ANALYSIS OF A TEN-DAY WAVE RECORD OBTAINED NEAR MIDDLETON ISLAND IN THE GULF OF ALASKA

RECOMMENDED:

Robin O. Brown

Robert W. Brown

Jim Maxwell

Vern Alexander

Thomas C. Royer
Chairman, Advisory Committee

W.S. Richards
Department Head

APPROVED:

K. B. Crapp
Dean of the College of Environmental Sciences

March 23 1976
Date

C. Lee
Vice President for Research

23 March 1976
Date

ANALYSIS OF A TEN-DAY WAVE RECORD OBTAINED NEAR MIDDLETON ISLAND IN THE GULF OF ALASKA

A

THESIS

Presented to the Faculty of the
University of Alaska in partial fulfillment
of the Requirements
for the Degree of

DOCTOR OF PHILOSOPHY

by

Jo Roberts, B.A., M.S.

Fairbanks, Alaska

May 1976

ABSTRACT

A bottom mounted surface wave gauge was operated in 70 m of water near Middleton Island in the Gulf of Alaska for 10 days in October and November 1973. Standard fast-Fourier transform techniques have been applied to the data, and a second-order lowpass Butterworth filter has been designed to examine low-frequency components in the record.

During the time the wave gauge was in operation, two earthquakes were reported with epicenters near the middle of the Aleutian Islands. The first had a surface wave magnitude of 6.4 on the Richter scale; the second, which occurred about 9 hours later, had a surface wave magnitude of 6.3. Spectra for data taken after the occurrence of these earthquakes have shown that generation of ocean waves by these quakes is questionable.

Hourly spectra from the first part of the record reveal a peak around 0.065 Hz which moves toward higher frequencies for about 18 hours. The frequency of the peak then remains constant for about 24 hours, after which it again increases. The changes are well correlated with a large storm which remained stationary in the North Pacific, then moved rapidly into the Gulf of Alaska and subsided. Wave group velocities are used to estimate possible distances of the wave source from the gauge. The actual distances of the storm from the gauge show a close correlation with wave-derived distances. Comparison with changes in wave spectra for a storm in the North Atlantic in March 1968 indicates the same time rate of change in the spectral peak as was found in the North Pacific for time periods when the storms are subsiding.

ACKNOWLEDGEMENTS

I am indebted to Dr. Thomas C. Royer, my major professor, for his guidance throughout the preparation of this work, and for its original idea.

I am grateful to James Dryden for his assistance with the computer programming; to Robert Seitz who, along with Dr. Royer, installed the wave gauge and obtained the data; and to Mauricette Nicpon for typing the manuscript. The reasearch was supported by the National Science Foundation under Grant Number GA-31544.

Finally, I wish to express gratitude to my husband, Tom, for his encouragement and advice during graduate school, as well as for his careful reading of this work.

TABLE OF CONTENTS

LIST OF FIGURES

CHAPTER 1

INTRODUCTION

From 0241 UT 30 October through 0102 UT 9 November 1973, a wave gauge was operated about 10 km off the coast of Middleton Island in the northern Gulf of Alaska. The water height was sampled every 4 seconds, giving approximately 214,000 data points. The purpose of this work is to develop techniques to analyze these data for periodicities and to carry out a detailed analysis of the wave record.

The number of points is too great for all of the data to be analyzed at one time; some means of reducing this number is necessary. The first step is to obtain an overall view of the record. This is done by averaging over 384 seconds (96 points) and taking each average as one point (Sections 3.6, 4.3). This reduces the number of points to 2234. Preliminary Fourier analysis shows this averaged record to be dominated by the tides.

The next step is to look at manageable sections of the raw data. To begin, sections of 1024 points (68 minutes 16 seconds) are taken from each day and Fourier analyzed. The resulting spectra show that for the first two days there are significant contributions to the average power by waves with periods from around 10 to 16 seconds. After two days, the spectra are nearly flat. For a finer look at the record for the first two days, 49 successive sections of 1024 points are Fourier analyzed. These spectra show details of a shift toward higher frequencies and simultaneous decay of a peak in the average power. These changes are correlated with a large storm in the area (Section 5.3).

Finally, we wish to analyze data sections which are more than a few hours long. This is because it is hoped that some evidence in the spectra can be seen of two earthquakes which occurred in the Aleutians while the wave gauge was operating. Earthquake-generated waves, or tsunamis, generally have periods from five minutes to an hour, so that longer sections of data need to be examined. The averaging and decimating procedure mentioned above is not deemed reliable enough for this purpose, nor is the method of using only every n^{th} data point. However, it is found that when the data are first lowpass filtered, the method of using only every n^{th} data point is quite satisfactory. Therefore, the entire record is lowpass filtered, then sampled, and various sections of these data are Fourier analyzed, the longest sections having 1536 data points (25.6 hours). Evidence in these spectra for tsunamis is shown to be inconclusive.

Chapter 2 contains a description of the area where the data were collected, with some notes on waves in the Gulf of Alaska. Chapter 3 gives details of the methods and assumptions which are used in analyzing and filtering the data. In Chapter 4, the methods described in Chapter 3 are used to search for possible evidence of tsunamis. Chapter 5 demonstrates the methods described in Chapter 3 by displaying the effects of a storm. A table of notation may be found in Appendix 1. All times in this work are given in Universal Time.

CHAPTER 2

BACKGROUND

2.1 The Gulf of Alaska

The Gulf of Alaska opens into the northern Pacific Ocean, being bounded on the eastern side by the Alexander Archipelago and by the Alaska Peninsula on the western side. The continental shelf, fairly wide in the eastern basin, is narrower on the northern and western sides. Near Middleton Island, in the northern gulf, the water depth increases from 200 to 4000 m in 75 km (Figure 4-2). South of Adak in the Aleutian Islands, water depth goes from 200 to 4000 m in 50 km, and to 6000 m, at the edge of the Aleutian Trench, in another 75 km. In the Aleutian Trench itself, water depths exceed 7000 m.

In winter, winds over the Gulf of Alaska are under the influence of the Aleutian Low. This is reflected in the general water circulation pattern, which is dominated by a counter-clockwise gyre, with current speeds immediately off the continental shelf exceeding 0.5 m/second (Royer, 1972). Severe storms in winter can create large waves with heights over 12 m. The storm of January, 1952, which caused the sinking of the S.S. *Pennsylvania* with all hands, for instance, was accompanied by waves with heights exceeding 15 m (Danielsen, Burt, and Rattray, 1957).

Middleton Island, a low, sandy island about 8 km long and 1.5 km wide, is located in the northern gulf at 59.5°N, 146.5°W, just north of the 200 m water depth (Figure 4-2). Tides at Middleton Island are semi-diurnal, with a marked inequality between successive low waters. The mean diurnal tidal range is 3.14 m (Rosenberg, 1972). The island is

often exposed to the full force of the storms that move in over the gulf. During the winter of 1973-74, for instance, storms caused the beach at Middleton Island to be eroded over 3 m.

2.2 The Data

In the summer of 1973 the Institute of Marine Science at the University of Alaska installed a wave gauge on the ocean floor about 10 km west of Middleton Island in about 70 m of water. The gauge was a B. J. Electronics Vibrotron Pressure Transducer, Model No. 120. Seitz (1975) has given details of the installation and the gauge.

The pressure was sampled every 4 seconds. At a depth of 70 m, pressure response for waves with periods of 8 seconds is about 2% that for 5 minute waves, so that aliasing of the spectrum from waves with periods under 8 seconds appeared to be no problem.

During the last of October and into November, 1973, the gauge ran continuously for almost 10 days, from 0241 UT 30 October to 0102 UT 9 November, giving a total of 214,496 data points. The data were recorded directly onto magnetic tape, the numbers representing a period output from the Vibrotron in nanoseconds. It was these numbers which were used in the analysis discussed in this work, since relative height, not actual height, of the waves was of interest. For an indication of actual height of the waves, Vibrotron period was converted to meters using the correspondence 1 nanosecond = 0.0477 m (Seitz, 1975).

CHAPTER 3

TECHNIQUES USED IN DATA ANALYSIS

3.1 Harmonic Analysis

All simple mechanical wave motions can be described by superposing trigonometric functions. Mathematically the importance of such functions, even in the case of complicated periodic phenomena such as ocean waves, depends on Fourier's theorem. This theorem states that every function $f(t)$, which is defined in the interval $t = 0$ to $t = 2\pi$, which has a continuous first derivative (except, at most, at a finite number of points in the interval), and which satisfies

$$\int_0^{2\pi} |f(t)| < \infty ,$$

can be expressed as an infinite series of trigonometric functions:

$$f(t) = \frac{a_o}{2} + a_1 \cos t + b_1 \sin t + a_2 \cos 2t + \ldots$$

with

$$a_o = \frac{1}{2\pi}\int_0^{2\pi} f(t)\, dt$$

$$a_n = \frac{1}{\pi}\int_0^{2\pi} f(t) \cos(nt)\, dt$$

$$b_n = \frac{1}{\pi}\int_0^{2\pi} f(t) \sin(nt)\, dt \qquad (n = 1, 2, 3, \ldots).$$

The process of expanding a function in the form of a trigonometric series is called harmonic analysis; the harmonic coefficients a_n and b_n are unique (Chapman and Bartels, 1940, p. 550).

In geophysics the conditions of Fourier's theorem are nearly always fulfilled. However, the fact that a function can be represented exactly over a chosen interval by an infinite series is of less importance for our purposes than the problem of approximating $f(t)$ by a finite series. In particular, we are presented with a discrete time series of pressure measurements representing the height of the ocean surface above its bottom at discrete time intervals for a time duration of T_1 and would like to approximate this signal by a finite trigonometric series. Such a representation will show which frequencies are predominant.

A discretely sampled signal can be regarded as having been derived from a continuous periodic signal $x(t)$ of length T_1 by sampling the signal at time increment Δ. This gives $N = T_1/\Delta$ sample values $x_k = x(t)$, where $t = k\Delta$. Assume N to be even and equal to $2n$, and let k run through the integers $-n,\ldots,0,1,\ldots,n-1$. [The FORTRAN subscripts of the data used by the computer for harmonic analysis must run from 1 to N, but interpretation of the results requires them to be transformed so as to run from $-N/2$ to $(N/2)-1$ (Kanasewich, 1973, p. 40).] Then the N pressure measurements may be written

$$\{x_k\} = \{x_{-n}, \cdots, x_0, \cdots, x_{n-1}\},$$

each x_k being 4 seconds apart in this experiment. An approximation to $x(k\Delta)$ in the interval $[-T_1/2, T_1/2]$ may be given by the finite Fourier series

$$\tilde{x}(k\Delta) = \tilde{x}_k$$

$$= A_o + 2 \sum_{m=1}^{n-1} \left\{ A_m \cos 2\pi m f_1 k\Delta + B_m \sin 2\pi m f_1 k\Delta \right\}$$

$$+ A_n \cos 2\pi n f_1 k\Delta$$

or, since the fundamental frequency is $f_1 = 1/T_1 = 1/N\Delta$,

$$\tilde{x}(k\Delta) = A_o + 2 \sum_{m=1}^{n-1} \left\{ A_m \cos \frac{2\pi mk}{N} + B_m \sin \frac{2\pi mk}{N} \right\}$$

$$+ A_n \cos \frac{2\pi nk}{N} \qquad (1)$$

(Jenkins and Watts, 1968, p. 19). The function $\tilde{x}(k\Delta)$ is thus composed of a sum of sine and cosine functions whose frequencies are multiples, or harmonics, of the fundamental frequency f_1 .

If the coefficients A_m and B_m are chosen so that

$$A_m = \frac{1}{N} \sum_{k=-n}^{n-1} x_k \cos \frac{2\pi mk}{N} \qquad (2a)$$

$$B_m = \frac{1}{N} \sum_{k=-n}^{n-1} x_k \sin \frac{2\pi mk}{N} , \qquad (2b)$$

then $\tilde{x}(k\Delta)$ as given by equation (1) is a least-squares approximation to the sampled function x_k ; that is,

$$\mu^2 = \frac{1}{N} \sum_{k=-n}^{n-1} x(k\Delta) - \tilde{x}(k\Delta)^2$$

is a minimum (Chapman and Bartels, 1940, p. 556). A_m is called the discrete Fourier cosine transform of $\{x_k\}$, and B_m is its discrete Fourier sine transform.

The mean square value of $\tilde{x}_k$ is

$$\frac{1}{N} \sum_{k=-n}^{n-1} \tilde{x}_k^2 \cdot \tag{3}$$

Using equation (1),

$$\frac{1}{N} \sum_{k=-n}^{n-1} \tilde{x}_k^2 = \frac{1}{N} \sum_{k=-n}^{n-1} \left[A_o + 2 \sum_{m=1}^{n-1} \left(A_m \cos \frac{2\pi mk}{N} + B_m \sin \frac{2\pi mk}{N} \right) + A_n \cos \frac{2\pi nk}{N} \right]^2$$

$$= A_o^2 + 2 \sum_{m=1}^{n-1} (A_m^2 + B_m^2) + A_n^2 \cdot \tag{4}$$

Equation (4) comes about owing to the orthogonality of $\sin (2\pi mk/N)$ and $\cos (2\pi mk/N)$ over the interval T_1 (Jenkins and Watts, 1968, p. 19). This orthogonality arises because of the assumption that the series $\{x_k\}$ has period T_1. Since the mean square value of $\tilde{x}_k$ is proportional to the average power associated with the wave (Lahti, 1968, p. 57), equation (4) shows how the average power of $\tilde{x}_k$ can be decomposed into contributions arising from each harmonic. The contribution from the m^{th} harmonic is $2(A_m^2 + B_m^2)$, while for the zero-th and n^{th} harmonics it is simply A_o^2 and A_n^2. A plot of the average power at each harmonic versus the frequency of the harmonic is called a Fourier line spectrum, or a periodogram.

When examining the record for periodicities, it is the relative sizes of the various contributions which are of interest. It is therefore assumed that the A_m and B_m are dimensionless quantities, so that their logarithm may be calculated. The periodogram then gives the log of the relative power at each harmonic.

The coefficients A_m and B_m were determined by a fast-Fourier

transform program called FOURG (Brenner, 1967). With FOURG, the number of data points to be transformed need not be a power of two, although a series whose number of points is a power of two will be transformed more rapidly. FOURG assumes that the normalization factor $1/N$ has been applied to equation (1), instead of to equations (2), so that A_m and B_m must be normalized before the periodogram is computed. A_o^2, the square of the mean of $\{x_k\}$, contains no information on periodicities in the data and is not plotted on the periodogram.

The discrete Fourier transform equations, equations (1) and (4), can be represented more compactly using complex variables. Let

$$X_m = A_m - jB_m \ . \tag{5}$$

Then, since

$$\cos\theta = \frac{1}{2}\,(e^{j\theta} + e^{-j\theta}) \tag{6a}$$

$$\sin\theta = \frac{-j}{2}\,(e^{j\theta} - e^{-j\theta}) \ , \tag{6b}$$

$\tilde{x}(k\Delta)$ as given by equation (1) can also be written as an exponential series:

$$\tilde{x}(k\Delta) = \sum_{m=-n}^{n-1} X_m\, e^{j(2\pi mk/N)} \ , \tag{7}$$

so that

$$X_m = \frac{1}{N} \sum_{k=-n}^{n-1} \tilde{x}_k\, e^{-j(2\pi mk/N)} \ . \tag{8}$$

When equations (7) and (8) hold, the functions $\tilde{x}(k\Delta)$ and X_m are said to be discrete Fourier transforms of each other. Proofs of equations (7) and (8) are given in Appendix 2.

The equalities $A_{-m} = A_m$ and $B_{-m} = -B_m$ imply that

$$X_{-m} = X_m^* , \tag{9}$$

where the asterisk denotes complex conjugation. Thus we have that the average power of the discrete function $\tilde{x}_k$ is

$$\frac{1}{N} \sum_{k=-n}^{n-1} \tilde{x}_k^2 = A_o^2 + \sum_{m=1}^{n-1} (A_m^2 + B_m^2) + \sum_{m=-1}^{-n+1} (A_m^2 + B_m^2) + A_n^2$$

$$= \sum_{m=-n}^{n-1} |X_m|^2 .$$

This equation is at the heart of our analysis, and we rewrite it for emphasis:

$$\frac{1}{N} \sum_{k=-n}^{n-1} \tilde{x}_k^2 = \sum_{m=-n}^{n-1} |X_m|^2 . \tag{10}$$

Thus the contribution to the average power at the m^{th} harmonic is divided into two parts, one at frequency mf_1 and the other at frequency $-mf_1$.

3.2 Other Analysis Procedures

A basic assumption in order that equation (3.1.4) hold is that the data are always taken over a fundamental period; i.e., that the data are periodic with period $N\Delta = T_1$, so that $x_{-n} = x_{n-1}$. In point of fact, actual data are seldom sampled exactly over one fundamental period, and there may be a large discrepancy between initial and final values of the experimentally determined $\{x_k\}$. For instance, consider the data shown in Figure 3-1. This figure shows the first 400 points (26 minutes 40 seconds) of the 10-day wave record, each point connected by a straight line. The record begins during ebb tide, and the downward trend evident

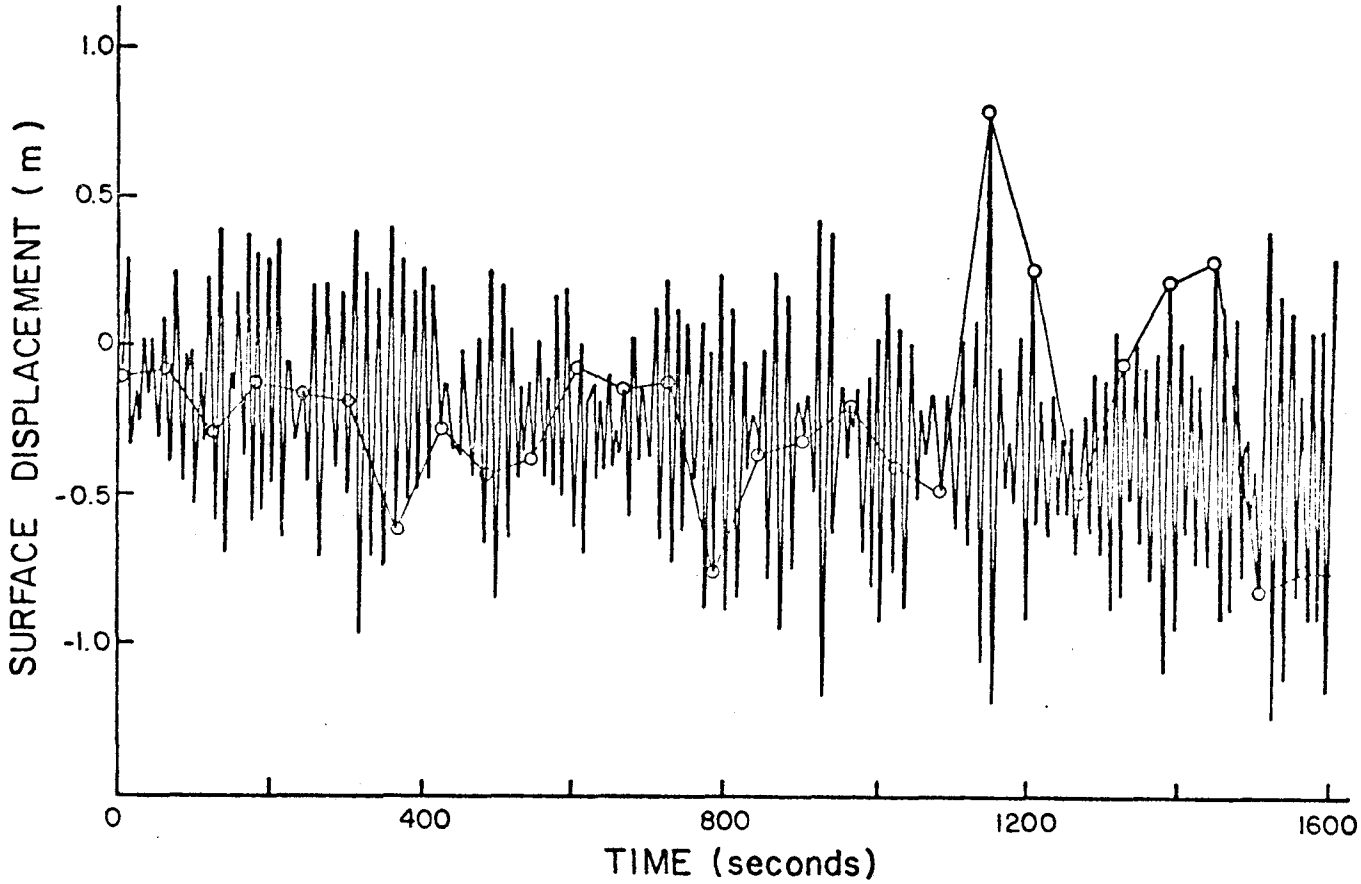

Figure 3-1. The first 400 points (1600 seconds) of raw data of pressure measurements taken near Middleton Island, starting at 0241 UT 30 October 1973. The heavy, solid line connects points 4 seconds apart; the open circles represent points 1 minute apart. For graphing, pressure has been converted to surface displacement using the relation given in Section 2.2.

in the figure continues for several hours. Figure 3-2a shows the periodogram for a series consisting of the first 1024 points of the wave record (68 minutes 16 seconds). The relative power at very low frequencies appears to be greater than 1000. Following a suggestion by Frankignoul (1974), the first and last points in the series of 1024 points were connected by a straight line, and this linear trend was subtracted from the data. Figure 3-2b shows the periodogram for the resulting series. Notice that the relative power at low frequencies is now less than 30, showing that a great deal of apparent relative power had been contributed to the periodogram by the downward trend. The relative power at higher frequencies is practically unchanged. Frankignoul's method was therefore adopted and routinely used before Fourier analyzing the experimental data.

Because the wave gauge was located beneath the surface of the water, the amplitude of the pressure variation was modified by K_p, a pressure response factor:

$$K_p = \frac{1}{\cosh\ (2\pi d/L)} \tag{1}$$

where L is the wavelength of a surface wave and d is the depth of the water (Kinsman, 1965, p. 143). From the dispersion relation for a linearized, small amplitude wave,

$$L = \frac{gT^2}{2\pi} \tanh \frac{2\pi d}{L} . \tag{2}$$

It is evident from this expression that, for a given wave period T and water depth d, L must be determined numerically.

An approximation to L, often called L_o, may be made as follows.

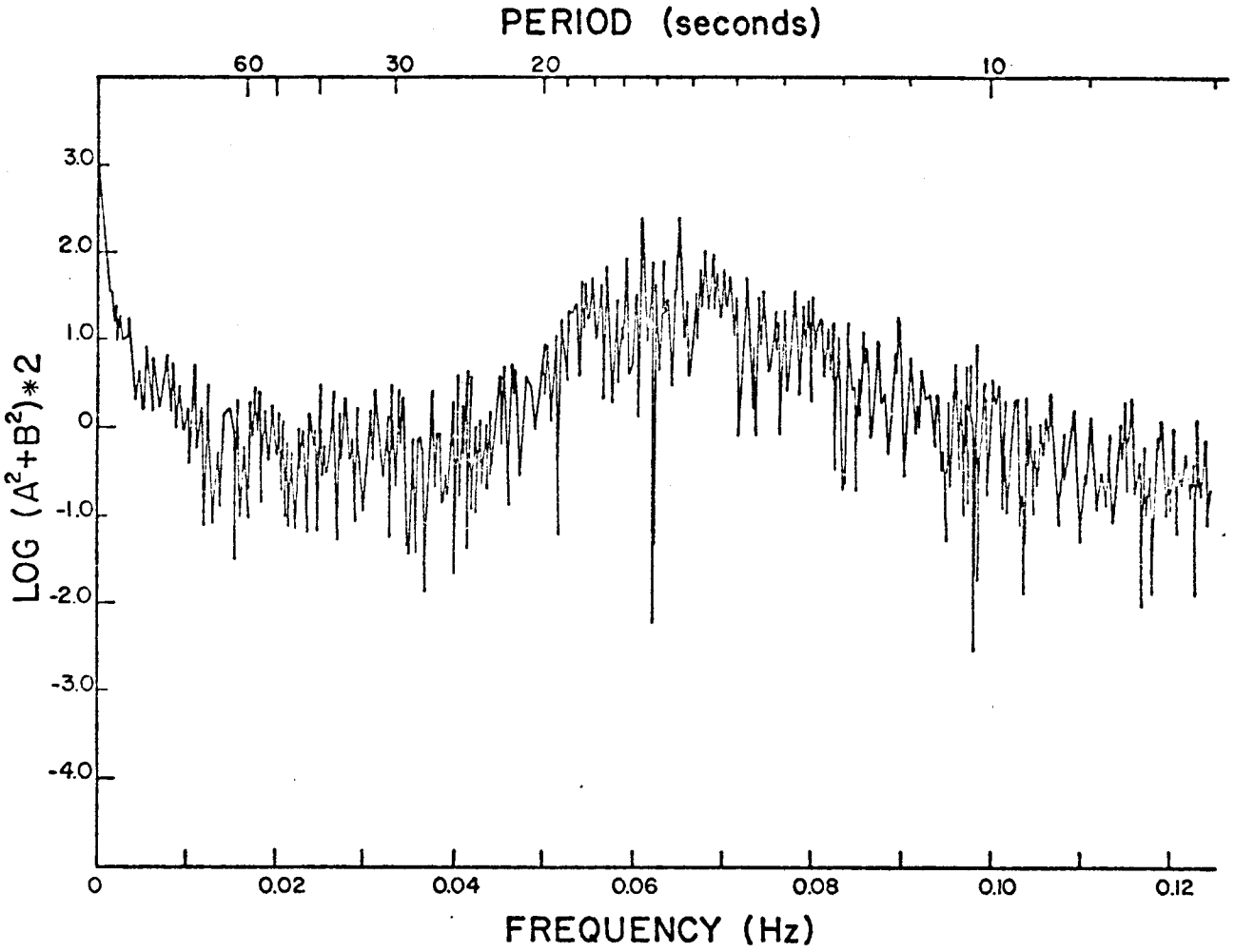

Figure 3-2a. Periodogram for the first 1024 points (68 minutes 16 seconds) of raw data.

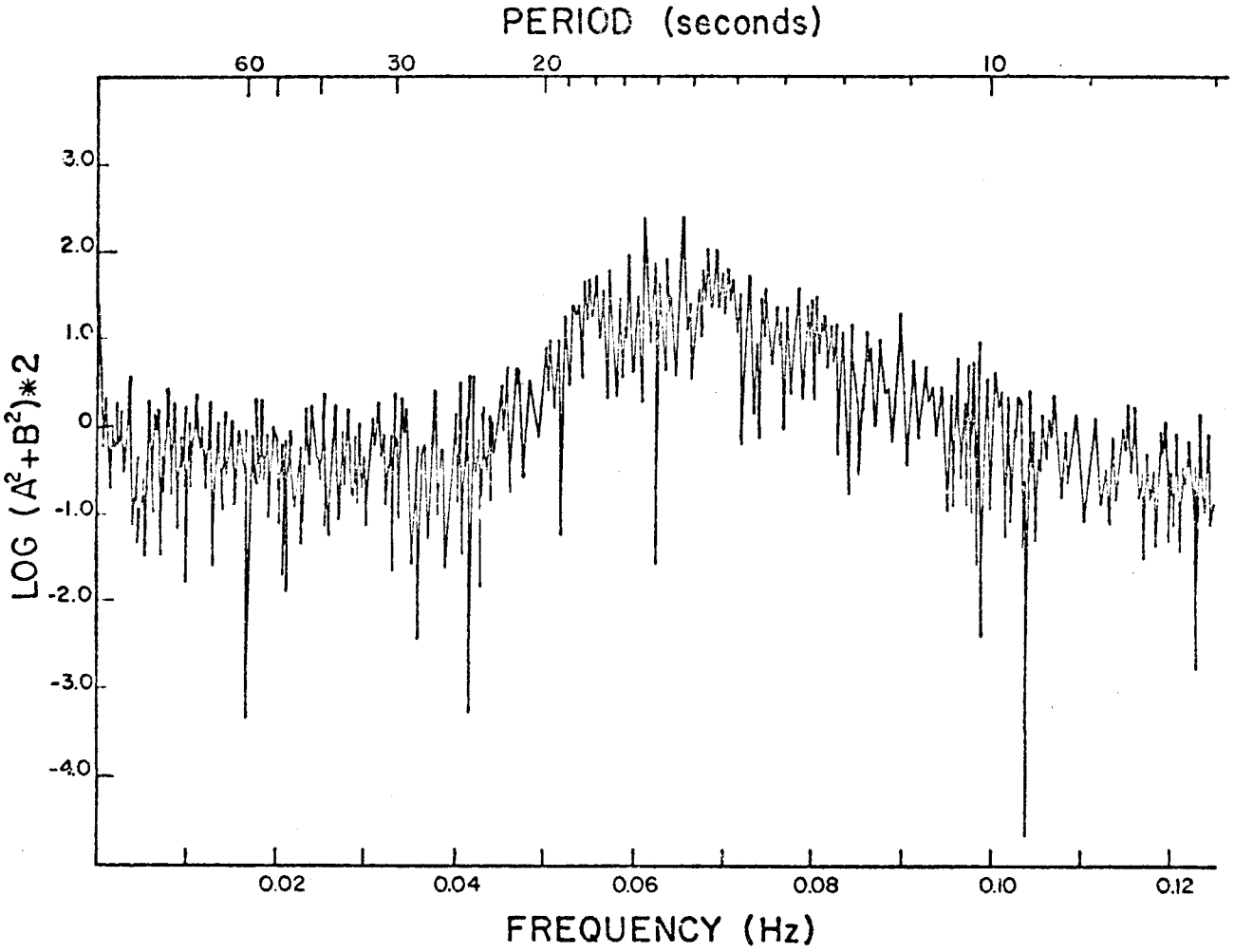

Figure 3-2b. Periodogram for the first 1024 points (68 minutes 16 seconds) after removal of the linear trend.

If we assume that the wavelength is much less than the depth of water, so that

$$\frac{d}{L} > > 1 \qquad \text{and} \qquad \tanh \frac{2\pi d}{L} \doteq 1,$$

then

$$L \doteq L_o = \frac{gT^2}{2\pi} . \tag{3}$$

For a given wave period T, L_o can be determined analytically.

In order to save computer time, expression (3) was used to determine the wavelength L_o, which in turn was used to compute the pressure response factor given by equation (1). Figure 3-3 compares a plot of K_p, the pressure response factor determined using L given by equation (2), with a plot of K_{p_o}, the pressure response determined by using L_o given in equation (3).

To obtain a surface wave periodogram, the observed periodogram should be divided by K_p^2 (Munk, Miller, Snodgrass, and Barber, 1963). Figure 3-4 shows the results of dividing the periodogram in Figure 3-2b by $K_{p_o}^2$, using $d = 69.5$ m.

The value of K_{p_o} is very close to unity for frequencies less than 0.017 Hz (periods greater than 60 seconds), as can be seen from Figure 3-3. Therefore, in this work only periodograms and spectra whose frequencies lie above 0.017 Hz have been divided by $K_{p_o}^2$.

3.3 Confidence Limits on the Spectrum

Oceanic wave data are seldom exactly normally distributed (Neumann and Pierson, 1966, p. 346), so that the confidence limits defined below will serve only as a pessimistic indication for the relative signifi-

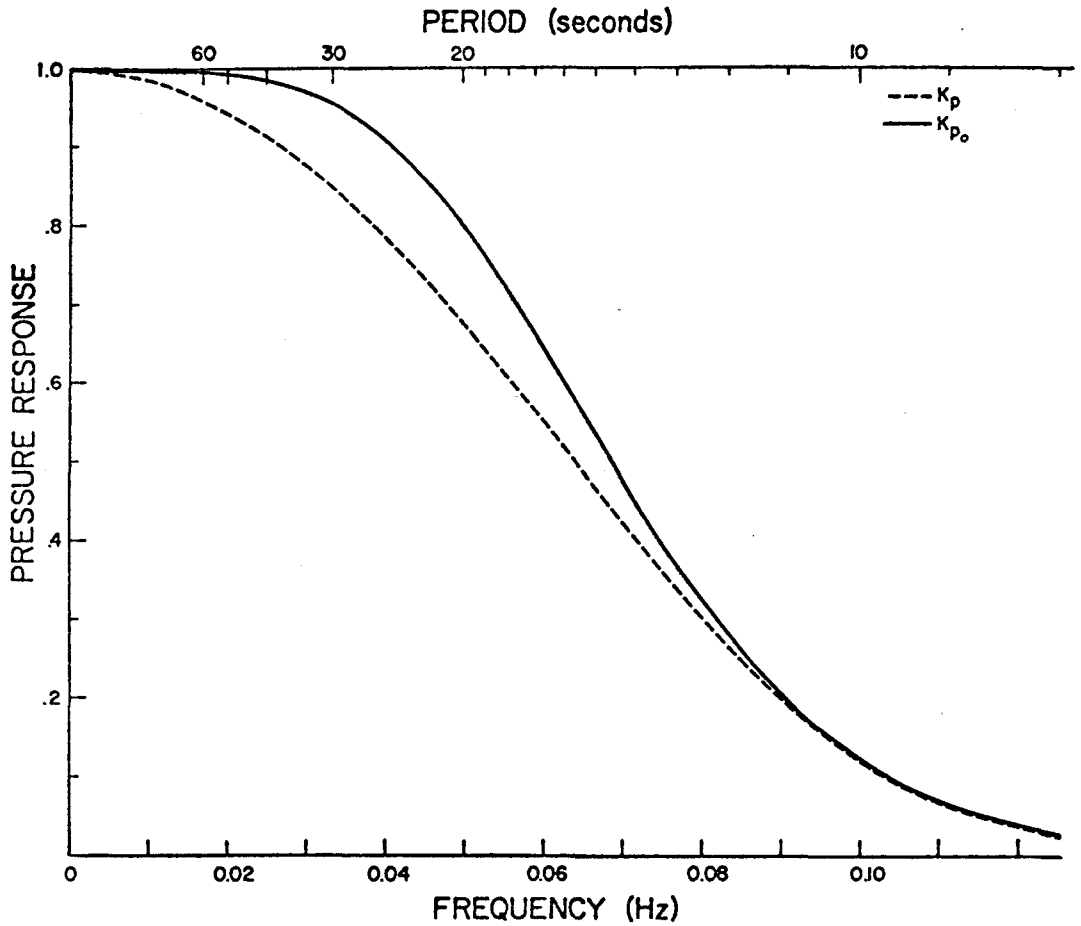

Figure 3-3. Comparison of pressure response factor computed using $L \doteq L_o = gT^2/2\pi$ (solid line) with pressure response factor computed using $L = (gT^2/2\pi) \tanh (2\pi d/L)$ with d = 69.5 m (dashed line).

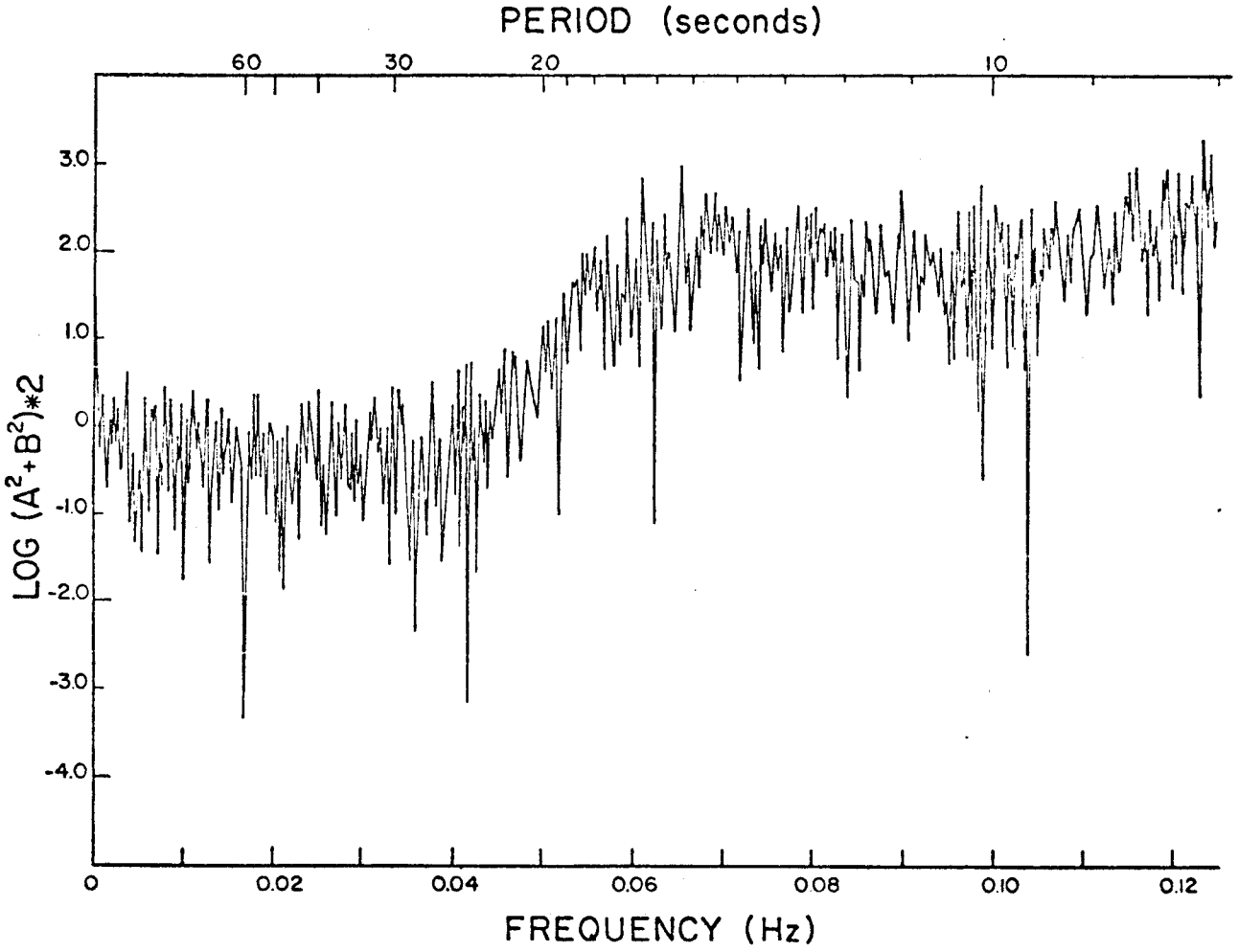

Figure 3-4. Periodogram for the first 1024 points (68 minutes 16 seconds). The linear trend has been removed from the data, and the periodogram has been divided by $[1/\cosh(4\pi^2 d/gT^2)]^2$, with d = 69.5 m.

cance of various peaks.

If the continuous time series, $x(t)$, from which the series $\{x(k\Delta)\}$ was derived can be regarded as one of many possible time series which might have been observed, that is, if it can be regarded as a realization of a stochastic process, then the variability in $x(t)$ is characterized by the random variables $\mathcal{X}(t)$ for $-T_1/2 \leqslant t \leqslant T_1/2$. Suppose that the random variables $\mathcal{X}(k\Delta)$, $-T_1/2 \leqslant (k\Delta) \leqslant T_1/2$, have been derived from $\mathcal{X}(t)$ by sampling the latter at increment Δ. Since $f_1 = 1/N\Delta$, the discrete Fourier sine and cosine transforms of $\mathcal{X}(k\Delta)$ may be written as

$$\mathcal{A}_{(mf_1)} = \frac{1}{N} \sum_{k=-n}^{n-1} \mathcal{X}(k\Delta) \cos(2\pi m f_1 k\Delta) = \mathcal{A}_m \tag{1a}$$

$$\mathcal{B}_{(mf_1)} = \frac{1}{N} \sum_{k=-n}^{n-1} \mathcal{X}(k\Delta) \sin(2\pi m f_1 k\Delta) = \mathcal{B}_m \tag{1b}$$

If $\mathcal{X}(k\Delta)$ is normally distributed, then so are $\mathcal{A}_m$ and $\mathcal{B}_m$, since the Fourier transform is a linear operation (Jenkins and Watts, 1968, p. 416; Papoulis, 1965, p. 475). Thus

$$|\mathcal{X}_m|^2 = \mathcal{A}_m^2 + \mathcal{B}_m^2$$

is the sum of two squared normal random variables and hence is distributed as a chi-squared random variable with two degrees of freedom; that is, as χ_2^2 (Papoulis, 1965, p. 250).

If $|\mathcal{X}_m|^2$ is distributed as χ_2^2, then the probability of $|\mathcal{X}_m|^2$ lying in the interval between $2|X_m|^2/\chi^2_{2;(\frac{\alpha}{2})}$ and $2|X_m|^2/\chi^2_{2;(1-\frac{\alpha}{2})}$ is $1 - \alpha$, where $0 < \alpha < 1$; i.e.,

$$\mathcal{P}\left\{\frac{2|X_m|^2}{\chi^2_{2;(\frac{\alpha}{2})}} < |\mathcal{X}_m|^2 \leq \frac{2|X_m|^2}{\chi^2_{2;(1-\frac{\alpha}{2})}}\right\} = 1 - \alpha \qquad (2)$$

(Jenkins and Watts, 1968, p. 254; Otnes and Enochson, 1972, pp. 216-220). The values of the upper and lower limits $2/\chi^2_{2;(\frac{1}{\alpha})}$ and $2/\chi^2_{2;(1-\frac{\alpha}{2})}$ may be obtained from tables (Otnes and Enochson, 1972, p. 221). These limits are very sensitive to the validity of the assumption that the Fourier coefficients are normal (Jenkins and Watts, 1968, p. 81).

For ν degrees of freedom, equation (2) becomes

$$\mathcal{P}\left\{\frac{\nu|X_m|^2}{\chi^2_{2;(\frac{\alpha}{2})}} < |\mathcal{X}_m|^2 \leq \frac{\nu|X_m|^2}{\chi^2_{2;(1-\frac{\alpha}{2})}}\right\} = 1 - \alpha \, . \qquad (3)$$

Equation (3) can be used to determine an interval within which $|\mathcal{X}_m|^2$ may be expected to lie for a given percentage of the time. For example, if $|X_m|^2 = 2$ and $\alpha = .2$, the lower and upper limits for $\nu = 2$ are found to be .405 and 9, so that 80% of the time $|\mathcal{X}_m|^2$ can be expected to lie between .810 and 18. The interval (.81,18) is called an 80% confidence interval for $|\mathcal{X}_m|^2$.

Notice that equation (3) is valid for a particular value of m only, so that a separate confidence interval is required for each frequency. This problem may be avoided if the log of the spectrum is plotted versus frequency. In that case, equation (3) becomes

$$\mathcal{P}\left\{\log_{10}|X_m|^2 + \log_{10}\left(\frac{\nu}{\chi^2_{2;(\frac{\alpha}{2})}}\right) < \log_{10}|\mathcal{X}_m|^2 \leq \log_{10}|X_m|^2 + \log_{10}\left(\frac{\nu}{\chi^2_{2;(1-\frac{\alpha}{2})}}\right)\right\} = 1 - \alpha \, , \qquad (4)$$

and the confidence interval for $\log_{10} |\mathcal{X}_m|^2$ is the same for all frequencies. For instance, suppose that $|X_1|^2 = 1$ and $|X_3|^2 = 3$. Using $\nu = 2$, and $\alpha = 0.2$, we have

$$\log_{10} \left(\frac{2}{\chi^2_{2;0.1}} \right) = -0.363$$

$$\log_{10} \left(\frac{2}{\chi^2_{2;0.9}} \right) = 0.977 .$$

When $m = 1$, equation (4) becomes

$$\mathcal{P} \left\{ 0 - 0.363 < \log_{10} |\mathcal{X}_1|^2 \leq 0 + 0.977 \right\} = 0.80$$

and the 80% confidence interval goes from 0.363 below to 0.977 above $\log_{10} |X_1|^2$; i.e., the 80% confidence interval is (-0.363, 0.977). On the other hand, when $m = 3$, equation (4) becomes

$$\mathcal{P} \left\{ 0.477 - 0.363 < \log_{10} |\mathcal{X}_3|^2 \leq 0.477 + 0.977 \right\} = 0.80 ,$$

and the 80% confidence interval is (0.114, 1.454), again from 0.363 below to 0.977 above $\log_{10} |X_3|^2$.

A plot of $2|X_m|^2$ for a signal such as ours which has highly irregular fluctuations will itself have irregular fluctuations (for instance, see Figure 3-2a). If $|\mathcal{X}_m|^2$ is distributed as χ^2_2, even the 80% confidence interval will be so wide that very few peaks, if any, will lie outside it. If the record $\{x(k\Delta)\}$ contains power at a certain frequency—that is, if waves with a certain period are present in the record—the plot of $2|X_m|^2$ will have a peak at that frequency, but the converse need not hold. Since the confidence interval can provide an indication of whether or not a peak is significant, it is desirable to be able to narrow it, if possible. One way this can be done is to

average adjacent blocks of Fourier coefficients. For instance, let

$$|X_1'|^2 = \frac{(A_1^2 + B_1^2) + \cdots + (A_L^2 + B_L^2)}{L}$$

$$|X_2'|^2 = \frac{(A_{L+1}^2 + B_{L+1}^2) + \cdots + (A_{2L}^2 + B_{2L}^2)}{L}$$

etc. Then each $|X_m'|^2$, being the sum of 2L squared normal random variables, is distributed as χ_{2L}^2, with a correspondingly narrower confidence interval.

In this work a plot of $2|X_m|^2$ versus frequency ($\nu = 2$) is referred to as a periodogram; plots of averaged Fourier coefficients versus frequency ($\nu > 2$) will be called spectra. It may be noted that this definition of a power spectrum as averages of $2|X_m|^2$ differs from, but is proportional to, the more usual definition of the one-sided sample Fourier power spectrum as averages of $2N\Delta|X_m|^2$ (for instance, Jenkins and Watts, 1968, p. 211). Since we have plotted the log of the spectrum, this difference amounts to an additive constant.

3.4 The Sampling Theorem

One of the assumptions thus far is that the discrete series of pressure measurements [i.e., the series $\{x(k\Delta)\}$] represents the actual continuous fluctuations of the ocean surface [i.e., the function $x(t)$ for $-T_1/2 \leq t \leq T_1/2$] well enough so that peaks in the spectrum of $\{x(k\Delta)\}$ would correspond to peaks in the spectrum of $x(t)$. That is, if the spectrum of $\{x(k\Delta)\}$ indicates considerable power at a certain frequency, we would expect waves of that frequency had actually occurred on the ocean surface. This assumption is true only if the sampling interval Δ

is sufficiently small. More precisely, we have the following theorem:

> A function $f(t)$ which has no harmonic components with frequency greater than ω_o, so that
>
> $$F(\omega) = 0 \quad \text{if} \quad \omega > \omega_o ,$$
>
> is uniquely determined by its samples taken at uniform intervals
>
> $$\Delta \leqslant \pi/\omega_o .$$

Here $F(\omega)$ is the Fourier transform of $f(t)$, ω_o is angular frequency $2\pi/T_o$, T_o is a specified period. This theorem is known as the Sampling Theorem (Lahti, 1968, p. 46).

One consequence of the Sampling Theorem is that the shortest period which can be analyzed is equal to twice the sampling interval. To see this, suppose that the spectrum $F(\omega)$ only has frequencies $\omega < \omega_o$ and suppose we choose a sampling interval $\Delta = \pi/\omega_o$. Then the minimum period period T_{min} of any component of $f(t)$ which we can detect is

$$T_{min} = 2\pi/\omega_{max} = 2\pi/\omega_o = 2\Delta .$$

Another consequence is that if the function $f(t)$ does have harmonic components with frequency greater than ω_o, and if the samples are taken at intervals $\Delta > \pi/\omega_o$, the resulting spectrum will be erroneous, particularly if $f(t)$ has considerable power at some frequency greater than ω_o (see Figure 3-5). The process by which components with frequencies greater than ω_o erroneously contribute to the spectrum is called aliasing.

3.5 Introduction to Digital Filters

In the course of analyzing the data record there were certain fre-

quencies we wished to suppress in order to examine others more carefully. Since the data were taken with no intentional filtering, aside from the unavoidable hydrodynamic filtering of higher frequencies, the best way to suppress undesired frequencies was by use of a digital filter. The original data were digitally filtered to obtain a filtered record which was then analyzed. It was decided to use a recursive filter, that is, one which uses past values of the output, since the cutoff for this type of filter is sharper than for non-recursive ones (Kaiser, 1966). The filter was designed in terms of the Z-transform. Z-transform notation is convenient and is used in many modern references on digital filters (Cadzow, 1973; Kaiser, 1966). A very brief description of the Z-transform and of transfer functions and their relation to the actual filtering operation are presented, followed by a detailed description of the filter which was used on the data.

3.6 Z-transforms and the Transfer Function

The Z-transform of a discrete-time system

$$\{x_k\} = \{x_o, x_1, x_2, \cdots, x_{N-1}, \cdots\}$$

is defined

$$Z\{x_k\} \equiv x_o + \frac{x_1}{z} + \frac{x_2}{z^2} + \cdots + \frac{x_{N-1}}{z^{N-1}} + \cdots$$

$$= \sum_{k=0}^{\infty} x_k z^{-k} = X(z) \ , \qquad (1)$$

where z is a complex variable. The Z-transform was known to Laplace (1779), but did not come into common use until the 1950's. We shall assume $x_k = 0$ for $k > N-1$, where N is the number of data points.

Thus the sum on the right-hand side of equation (1) is finite and will converge, so long as $0 < |z| < \infty$.

One of the most important properties of the Z-transform is its time-shifting property. If $x_k = 0$ for $k < 0$, then

$$Z\left\{x_{k-m}\right\} = z^{-m}\, Z\left\{x_k\right\} \tag{2}$$

because

$$Z\left\{x_{k-m}\right\} = x_{-m} + \frac{x_{-m+1}}{z} + \frac{x_{-m+2}}{z^2} + \cdots + \frac{x_o}{z^m} + \frac{x_1}{z^{m+1}} + \cdots$$

[by definition of $Z\{\cdot\}$]

$$= \frac{x_o}{z^m} + \frac{x_1}{z^{m+1}} + \cdots \qquad [x_k = 0 \text{ for } k < 0]$$

$$= \sum_{k=0}^{\infty} x_k z^{-(k+m)}$$

$$= z^{-m} \sum_{k=0}^{\infty} x_k z^{-k} \ .$$

Consider a discrete, linear system whose initial conditions are all zero and whose input is the sequence $\left\{x_k\right\}$. The k^{th} element of the output sequence $\left\{y_k\right\}$ is given by

$$y_k = \sum_{i=0}^{\infty} h_i x_{k-i} \tag{3}$$

(Jenkins and Watts, 1968, p. 34). This may be equivalently written

$$y_k = b_1 x_k + b_2 x_{k-1} + \cdots + b_{m+1} x_{k-m} - a_1 y_{k-1} - \cdots - a_\ell y_{k-\ell} \tag{4}$$

(Cadzow, 1973, p. 92), where the coefficients a_i and b_i depend on the coefficients h_i in equation (3). Equation (3) is called a convolution summation, and the sequence $\left\{h_k\right\}$ is called the system weighting sequence. However, we shall be less concerned with it than with its

Z-transform, $H(z)$.

Writing $Y(z)$, $H(z)$, and $X(z)$ for the Z-transforms of the sequences $\{y_k\}$, $\{h_k\}$, and $\{x_k\}$, respectively, where $\{y_k\}$ is given by equation (3), we have the important relation

$$Y(z) = H(z)\, X(z) \ . \tag{5}$$

Freeman (1965, p. 40) has given a proof of this statement. $H(z)$ is called the transfer function of the system, and its importance will now be shown.

Taking $z = e^{j2\pi m/N}$, where m is some integer $0 < m < N-1$, it may be shown that $2|X(z)|^2$ is the contribution to the average power of the input signal $\{x_k\}$ at the m^{th} harmonic. From equation (5),

$$|Y(z)|^2 = |H(z)|^2 \ |X(z)|^2 \ ,$$

showing that at the m^{th} harmonic this contribution has been modified by a factor $|H(z)|^2$. $|H(z)|$ is called the gain function. Writing radian frequency $\omega = 2\pi m/N\Delta$, where as before Δ is the sampling interval for the data, we have

$$|H(z)| = |H(e^{j2\pi m/N})| = |H(e^{j\omega\Delta})| \ .$$

We therefore wish to determine coefficients a_i and b_i in equation (4) so that the gain function will suppress contributions to the average power at the appropriate radian frequencies ω. In general, it is quite difficult to determine $H(z)$ from $|H(z)|^2$. However, once this has been done we have, for a linear time-invariant system, a transfer function which is a ratio of polynomials, and the coefficients of these polynomials are the desired a_i and b_i, as will now be shown.

Multiplying equation (4) by z^{-k}, rearranging, and summing over k

we have

$$\sum_{k=0}^{\infty}\left[y_k z^{-k} + a_1 y_{k-1} z^{-k} + \cdots + a_\ell y_{k-\ell} z^{-k}\right]$$

$$= \sum_{k=0}^{\infty}\left[b_1 x_k z^{-k} + \cdots + b_{m+1} x_{k-m} z^{-k}\right].$$

As a consequence of equation (2), this becomes

$$\sum_{k=0}^{\infty} y_k z^{-k} + a_1 z^{-1} \sum_{k=0}^{\infty} y_k z^{-k} + \cdots + a_\ell z^{-\ell} \sum_{k=0}^{\infty} y_k z^{-k}$$

$$= b_1 \sum_{k=0}^{\infty} x_k z^{-k} + \cdots + b_{m+1} z^{-m} \sum_{k=0}^{\infty} x_k z^{-k},$$

or, by equation (1),

$$Y(z)\left[1 + a_1 z^{-1} + \cdots + a_\ell z^{-\ell}\right] = X(z)\left[b_1 + \cdots + b_{m+1} z^{-m}\right],$$

whence, from equation (5),

$$H(z) = \frac{b_1 + b_2 z^{-1} + \cdots + b_{m+1} z^{-m}}{1 + a_1 z^{-1} + \cdots + a_\ell z^{-\ell}}. \tag{6}$$

Thus the coefficients of the transfer function may be used directly to compute $\{y_k\}$, the filtered output of the input sequence $\{x_k\}$. The system weighting sequence $\{h_k\}$ may be found by taking the inverse Z-transform of $H(z)$. In our case, however, once the transfer function has been found, there is no need to find a specific expression for the weighting sequence.

3.7 A Lowpass Filter

In order to examine large portions of the record, it was desirable to reduce the number of data points so they could be accommodated by the

discrete Fourier transform program. This could have been done in several ways: (a) average the data over some interval and choose the mean as a single point for that interval; (b) use only every n^{th} point of data; (c) filter the record first to remove high-frequency waves, then use method (b).

Method (a) has the capability of smoothing the data and substantially reducing the number of data points. This method is demonstrated in Section 4.3. The averaged output can be considered as the output of a lowpass filter. However, the gain function for such a filter has a fairly complicated form (Blackman and Tukey, 1958, pp. 129-135), and it cannot be sufficiently assured that no aliasing from high-frequency waves will occur.

Method (b) was tested on the first 1024 data points of the record. The raw data were sampled every minute, then the linear trend was removed. Figure 3-5 compares the periodogram of these data (Δ = 60 seconds, dashed line) with the results in Figure 3-2b (Δ = 4 seconds, solid line). Note that when Δ = 60 seconds, only frequencies greater than 1/(2 x 60 seconds) can be analyzed (Section 3.4), so the periodogram in this case is considerably shorter than when Δ = 4 seconds. Aliasing of the periodogram in Figure 3-5 is evident, probably from contributions with frequencies around 0.06 Hz. Method (b) was therefore abandoned. It may be added that this method probably could have been used, had we been willing to take Δ smaller than 60 seconds, say Δ = 8 or even 16 seconds, and analyzed only those parts of the data record where contributions from frequencies around 0.06 Hz were not so large.

It was therefore decided to try method (c). The filter used was a

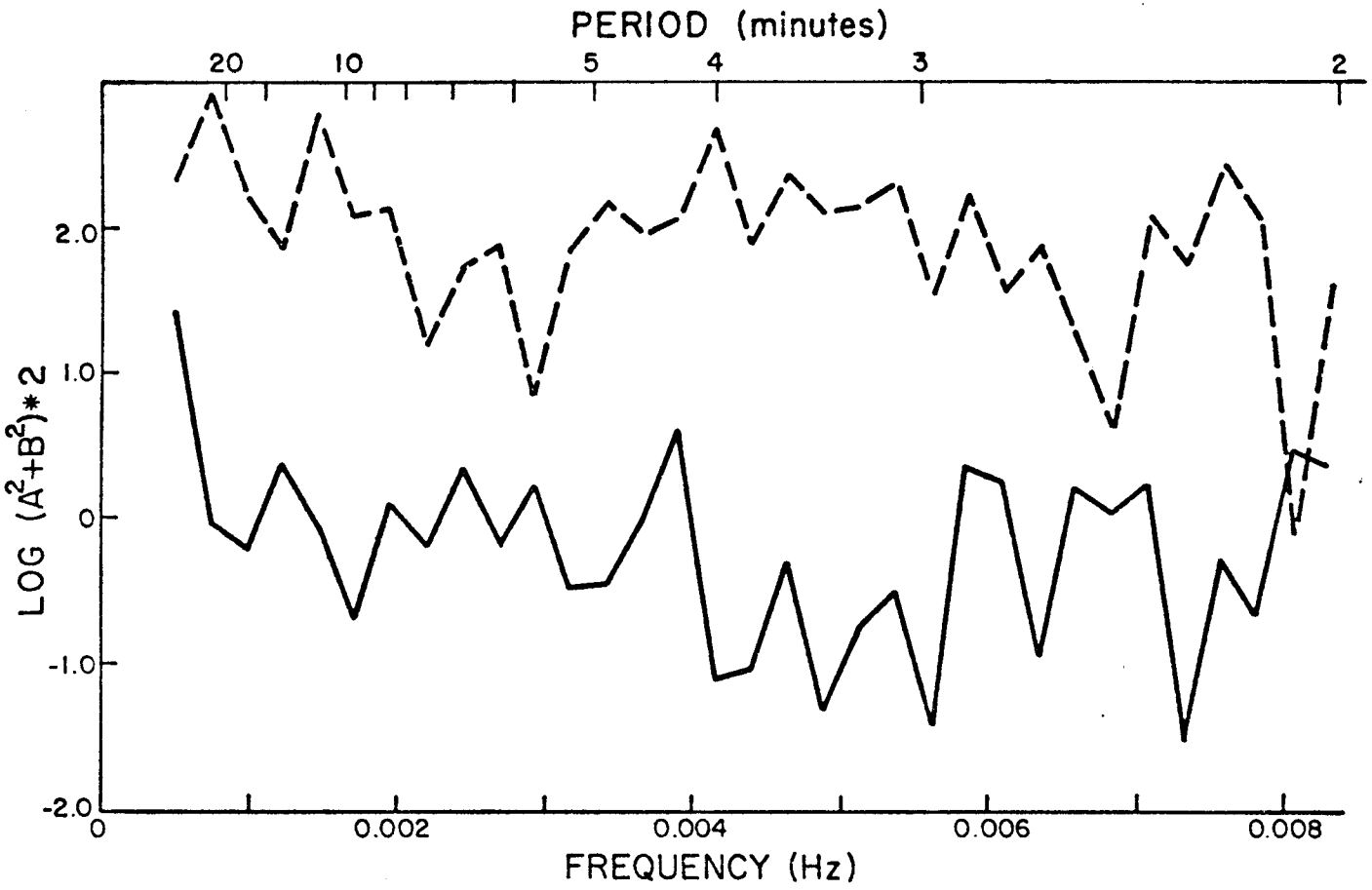

Figure 3-5. Comparison of periodograms for the first 1024 data points for Δ = 4 seconds (solid line) with Δ = 60 seconds (dashed line).

second order lowpass Butterworth filter designed according to Cadzow (1973, p. 336 ff.) and called LPFILTER. Its gain function has the form

$$|H(e^{j\omega\Delta})| = \left[\frac{1}{1 + \dfrac{\tan^2(\frac{\omega\Delta}{2})}{\tan^2\left(\frac{\omega_c\Delta}{2}\right)}} \right]^{1/2} \qquad (1)$$

where ω_c is the cutoff radian frequency;

$$|H(e^{j\omega_c\Delta})|^2 = 0.5 ,$$

as can be seen from equation (1).

For the tsunami problem in Chapter 4, only periodicities greater than about 5 minutes were of interest, so it was decided to take

$$\omega_c = 2\pi/4 \text{ minutes} ,$$

$$\text{or } f_c = 1/4 \text{ minutes} = 4.17 \times 10^{-3} \text{ Hz.}$$

The transfer function of this filter has the form

$$H(z) = \frac{b(z+1)^2}{(z-p_1)(z-p_2)} \qquad (2)$$

where p_1 and p_2 are the poles of the filter and b is chosen so that

$$|H(1)|^2 = 1 .$$

Using formulae from Cadzow (1973, p. 338) the values for b, p_1, and p_2 for LPFILTER were found to be

$$b = 0.002550$$

$$p_1 = 0.926073 + j\ 0.068825$$

$$p_2 = 0.926073 - j\ 0.068825$$

In order to determine if a filter is stable, that is, whether any bounded input will result in a bounded output, it is necessary and sufficient to determine whether or not the magnitudes of all its poles are

less than unity (Freeman, 1965, p. 171, 173). (While this is true in theory, the round-off error may make a theoretically stable filter unstable.) In the case of LPFILTER,

$$|p_1| = |p_2| = 0.928627$$

so that the filter is theoretically stable.

Putting the transfer function for LPFILTER in the form of equation (3.6.6), we have

$$H(z) = \frac{b_1 + b_2 z^{-1} + b_3 z^{-2}}{1 + a_1 z^{-1} + a_2 z^{-2}}$$

$$= \frac{0.002551 + 0.005101\ z^{-1} + 0.002551\ z^{-2}}{1.0 - 1.852146\ z^{-1} + 0.862349\ z^{-2}} \quad .$$

To find $|H(z)|^2$ in terms of the calculated numbers b, p_1, and p_2 (such an expression, when compared to equation (1), serves as a check on the calculations), we take

$$|H(z)|^2 = H(z)H(z^{-1})$$

$$= \frac{b^2(z+1)^2(z^{-1}+1)^2}{(1+a_1 z+a_2 z^2)(1+a_1 z^{-1}+a_2 z^{-2})}$$

$$= b^2 \frac{6 + 4(z + z^{-1}) + (z^2 + z^{-2})}{(1+a_1^2+a_2^2) + (a_1+a_1 a_2)(z+z^{-1}) + a_2(z^2+z^{-2})}$$

$$= b^2 \frac{6 + 8 \cos \omega\Delta + 2 \cos 2\omega\Delta}{(1+a_1^2+a_2^2) + 2(a_1+a_1 a_2) \cos \omega\Delta + 2a_2 \cos 2\omega\Delta}$$

since

$$z^n + z^{-n} = e^{jn\omega\Delta} + e^{-jn\omega\Delta} = 2 \cos n\omega\Delta \ .$$

A graph of $|H(z)|$ for LPFILTER is shown in Figure 3-6. The response of

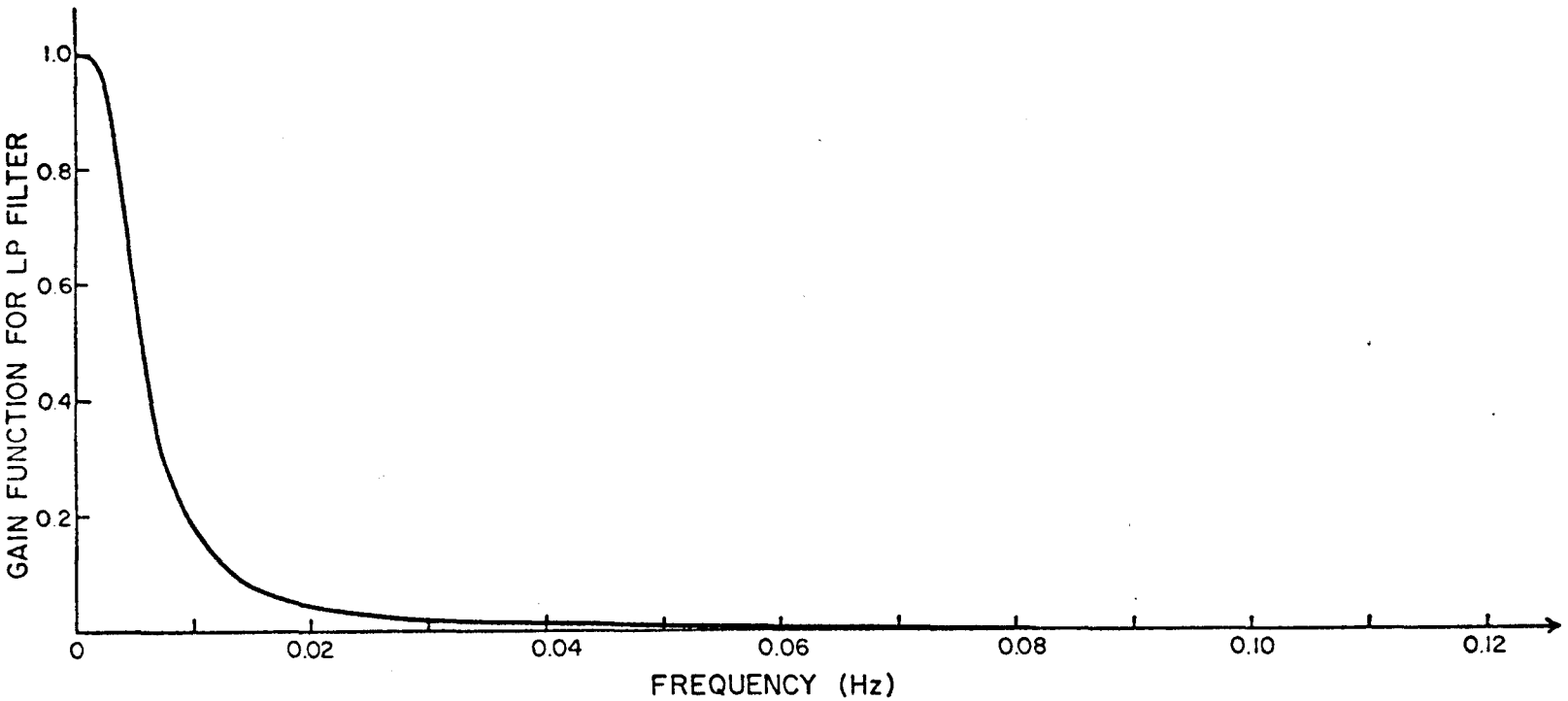

Figure 3-6. Gain function, $|H(z)|$, for LPFILTER, a second-order Butterworth lowpass filter with cutoff frequency at 4.17×10^{-3} Hz (T = 4 minutes).

LPFILTER to an impulse is shown in Figure 3-7.

LPFILTER was tested on the first 1024 points of the data record. The first 400 points of filtered output are shown in Figure 3-8. This may be compared to the unfiltered data in Figure 3-1. Figure 3-9 shows the periodogram for these 1024 points of filtered data (linear trend and pressure response removed). Then, as in method (b) above, the filtered data were sampled every minute and the linear trend removed. Figure 3-10 compares the periodogram of these data (Δ = 60 seconds, dashed line) with the results in Figure 3-9 (Δ = 4 seconds, solid line). For comparison, the periodogram for unfiltered data sampled every 4 seconds is shown with a dotted line in Figure 3-10. It appears that the periodogram will not be unacceptably distorted below 5.6×10^{-3} Hz (T = 3 minutes) by sampling the filtered record every minute. Method (c) was thus adopted for the analysis of the records discussed in Section 4.4.

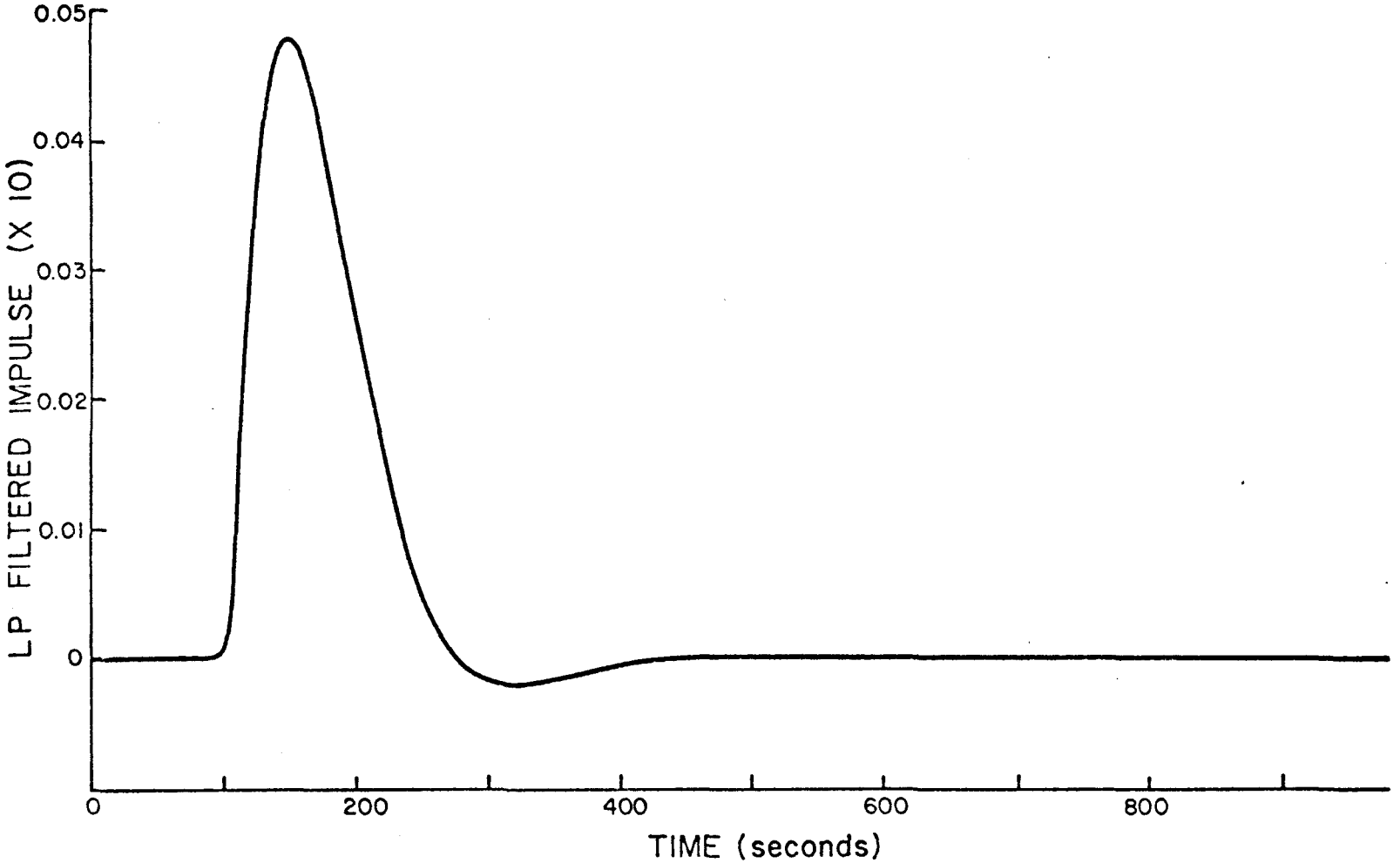

Figure 3-7. The response of LPFILTER to a unit impulse applied at 100 seconds.

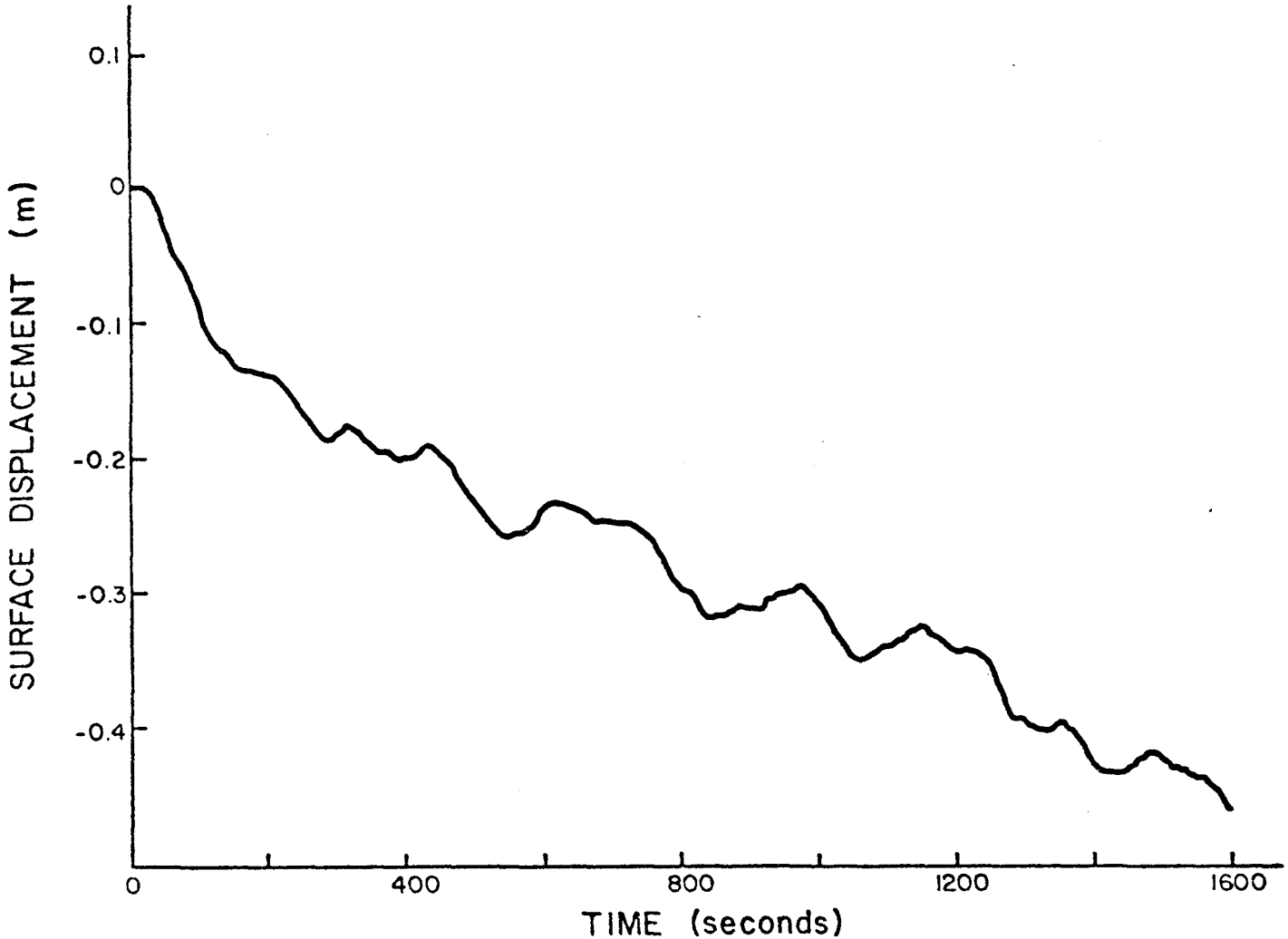

Figure 3-8. The first 400 points (1600 seconds) of the data record after filtering with LPFILTER. Compare with Figure 3-1. For graphing, pressure has been converted to surface displacement using the relation given in Section 2.2.

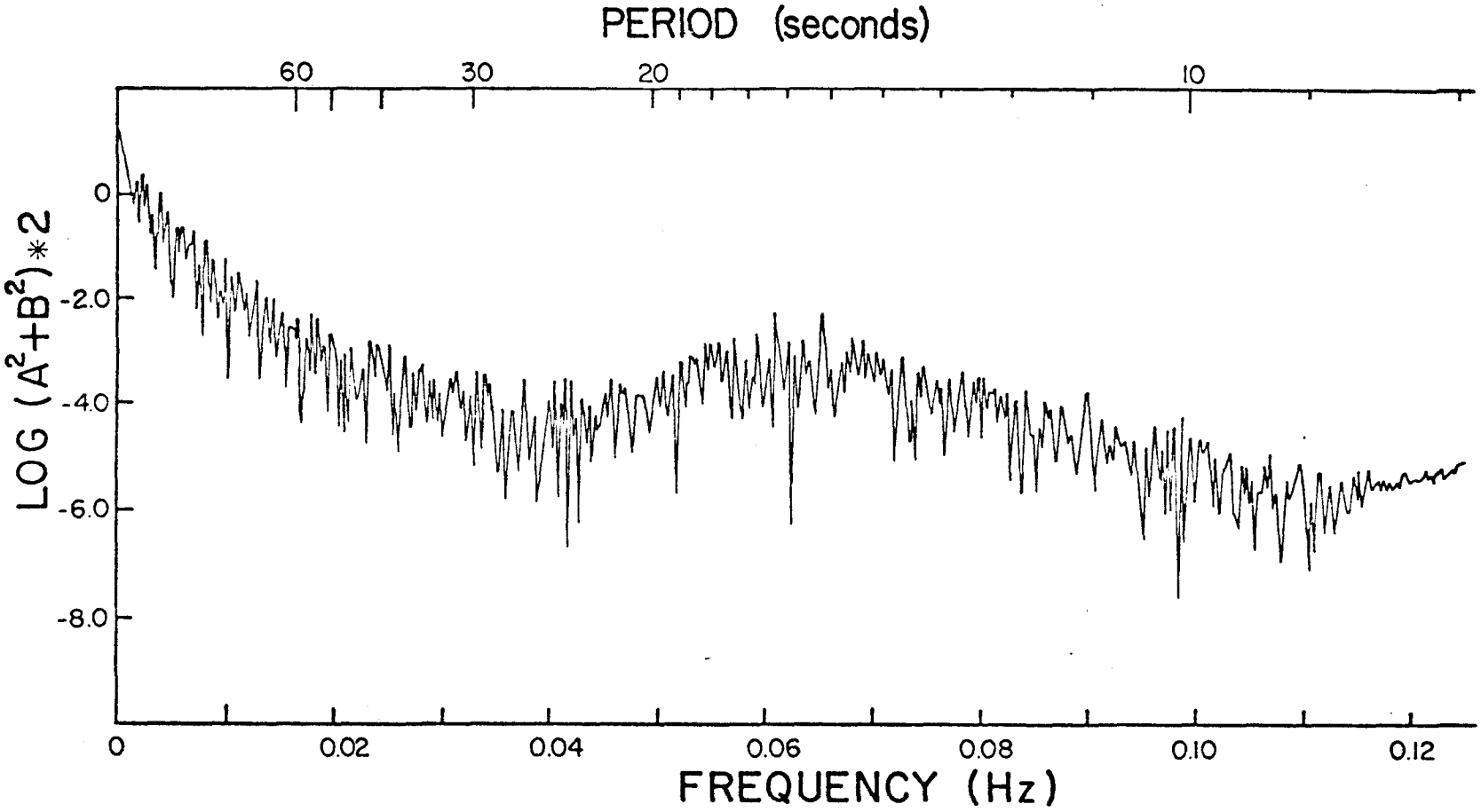

Figure 3-9. Periodogram of the first 1024 points of the data record after filtering with LPFILTER. The linear trend has been removed from the data, and the periodogram has been divided by $[1/\cosh(4\pi^2 d/gT^2)]^2$, with d = 69.5 m.

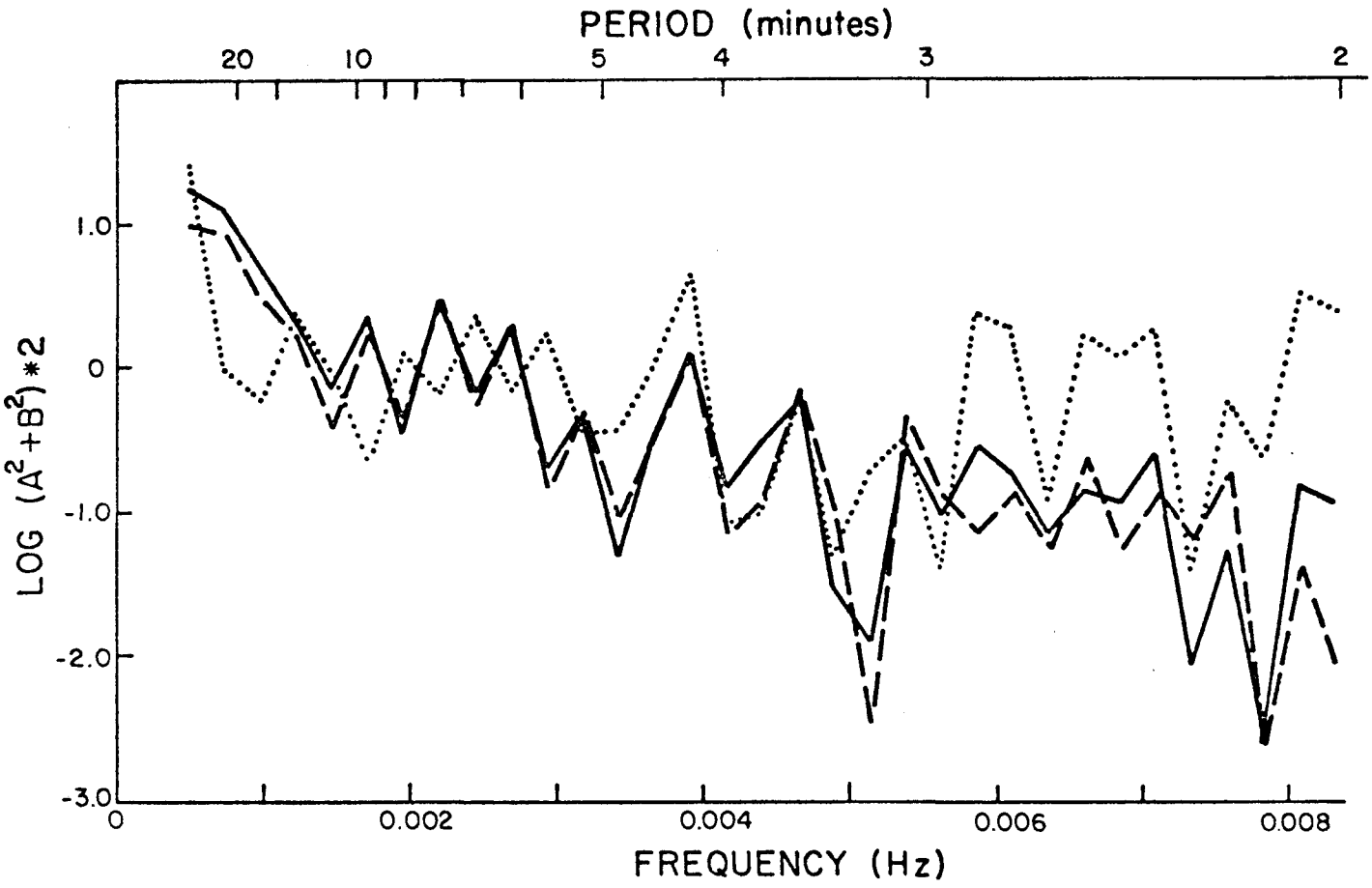

Figure 3-10. Periodograms for the first 1024 data points after filtering with LPFILTER when Δ = 4 seconds (solid line) and Δ = 60 seconds (dashed line). The periodogram for the unfiltered data with Δ = 4 seconds is shown by a dotted line.

CHAPTER 4

SECONDARY TSUNAMIS

4.1 Introduction

The idea that small earthquakes can generate small tsunamis, suggested by Iida (1963), was explored by Royer and Reid (1971). They found evidence that aftershocks of the 9 March 1957 earthquake in the Aleutians (which generated a very large tsunami) themselves generated long-period surface waves of considerable amplitude. The importance of such waves, which Royer and Reid termed "secondary tsunamis", is evident: one need not wait for the rare occurrence of a cataclysmic earthquake in order to study the various properties of tsunamis; milder, more frequent quakes would suffice. The likelihood of detecting secondary tsunamis, however, is not particularly promising. Not all earthquakes, even very large ones, generate tsunamis of any sort (Adams and Furumoto, 1970); and evidence indicates that when a tsunami is generated by an earthquake with magnitude less than 6.5 on the Richter scale, it will usually be quite small (Figure 4-1).

Theoretically, a tsunami can be considered to be caused by a suddenly occurring discontinuity on a small square of the earth's crust (Podyapolsky, 1970). In the water above it, the disturbance generates waves whose frequencies lie in a continuous band. These waves then propagate radially out of the region, dissipating and dispersing. An energy spectrum of a large tsunami indicates that there is a great deal of power encompassing many frequencies. The shape of the spectrum for a particular tsunami varies from location to location. The peaks usually

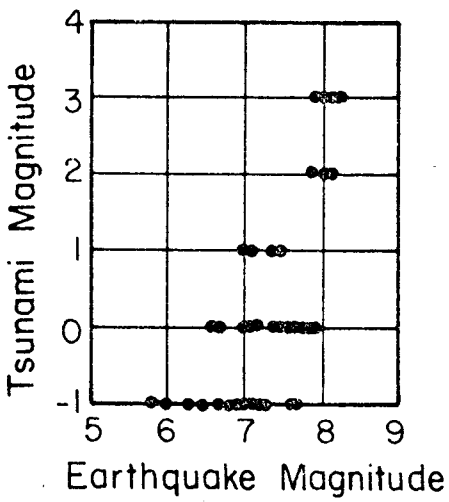

Figure 4-1. Earthquake magnitude on the Richter scale versus tsunami magnitude, defined as $\log_2 h$, where h is the maximum height of the tsunami, in meters, measured at a coast 10 to 300 km from the tsunami origin. (After Iida, 1963).

correspond to periods from around 5 minutes to about an hour (Miller, Munk, and Snodgrass, 1962). However, as Royer and Reid state, the periods of secondary tsunamis are unknown; the largest of the waves which they identified as secondary tsunamis had periods from around 55 to 100 minutes.

4.2 Earthquakes on 6 November 1973

During the time the wave gauge was operating, two significant earthquakes in the Pacific Ocean were reported (U.S. Department of the Interior, 1973) with epicenters near Adak in the middle of the Aleutians. The first, with body wave magnitude of 5.8 on the Richter scale, surface wave magnitude of 6.4, and depth of 34 km, occurred at 51.6°N, 175.4°W at 0936 UT 6 November 1973. The second, with body wave magnitude of 5.9, surface wave magnitude of 6.3, and depth of 41 km, occurred at 51.6°N, 175.2°W at 1826 UT the same day.

In order to estimate the approximate arrival time at Middleton Island of any waves generated by these earthquakes, we used the long wave phase speed

$$c_p = \sqrt{gd} \ ,$$

where d is the depth of the water and g is the acceleration due to gravity. According to Braddock (1970), a tsunami propagating along the Alaskan coastline will tend to follow the Aleutian Trench, rather than a great circle, giving it a faster travel time. Taking this into account, the expected tsunami path was broken into four sections, one section following the trench. The water depth d was assumed constant in each section.

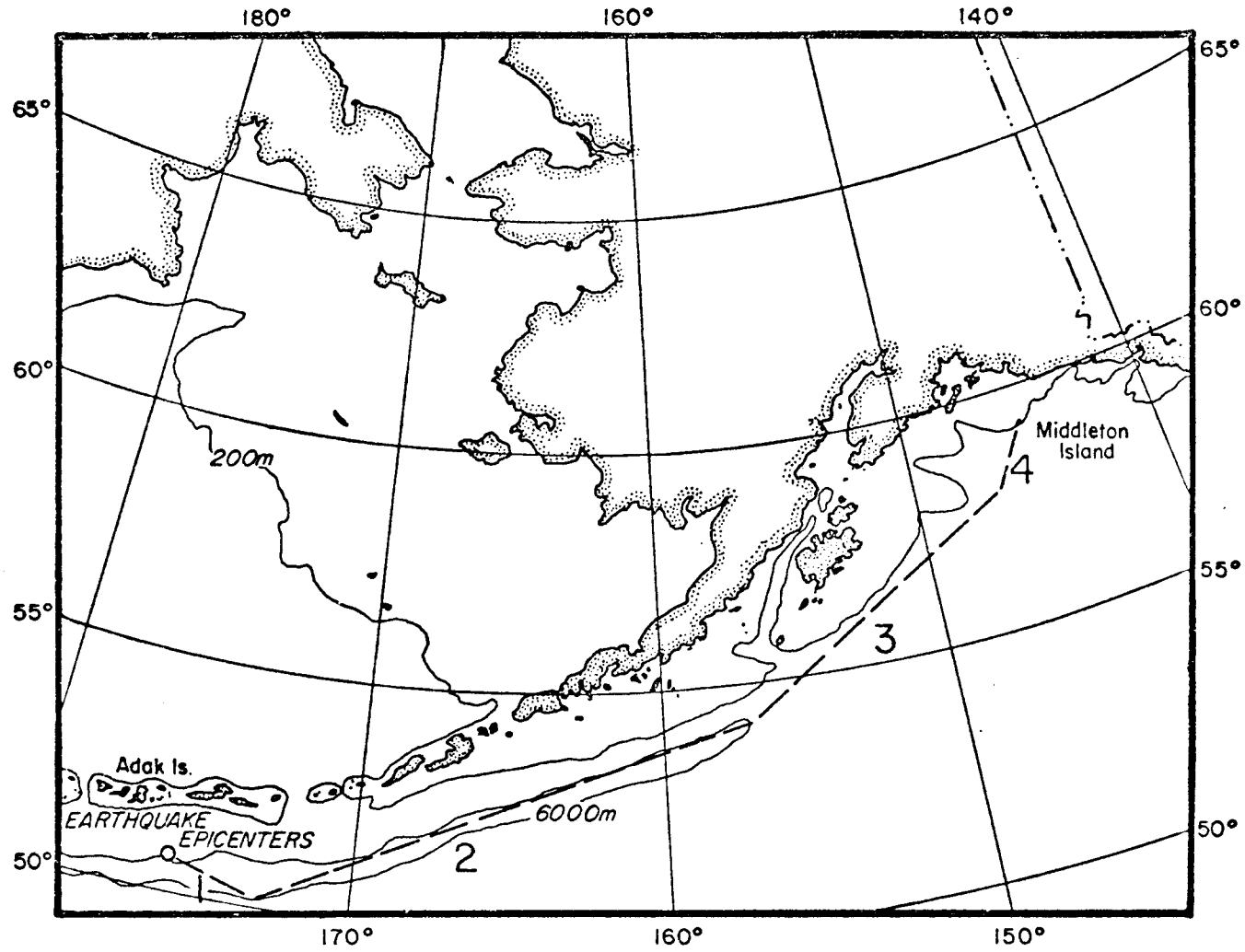

Figure 4-2. The assumed path to Middleton Island of a tsunami generated at 51.6°N, 175.3°W. Numbers refer to sections where water depth was assumed to be constant.

The assumed path is shown in Figure 4-2. The travel times for each section are as follows:

Section	Distance (km)	d (m)	Travel time (minutes)
1	250	2000	29.46
2	1250	7500	76.07
3	750	5000	55.90
4	200	500	47.14
Totals	2450		208.57

Thus, the minimum travel time was estimated to be 208.57 minutes, or 3.48 hours.

4.3 Evidence of Tsunamis in the Time Series

In order to determine if the earthquakes on 6 November had generated tsunamis which were large enough to be seen in the record, the data were averaged over 384 seconds, each average considered to be one point, and the points were plotted versus time. Averaged pressures for 6 November are shown in Figure 4-3. No well-defined disturbances can be discerned around the expected arrival times for tsunamis. The roughness around 1100 UT is probably due to the wind, which increased slightly during this time (other sections of the averaged data show similar roughness with increased wind).

To show that if tsunamis were large enough to be seen in the original record then one might reasonably expect to see some evidence of them in an averaged record, data from Wake Island following the earth-

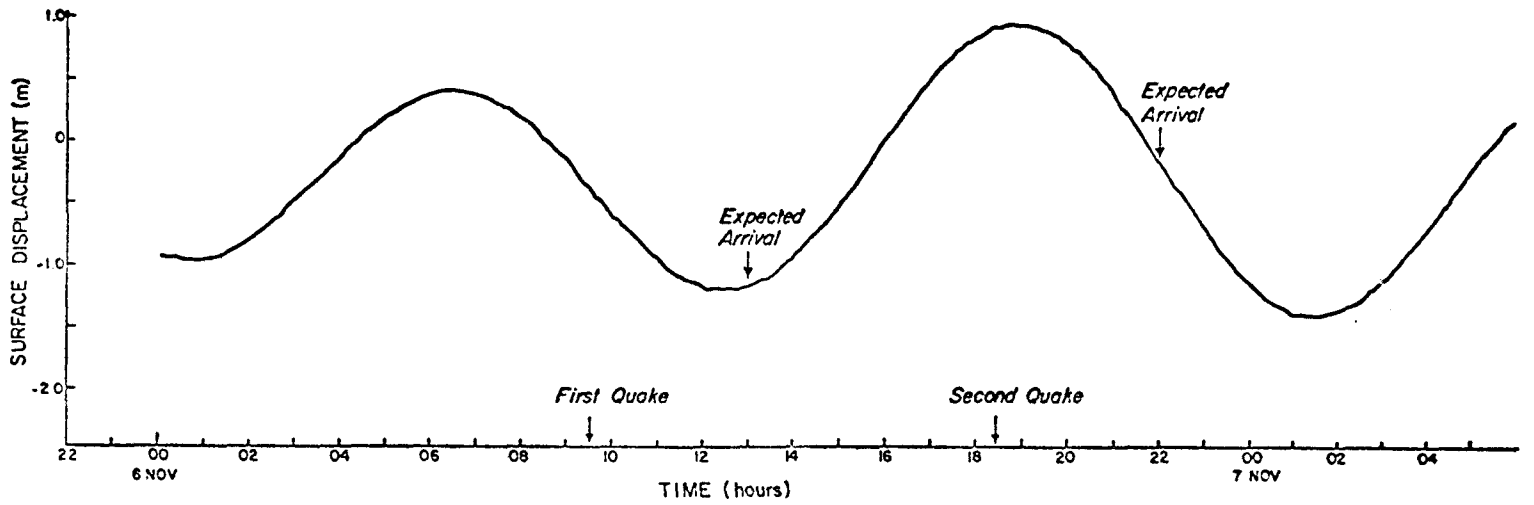

Figure 4-3. Pressure data from Middleton Island averaged over 384 seconds (96 points). For graphing purposes, pressure has been converted to surface displacement using the relation given in Section 2.2.

quake on 7 March 1957 were averaged over 600 seconds and each average considered to be one point. The results are shown in Figure 4-4. The numbers on the vertical axis are scale divisions, 1.81 divisions per centimeter. The record begins around 8 hours before the arrival of the first trough of the tsunami and continues for about 4.5 days. Despite the fact that the data were averaged over a larger interval, tsunamigenic waves are quite evident, dominating even the tide.

4.4 Evidence of Tsunamis in the Spectrum

As mentioned in Section 4.1, typical or characteristic periods for secondary tsunamis are not known. However, it seemed reasonable to suppose that the range would be approximately the same as that for larger tsunamis, namely, from about 5 minutes to about an hour (Miller, Munk, and Snodgrass, 1962). The earthquakes on 6 November occurred about 9 hours apart; thus, the longest time series which could be used to compare spectra following each quake would be on the order of 9 hours duration.

Figure 4-5 shows the spectrum for 25.6 hours (1536 filtered data points, Δ = 60 seconds) beginning at 0000 UT 6 November 1973. It is fairly flat, with no large peaks. Figure 4-6 shows spectra for 8.5 hours of data (512 data points) beginning (a) 3 hours after the first quake (solid line); (b) 3 hours after the second quake (dashed line); (c) about 13 hours before the first quake (dotted line), as a baseline comparison. The data were first lowpass filtered with LPFILTER, then sampled every minute (Section 3.7). The Fourier coefficients were averaged in groups of 10, to give 20 degrees of freedom. In Figure 4-6,

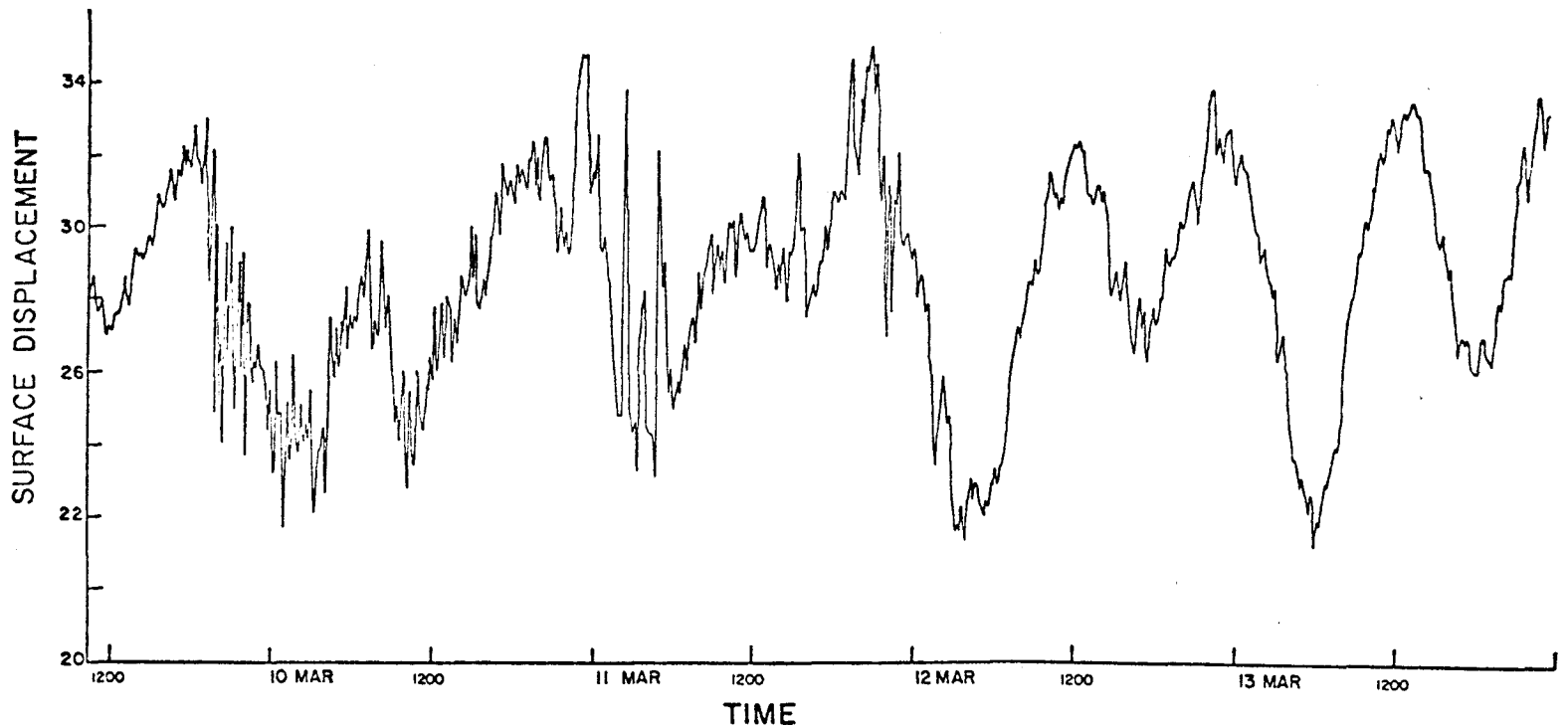

Figure 4-4. Surface displacement data from Wake Island beginning 9 March 1957, and averaging over 600 seconds (20 points). The vertical axis is given in scale divisions, 1.81 divisions per centimeter.

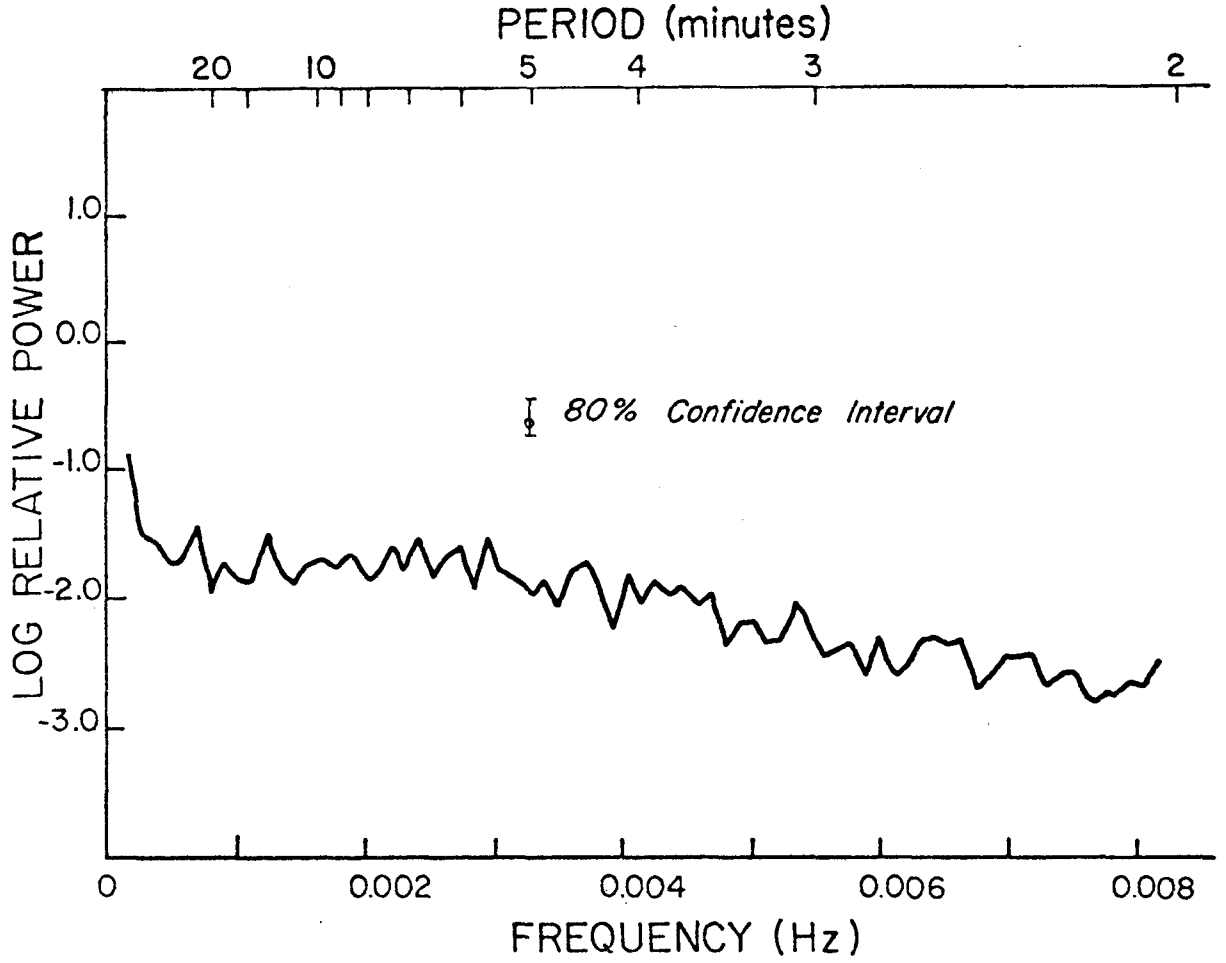

Figure 4-5. Spectrum for 25.6 hours (1536 points, Δ = 60 seconds) beginning at C000 UT 6 November 1973. The data have been filtered with LPFILTER and sampled every minute; the Fourier coefficients were averaged in groups of 10.

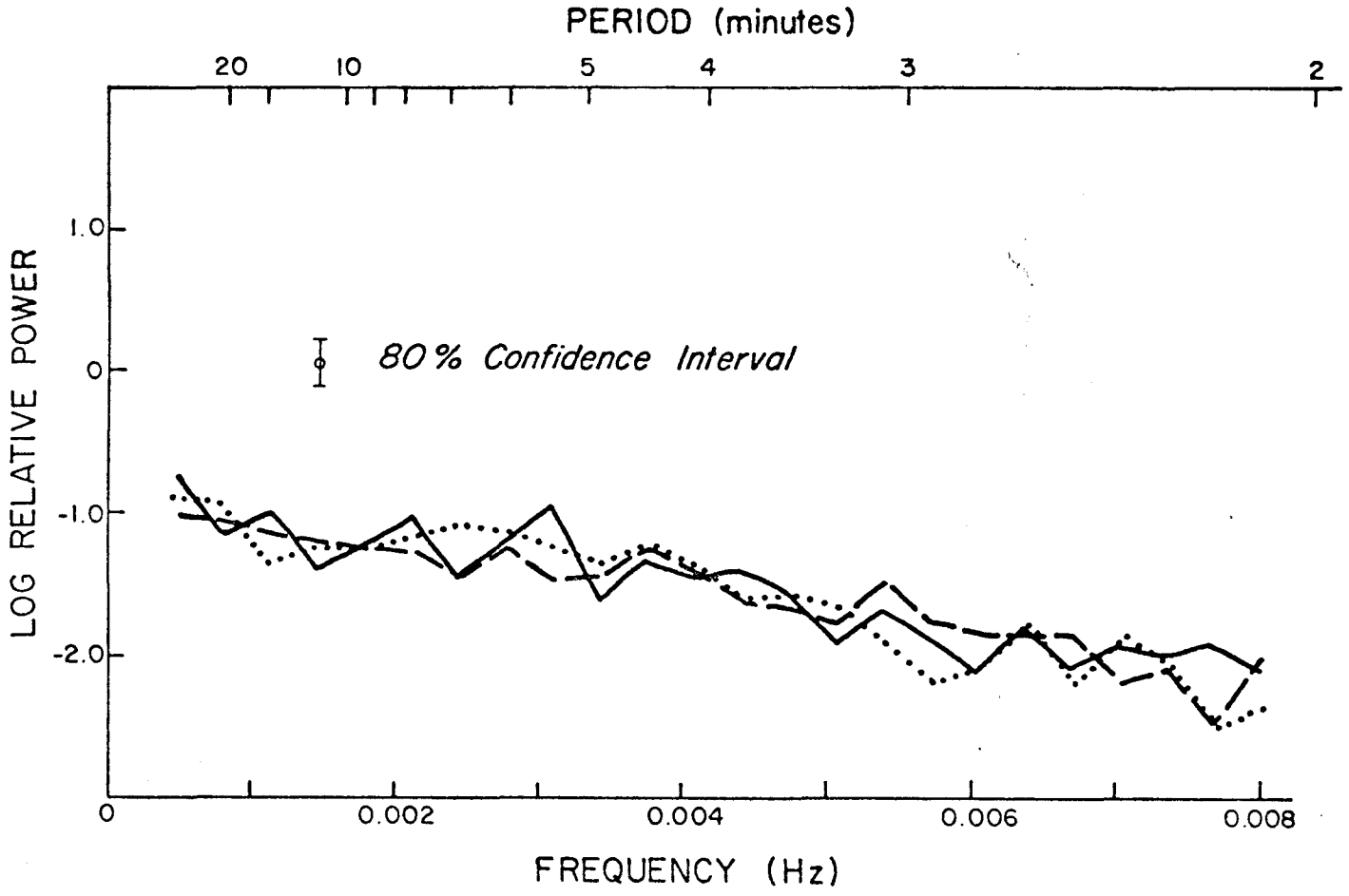

Figure 4-6. Spectra for 8.5 hours of data (512 points) beginning at 1235 UT 6 November 1973, 3 hours after the first quake (solid line); 2117 UT 6 November, 3 hours after the second quake (dashed line); 2059 UT 5 November, as a comparison (dotted line). The data were filtered with LPFILTER and sampled every minute; Fourier coefficients were averaged in groups of 10.

detectable peaks could occur between the second and the next-to-last points, that is, between 8.138×10^{-4} Hz and 7.6×10^{-3} Hz. Averaging the Fourier coefficients compresses the frequency scale. Therefore, in order to look for peaks at lower frequencies, the first 24 unaveraged Fourier coefficients for the same data were plotted in Figure 4-7. In this figure, the log of the relative power has been averaged with a three-point moving average to smooth the curves. Now detectable peaks could occur between 1.3×10^{-4} Hz and 8.138×10^{-4} Hz.

There are several noticeable maxima in the spectra for the time series following the earthquakes, particularly after the first quake. For instance, there is a 3 db peak at 4.56×10^{-4} Hz in Figure 4-7 (solid line), and a 6.5 db peak at 3.09×10^{-3} Hz in Figure 4-6 (solid line). The second peak at 3.09×10^{-3} Hz appears off and on throughout the record, and does not seem to be uniquely associated with any given section of data. The fact that the first earthquake was somewhat shallower than the second one favors the interpretation of the first peak as a possible secondary tsunami since, given two quakes of equal magnitude, the shallower one is slightly more likely to be tsunamigenic (Iida, 1970).

On the other hand, the method used in Figure 4-7 was applied to test data consisting of a 2 m sinusoidal tide, T = 12 hours; plus a 0.1 m exponentially decaying tsunami, T = 30 minutes, with a decay time of 12 hours (Miller, Munk, and Snodgrass, 1962). The spectrum showed a 22 db peak for the tsunami. Moreover, considering that there is no immediately recognizable evidence of a tsunami in either the filtered or unfiltered wave record, it must be stated that the possibility for generation of tsunamis by the first earthquake of 6 November is somewhat questionable.

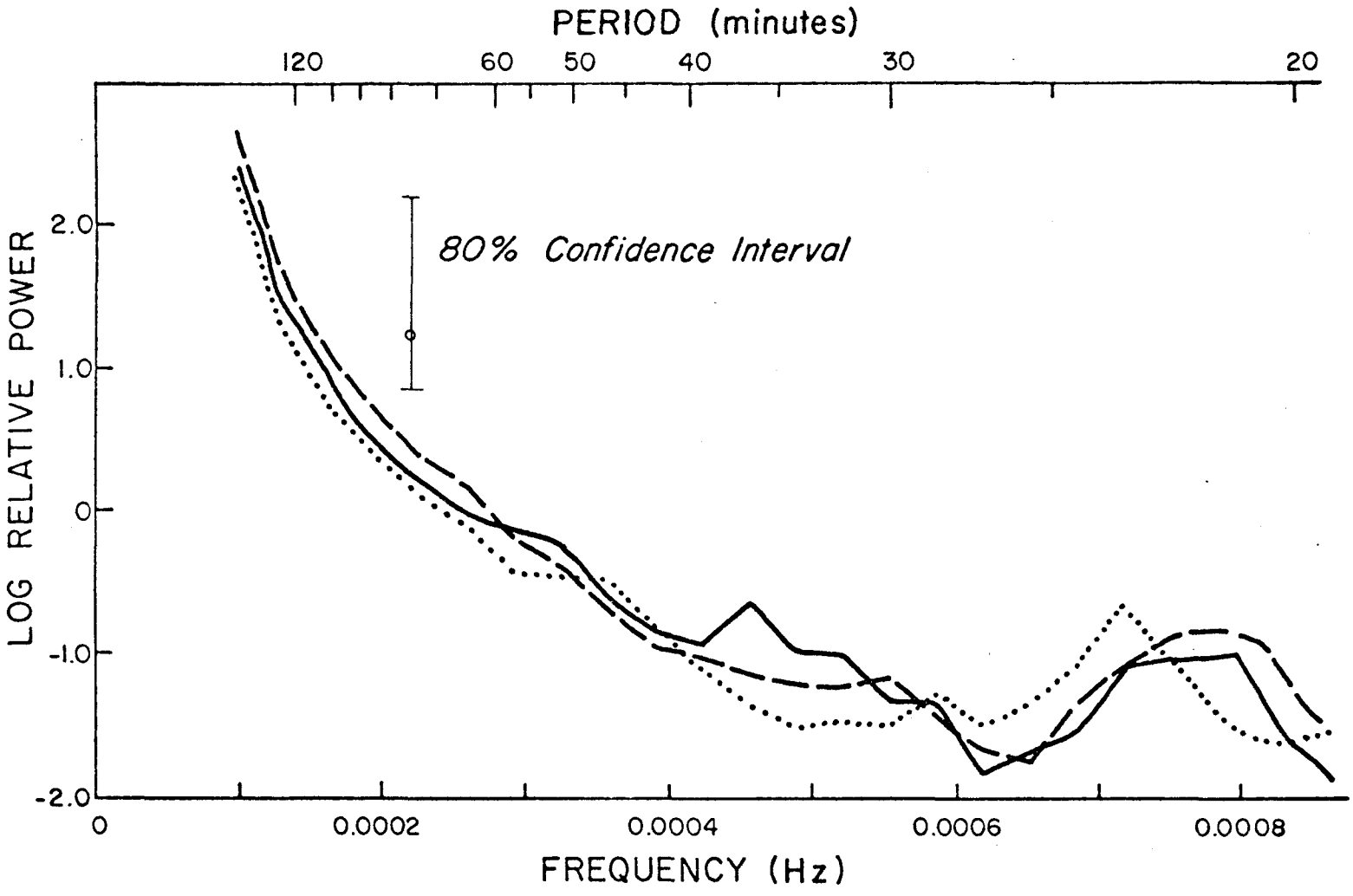

Figure 4-7. The first 24 unaveraged Fourier coefficients for the same data shown in Figure 4-5. The log of the coefficients has been averaged with a three-point moving average for smoothing.

CHAPTER 5

WAVES WITH PERIODS UNDER FIVE MINUTES

5.1 Some Typical Spectra from the Record

Spectra of 25.6 hour sections (1536 filtered points, Δ = 60 seconds) of the record are typically quite flat. The spectrum from 6 November (Figure 4-5), for instance, exhibits a smooth, almost linear decrease in log relative power from around -1.5 at 2.5×10^{-4} Hz to around -2.75 at 0.008 Hz. The spectrum for the first day, 30 October (Figure 5-1), has a nearly identical shape and slope, although it contains more total energy than does the spectrum from 6 November. This is due to a storm in the area, discussed below in Section 5.3. The decrease in energy in both spectra above 0.003 Hz may be attributed to the lowpass filter, which has a cutoff frequency of 4.16×10^{-3} Hz.

The spectrum from a 68 minute section of unfiltered data (1024 points, Δ = 4 seconds) from 6 November (Figure 5-2) is fairly flat, with a slight peak around 0.065 Hz. It is typical of 68 minute spectra for the entire record, with the exception of those from the first two days.

5.2 A Series of 68 Minute Spectra

Beginning at the first of the record, spectra of the unfiltered data (Δ = 4 seconds) were taken over successive sections of 1024 points (68 minutes 16 seconds). Forty-nine spectra were taken in all, covering about 56 hours of data from the beginning of the record at 0241 UT 30 October to 1021 UT 1 November 1973. The Fourier coefficients for each spectrum were averaged in groups of 5 to give 10 degrees of freedom.

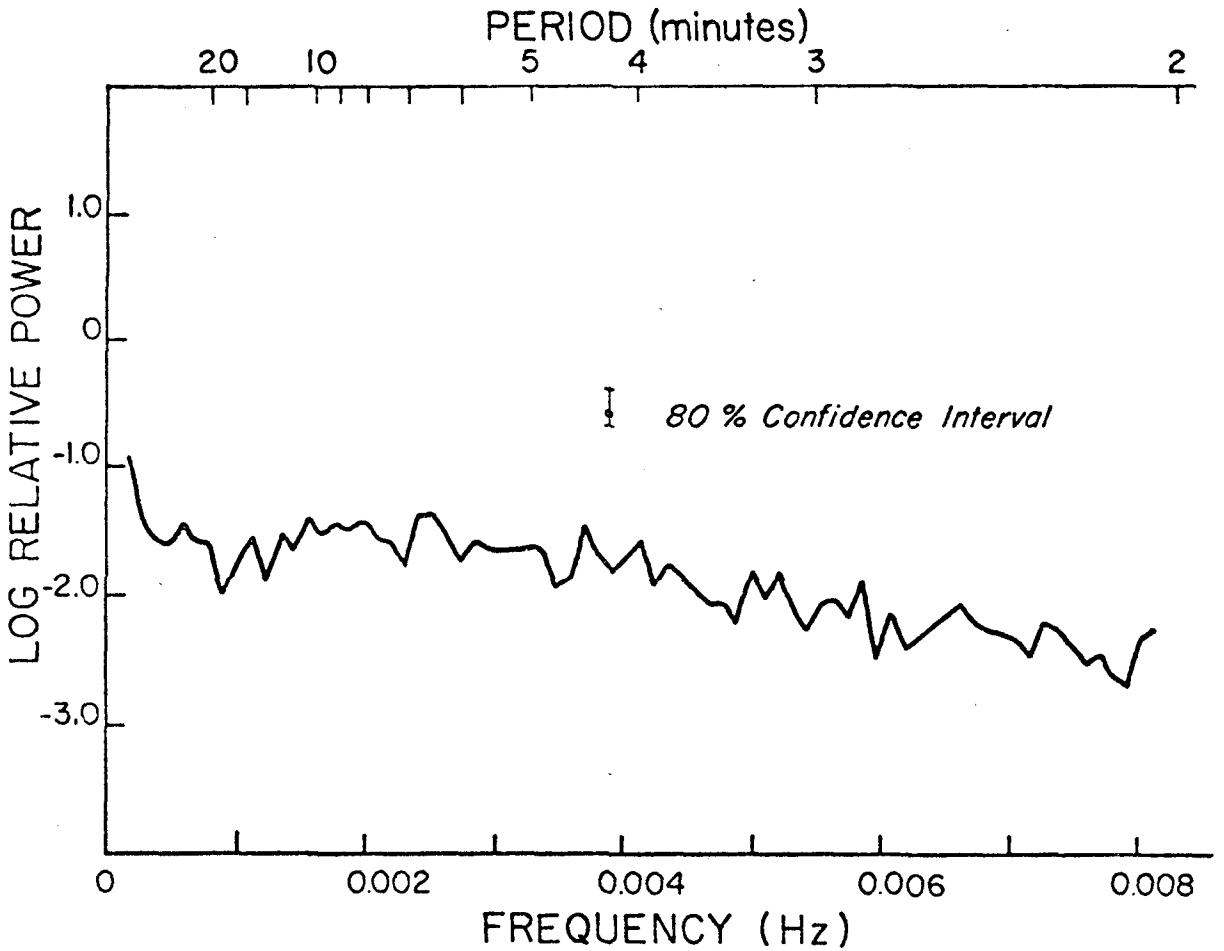

Figure 5-1. Spectrum of the initial 25.6 hours of the record, beginning at 0241 UT 30 October 1973. The data have been filtered with LPFILTER and sampled every minute. The Fourier coefficients have been averaged in groups of 10.

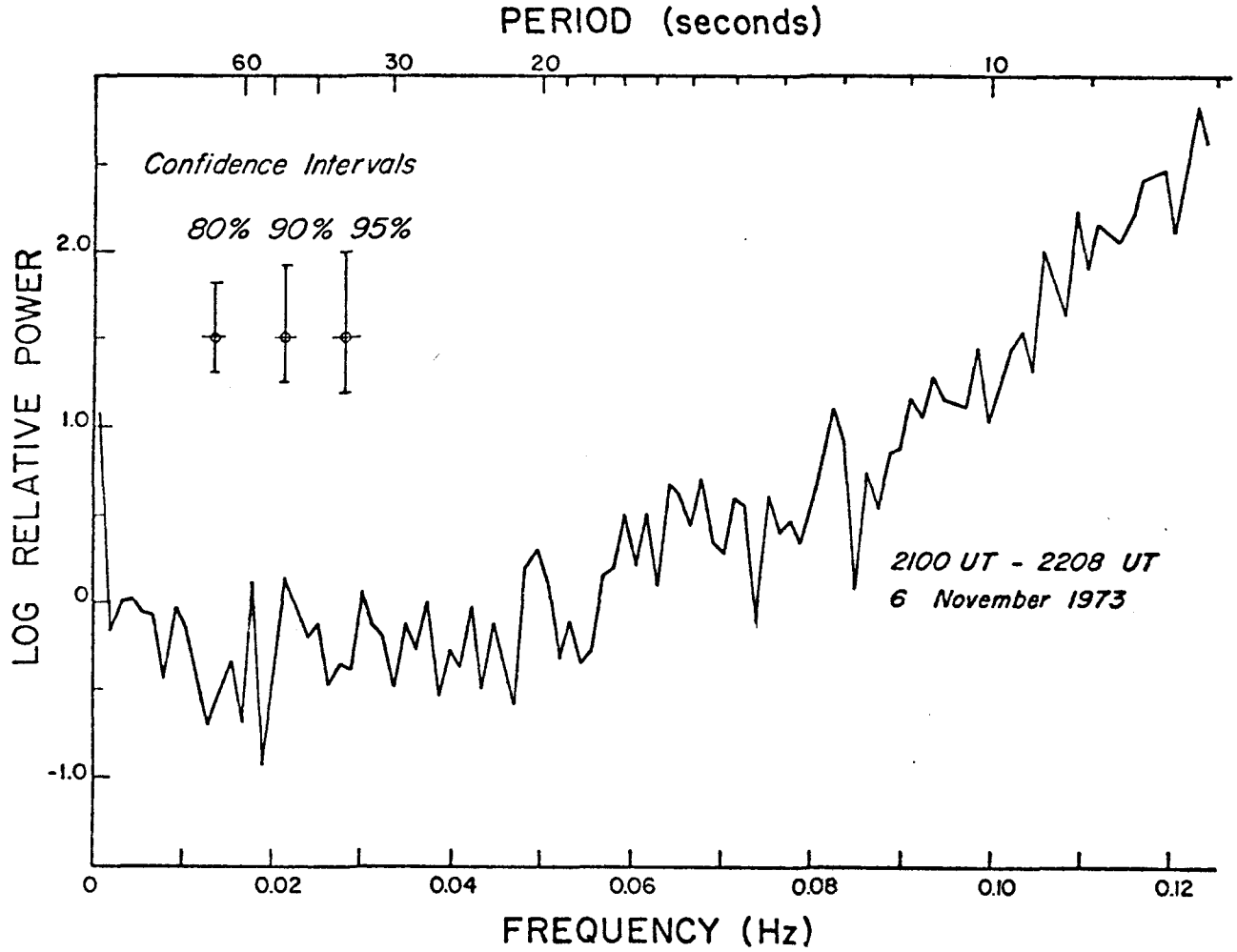

Figure 5-2. Spectrum of 1024 unfiltered data points (68 minutes 16 seconds) beginning at 2100 UT 6 November 1973. The Fourier coefficients have been averaged in groups of 5, and the resulting spectra divided by $[1/\cosh(4\pi^2 d/gT^2)]^2$, with d = 69.5 m.

Figures 5-3 through 5-15 show every fourth spectrum of this series.

The most striking feature of these spectra is the peak which starts out about 20 db above the baseline around 0.0625 Hz, and slowly shifts toward higher frequencies, decreasing in amplitude as it shifts, until by 1032 UT 31 October (Figure 5-10), the peak has fallen to 10 db above the baseline and is centered around 0.087 Hz. Between 0600 and 1000 UT 31 October there is a marked decrease in power around 0.085 Hz (Figures 5-9 and 5-10), and another decrease around the same frequency between 0444 and 0900 UT 1 November (Figures 5-14 and 5-15). Around 0200 UT 31 October there is a marked decrease in total power, and another peak around 0.06 Hz becomes evident (Figure 5-8). This peak shifts back and forth slightly in successive spectra, but it is present even in the last one, Figure 5-15.

Figure 5-16 shows the spectra in Figures 5-1, 5-9, and 5-15 as solid, dashed, and dotted lines, respectively. The shift and decay of the spectral peaks is evident. In the next section we examine some possible causes for these observed changes in the spectra.

5.3 Influence of a Storm in the Gulf of Alaska

On 27 October 1973, a storm in the northwest Pacific around 3600 km from Middleton Island, centered at 45°N, 164°E and having winds up to 30 m/second (60 knots), began moving eastward. Figure 5-17 shows the path of the storm. By 1200 UT 28 October it was at 48°N, 162°W, and the winds had decreased to about 20 m/second (40 knots). By 0000 UT 29 October it had moved into the Gulf of Alaska (Figure 5-18); 20 m/second winds were still being reported. At about 0600 UT 30 October the storm

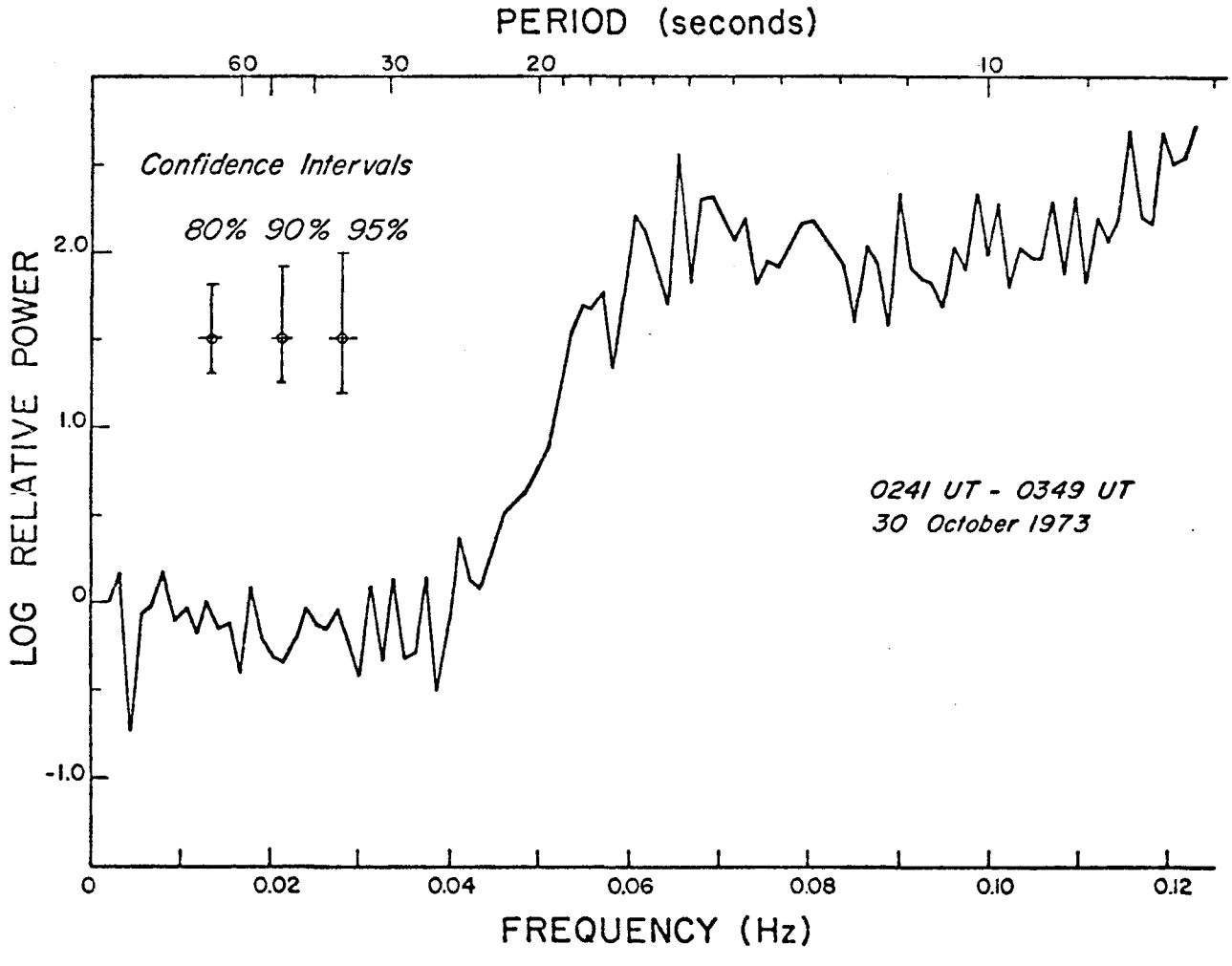

Figure 5-3. Spectrum of 1024 unfiltered data points (68 minutes 16 seconds) beginning at 0241 UT 30 October 1973. The Fourier coefficients have been averaged in groups of 5, and the resulting spectra divided by $[1/\cosh(4\pi^2 d/gT^2)]^2$, with d = 69.5 m.

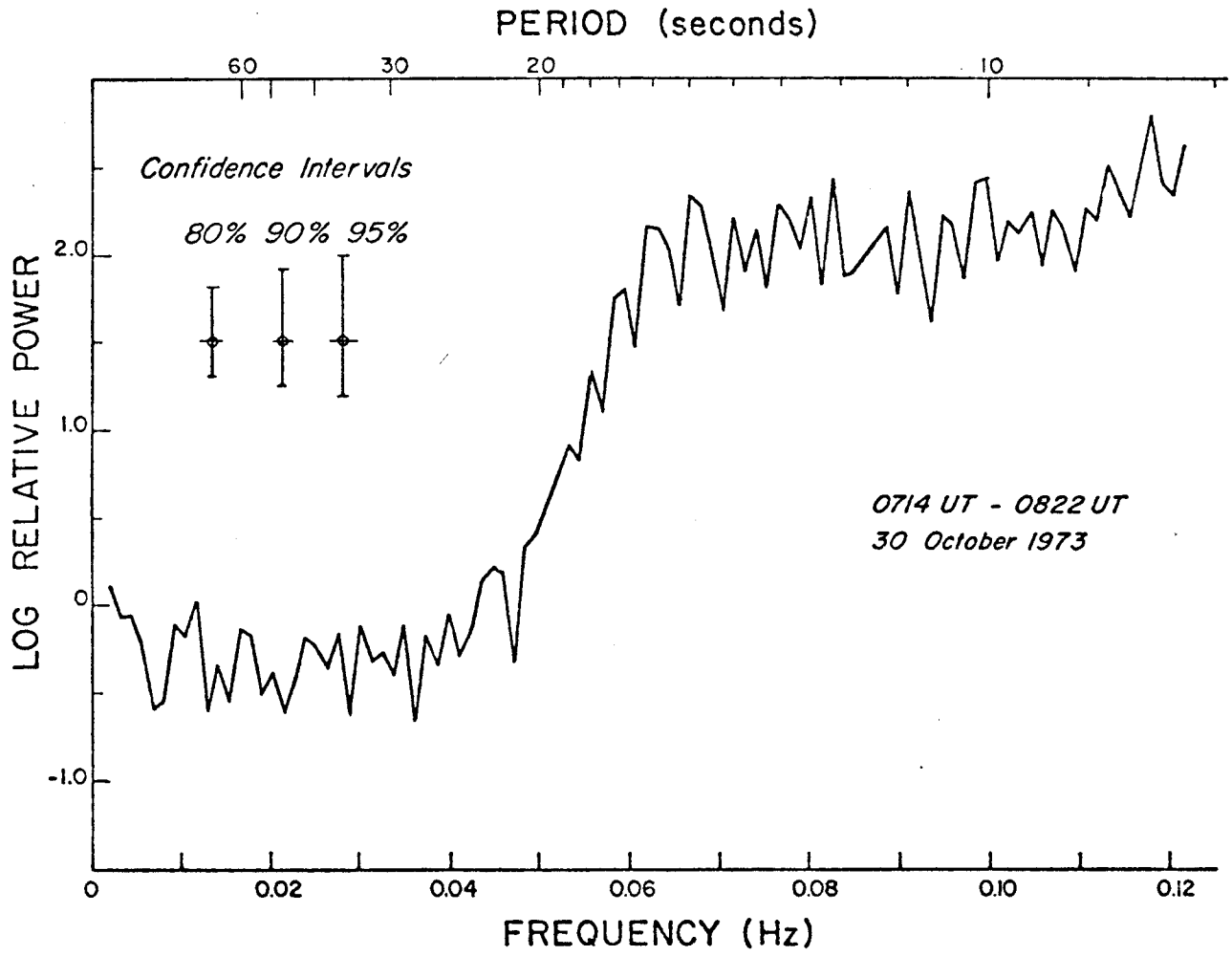

Figure 5-4. Spectrum of 1024 unfiltered data points (68 minutes 16 seconds) beginning at 0714 UT 30 October 1973.

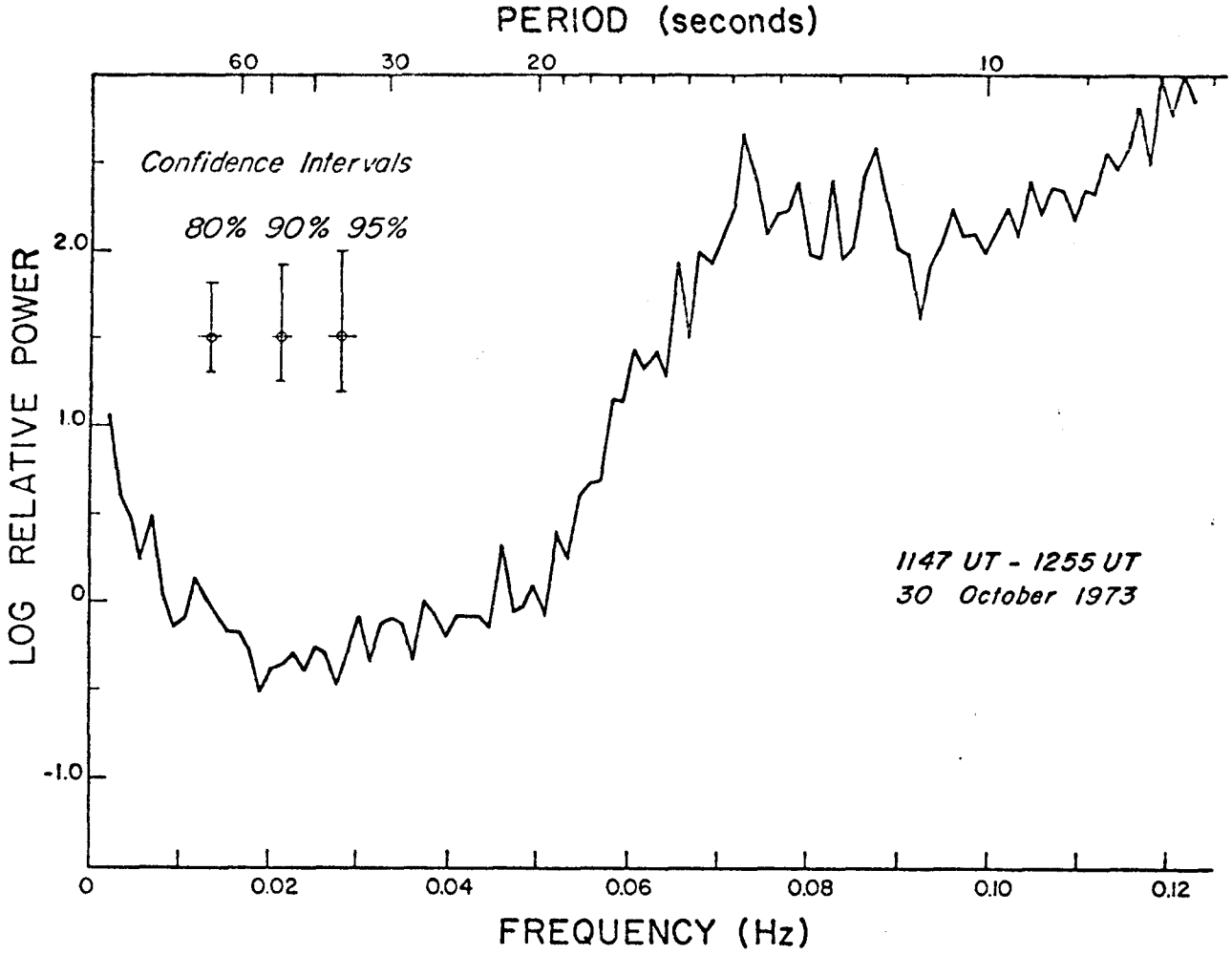

Figure 5-5. Spectrum of 1024 unfiltered data points (68 minutes 16 seconds) beginning at 1147 UT 30 October 1973.

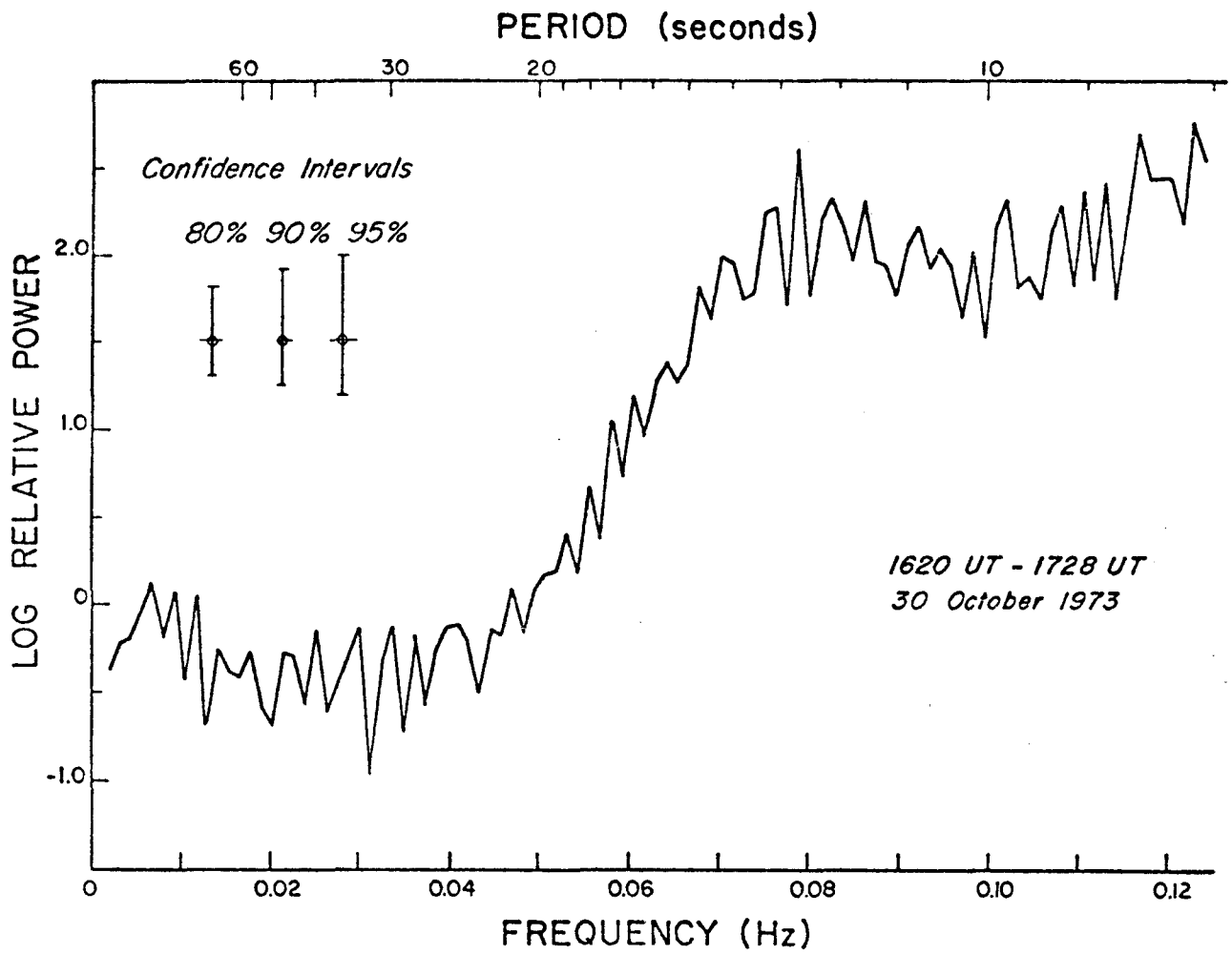

Figure 5-6. Spectrum of 1024 unfiltered data points (68 minutes 16 seconds) beginning at 1620 UT 30 October 1973.

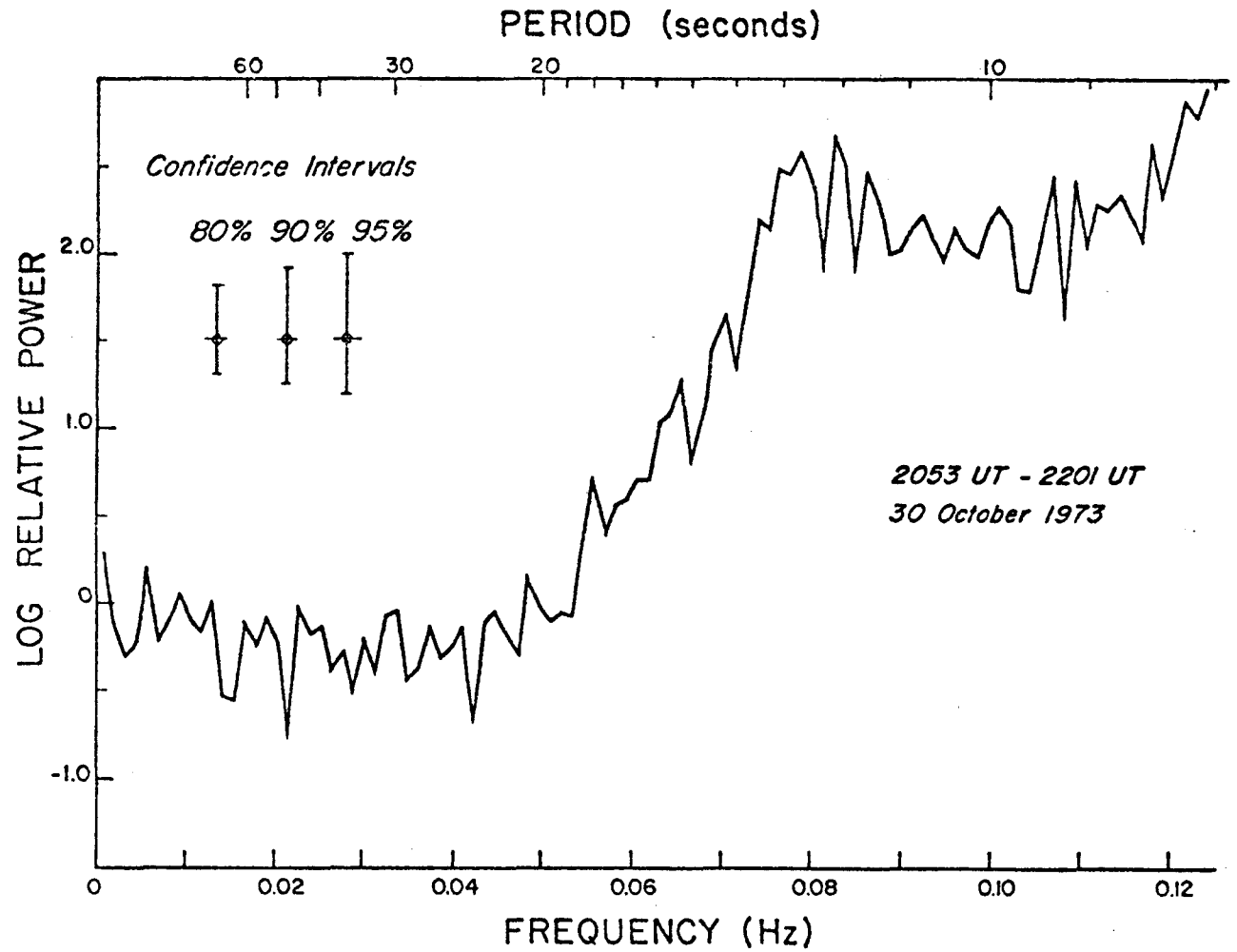

Figure 5-7. Spectrum of 1024 unfiltered data points (68 minutes 16 seconds) beginning at 2053 UT 30 October 1973.

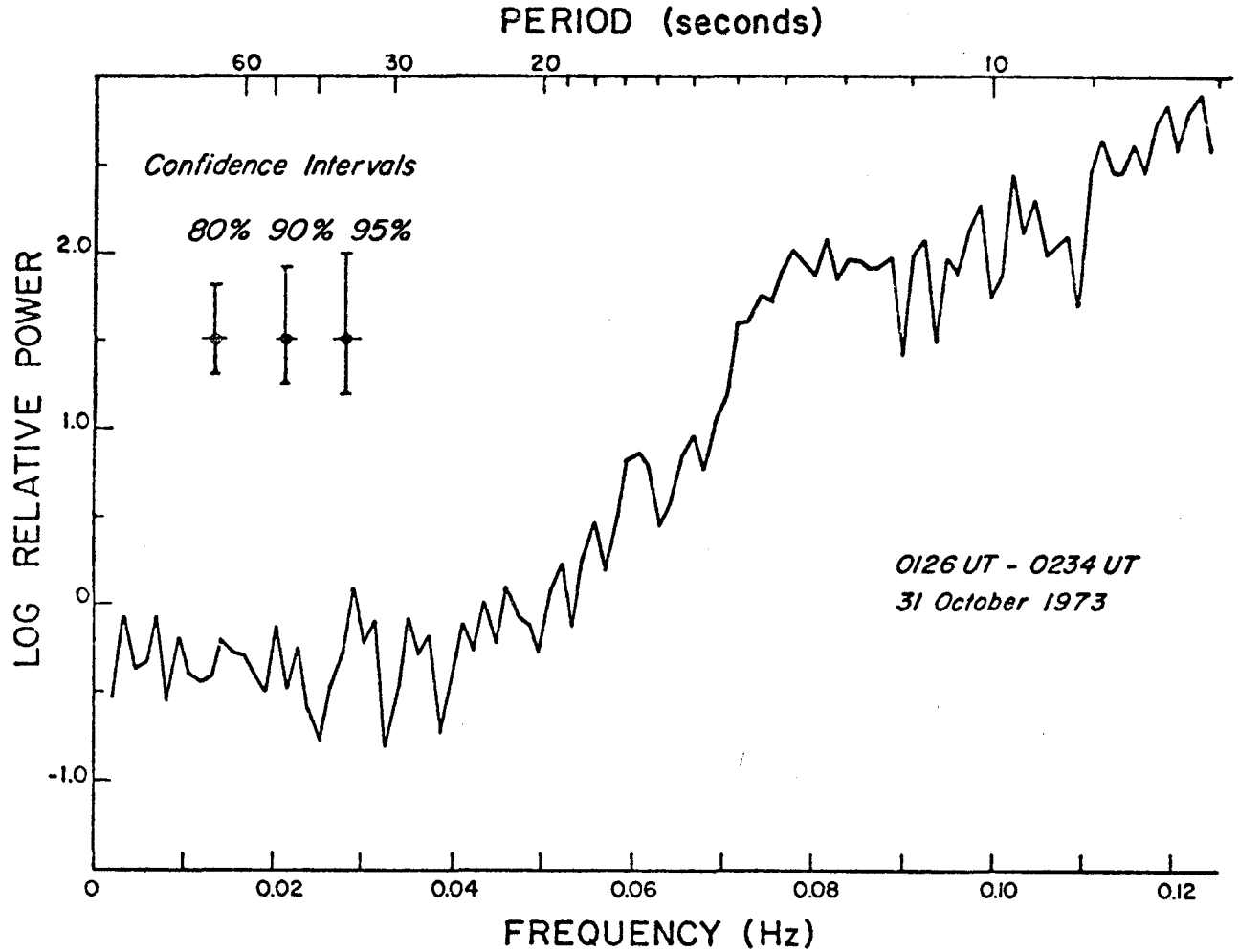

Figure 5-8. Spectrum of 1024 unfiltered data points (68 minutes 16 seconds) beginning at 0126 UT 31 October 1973.

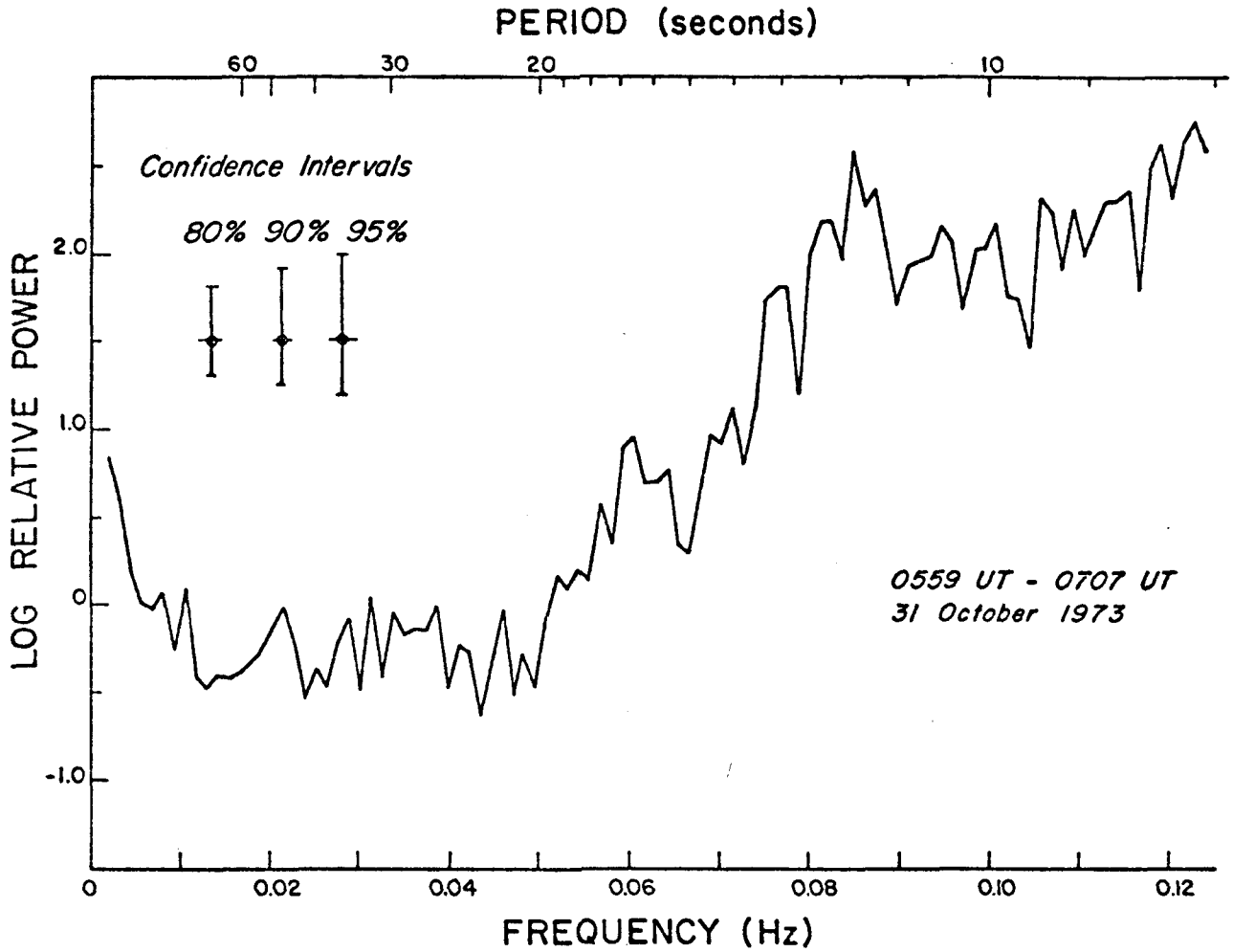

Figure 5-9. Spectrum of 1024 unfiltered data points (68 minutes 16 seconds) beginning at 0559 UT 31 October 1973.

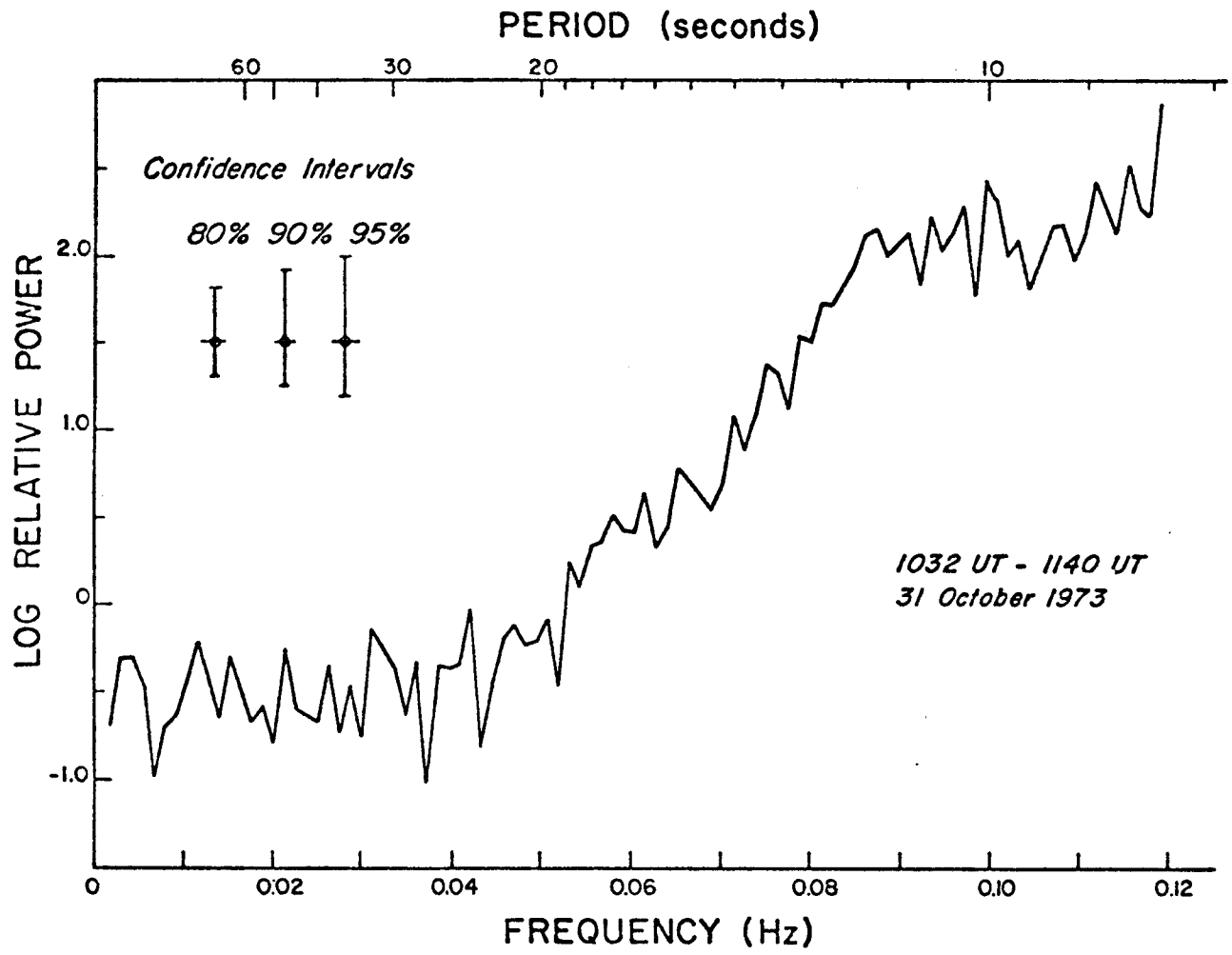

Figure 5-10. Spectrum of 1024 unfiltered data points (68 minutes 16 seconds) beginning at 1032 UT 31 October 1973.

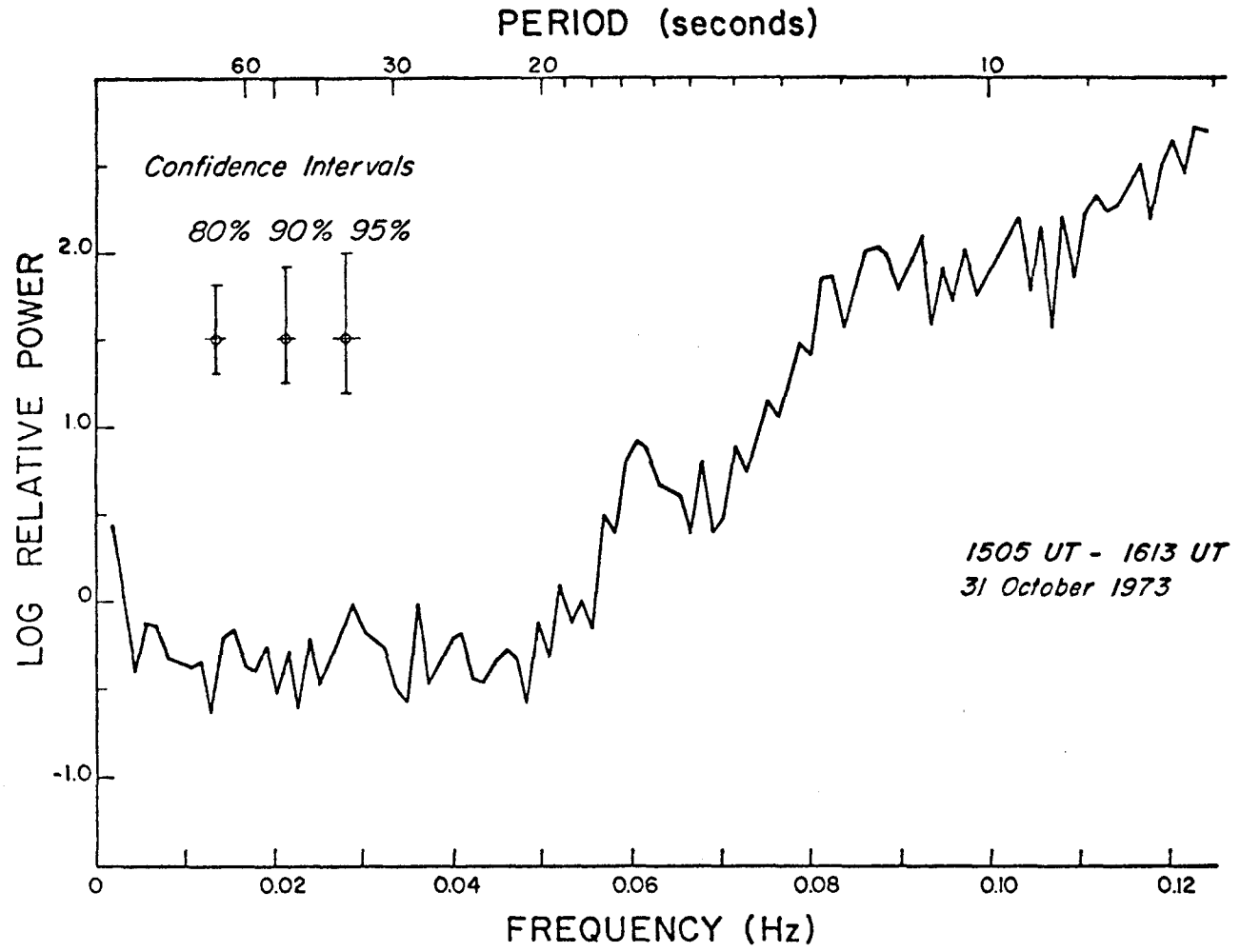

Figure 5-11. Spectrum of 1024 unfiltered data points (68 minutes 16 seconds) beginning at 1505 UT 31 October 1973.

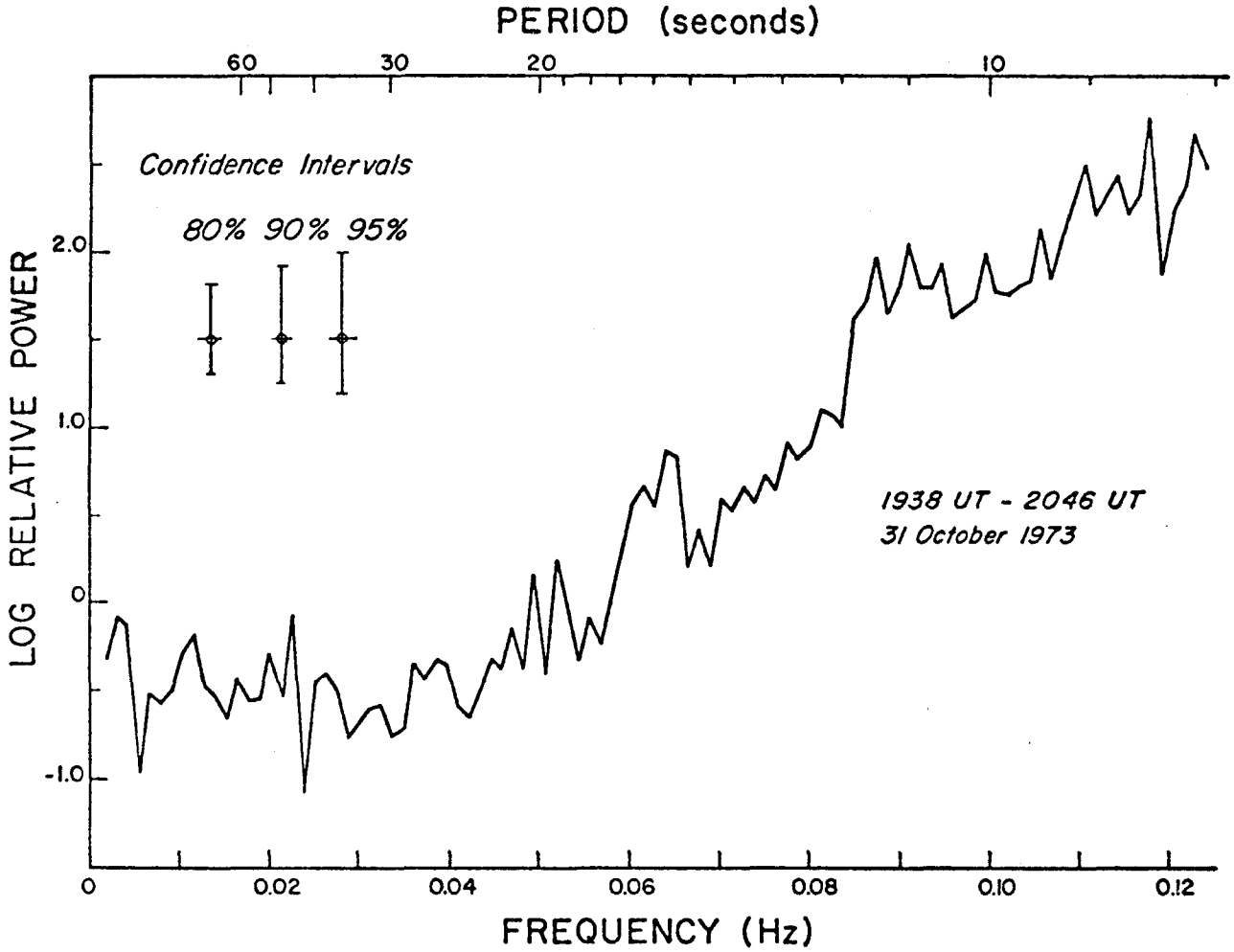

Figure 5-12. Spectrum of 1024 unfiltered data points (68 minutes 16 seconds) beginning at 1938 UT 31 October 1973.

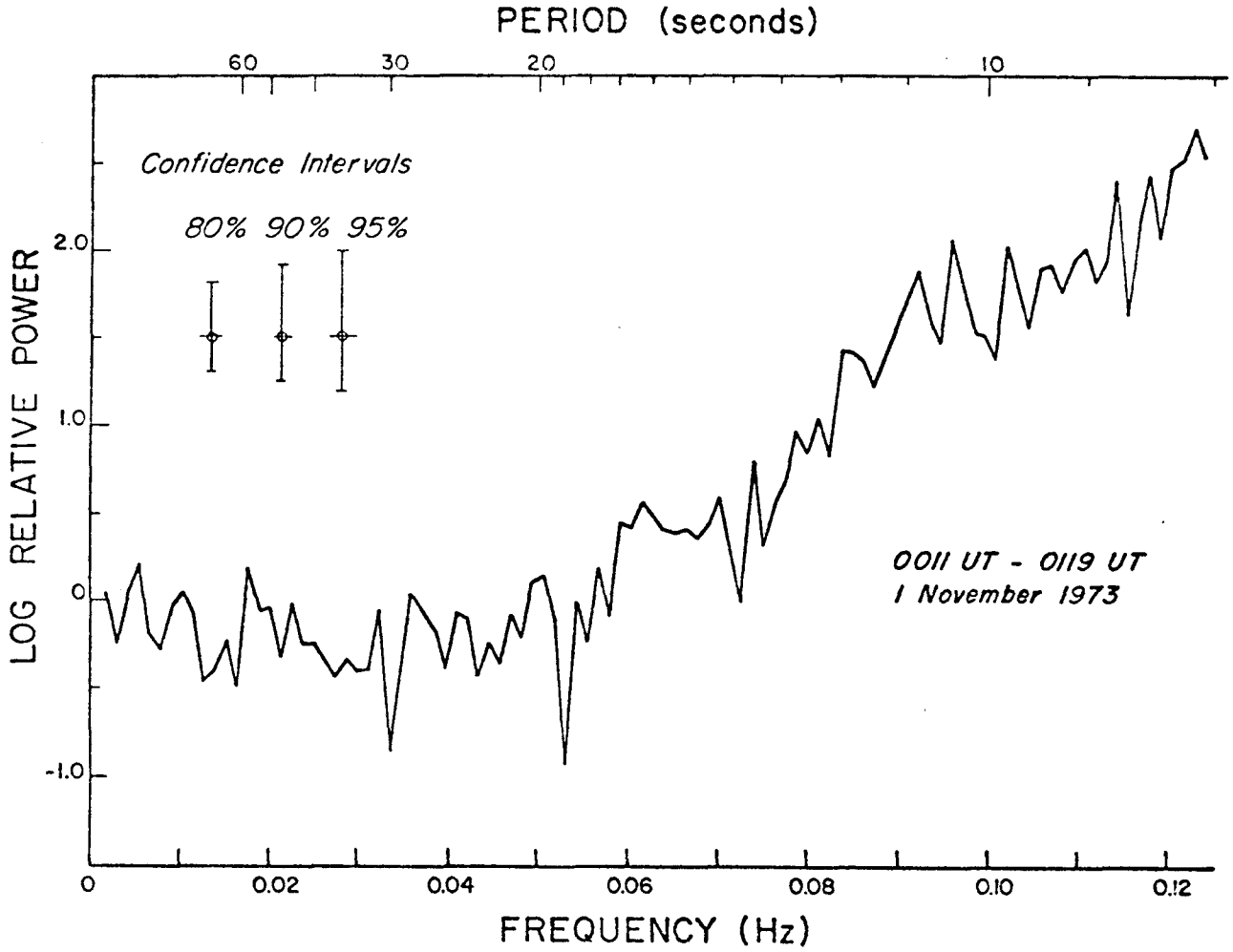

Figure 5-13. Spectrum of 1024 unfiltered data points (68 minutes 16 seconds) beginning at 0011 UT 1 November 1973.

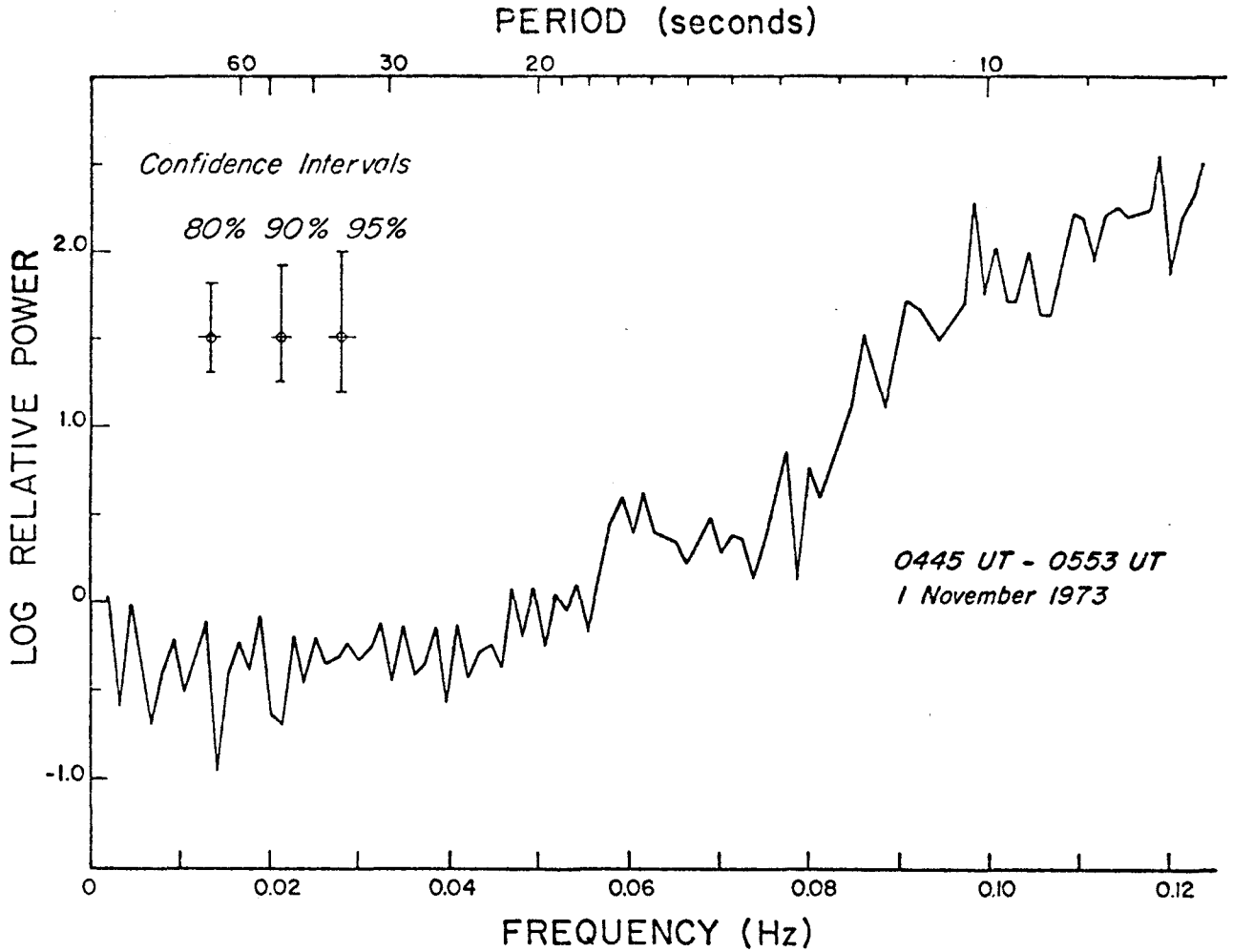

Figure 5-14. Spectrum of 1024 unfiltered data points (68 minutes 16 seconds) beginning at 0445 UT 1 November 1973.

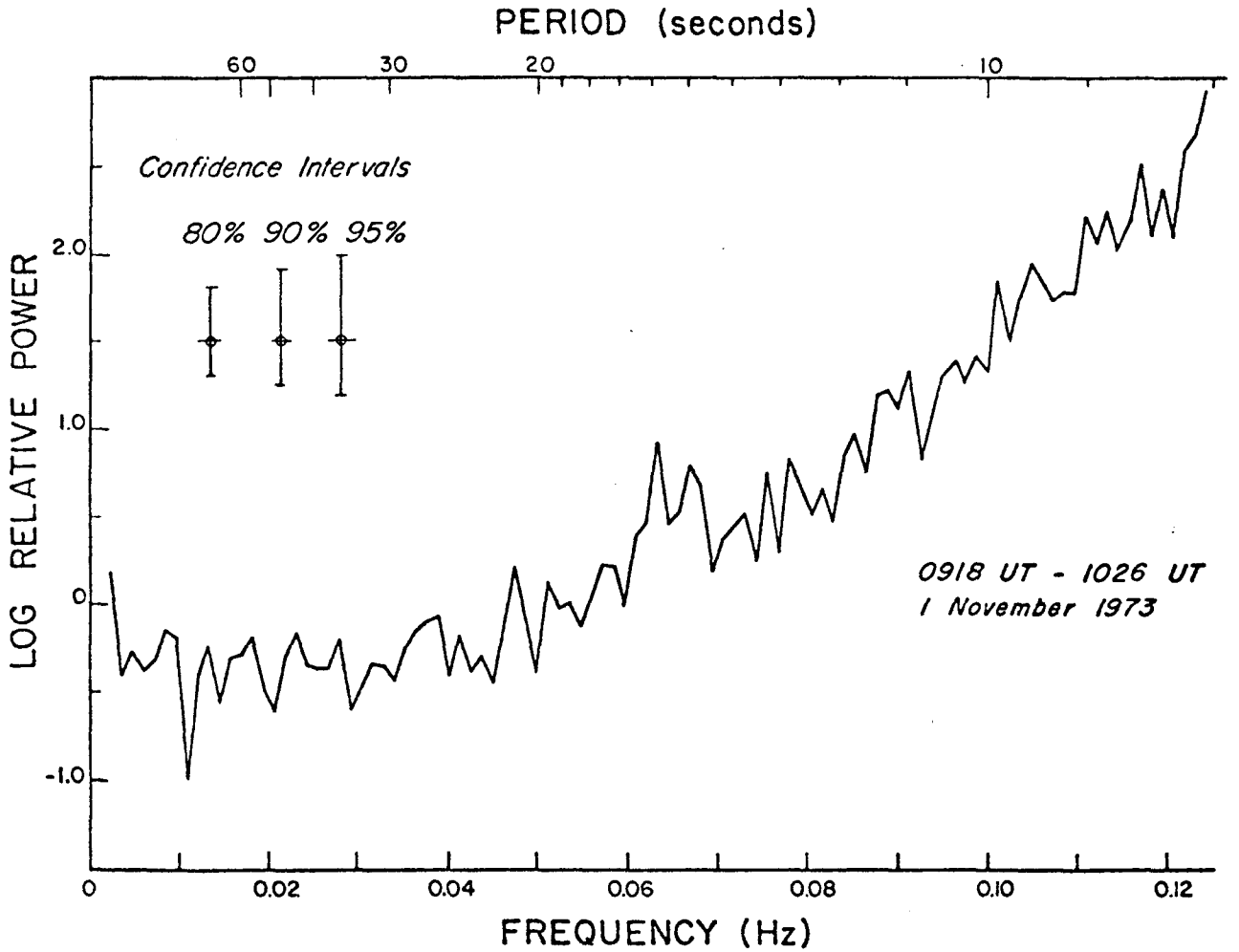

Figure 5-15. Spectrum of 1024 unfiltered data points (68 minutes 16 seconds) beginning at 0918 UT 1 November 1973.

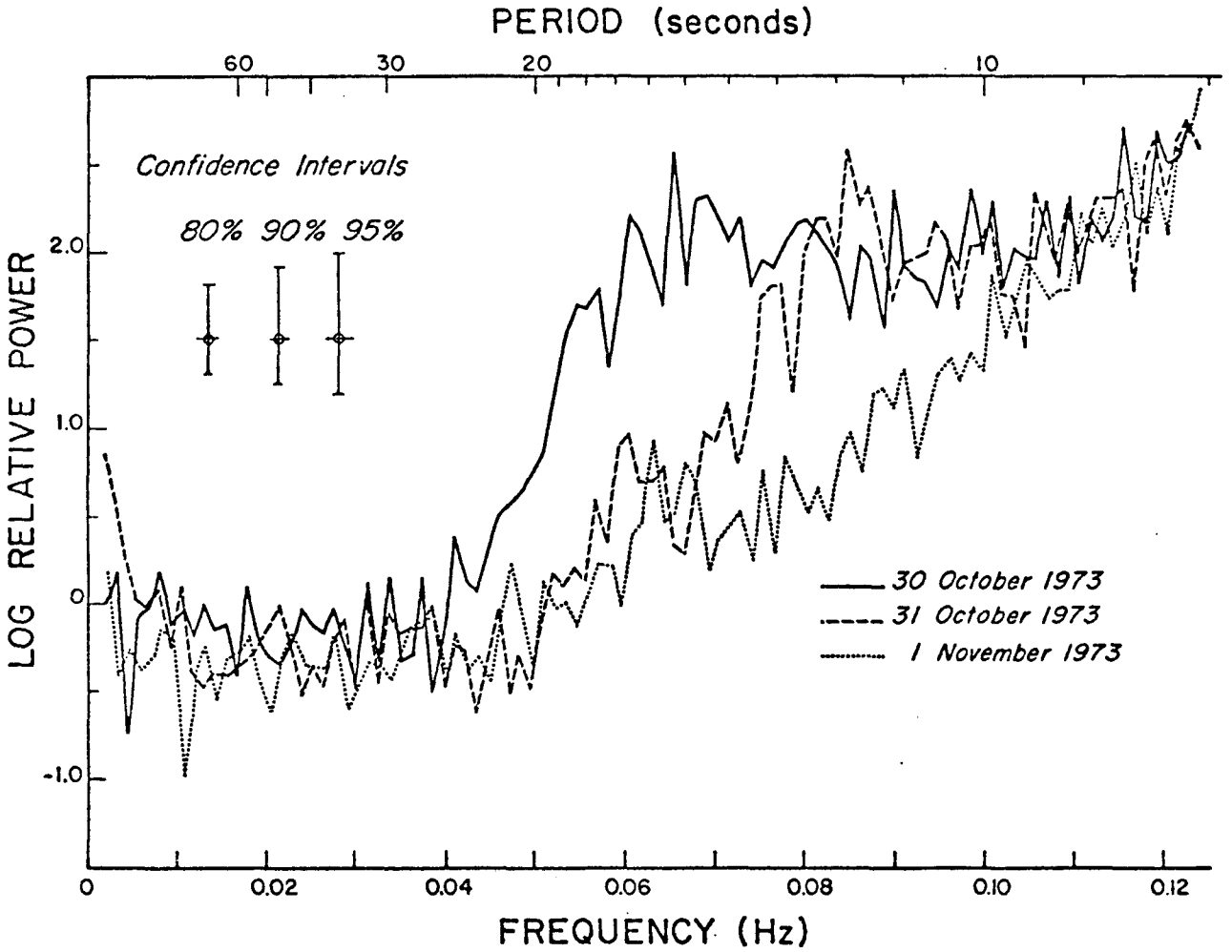

Figure 5-16. Comparison of the spectra in Figure 5-3 (solid line), in 5-9 (dashed line), and in 5-15 (dotted line).

began to diminish, although 20 m/second winds were still being reported near the Canadian Coast. At 0300 UT 31 October the winds had fallen below 5 m/second, and on 1 November a high pressure system moved in over the gulf.

The changes in the spectra reported in Section 5.2 are closely correlated with this storm. These changes are summarized by plotting frequency of the peak and log power of the peak versus time (Figure 5-19). The points in Figure 5-19 represent the successive spectra shown in Figures 5-3 to 5-15; thus, each point is 4 hours, 33 minutes, 4 seconds apart.

Figure 5-20 shows distances from Middleton Island of the low-pressure disturbance versus time. Direction is not indicated, since the data were taken with only one sensor. The lines in Figure 5-20 show possible time and distance from Middleton Island for the source of waves associated with peaks in the spectra. These lines are computed using the relation for the group velocity of deep water waves

$$c_g = \frac{1}{2}\left(\frac{g}{2\pi f}\right) \tag{1}$$

(Kinsman, 1965, p. 153) and the relation

$$D = c_g \tau \tag{2}$$

where D is distance and τ is elapsed time. For instance, waves with a frequency of 0.0726 Hz (the frequency of the spectral peak at 1147 UT 30 October) travel with a group velocity of 10.7 m/second. Thus, when τ = 2 hours, D = 77 km; when τ = 4 hours, D = 154 km, etc. It may be seen from Figure 5-20 that there is rough agreement between the path of the storm and the generating lines for the observed peaks in the spectra.

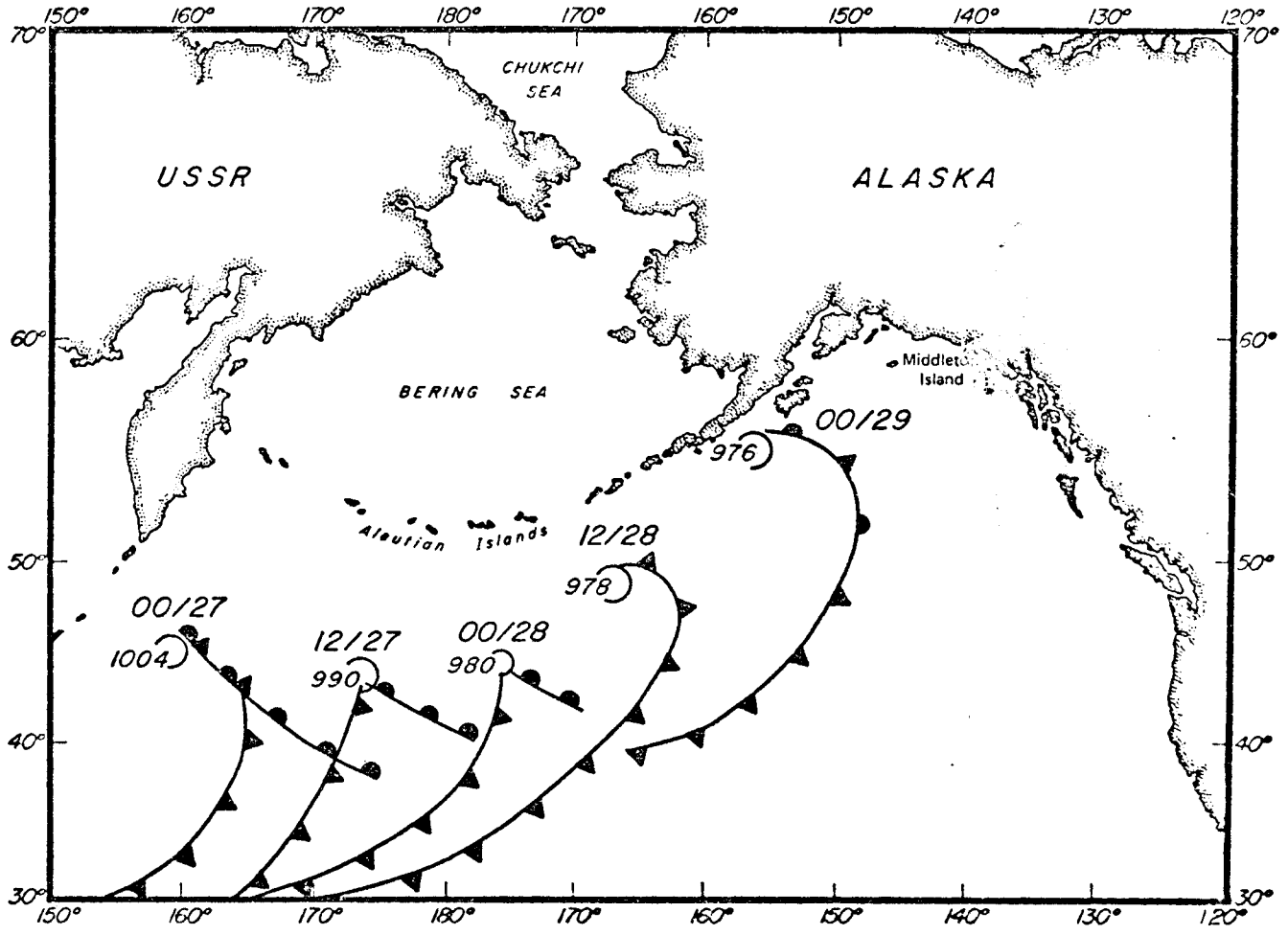

Figure 5-17. Twelve-hour positions of the center and front of a storm in the North Pacific, from 0000 UT 27 to 0000 UT 29 October 1973. The numbers above the center refer to the hour and day of the month when the data were reported. The number inside the centers refer to barometric pressure (Japan Meteorological Agency, 1973; U.S. Department of Commerce, 1973).

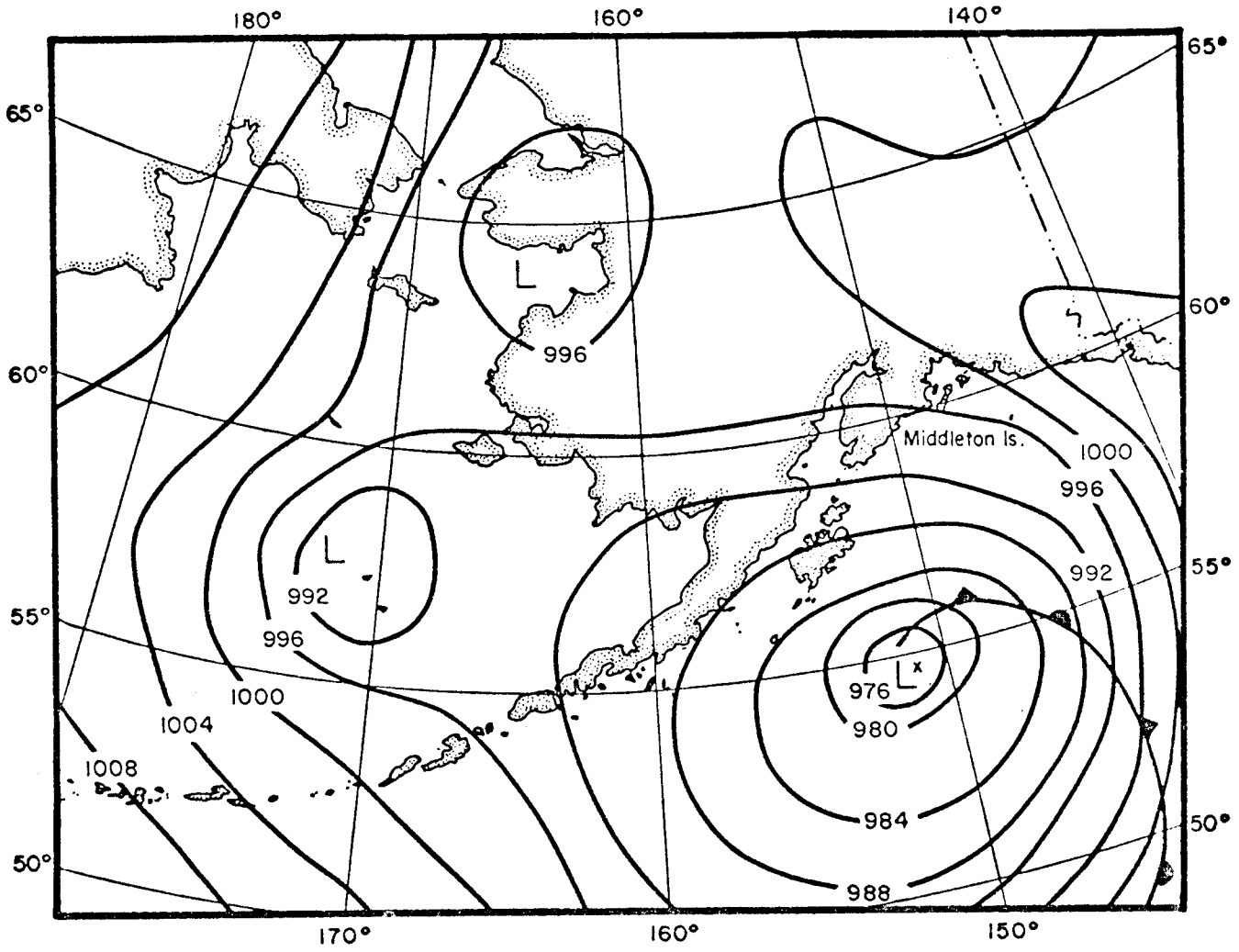

Figure 5-18. Weather over the Gulf of Alaska at 0000 UT 29 October 1973.

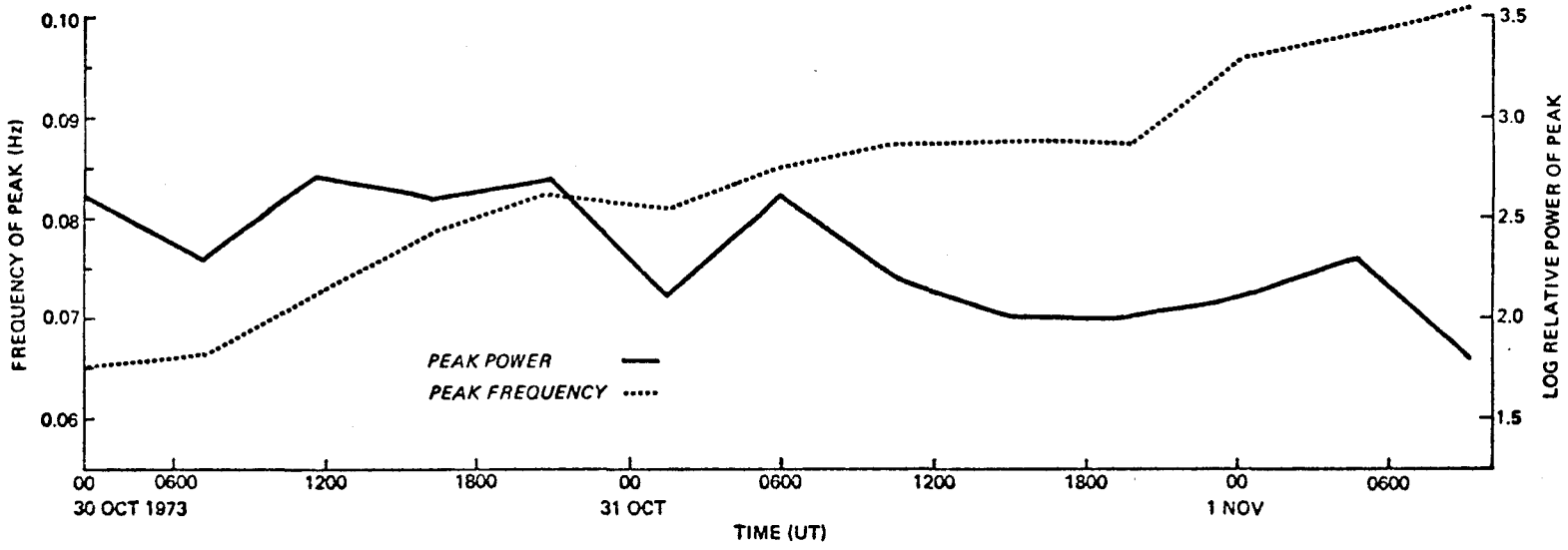

Figure 5-19. Frequency and log relative power of the spectral peak shown in Figures 5-3 to 5-15. From each of these spectra, frequency and log relative power of the peak were determined. Each point was then plotted at the time its respective time series started, and the points were connected by straight lines.

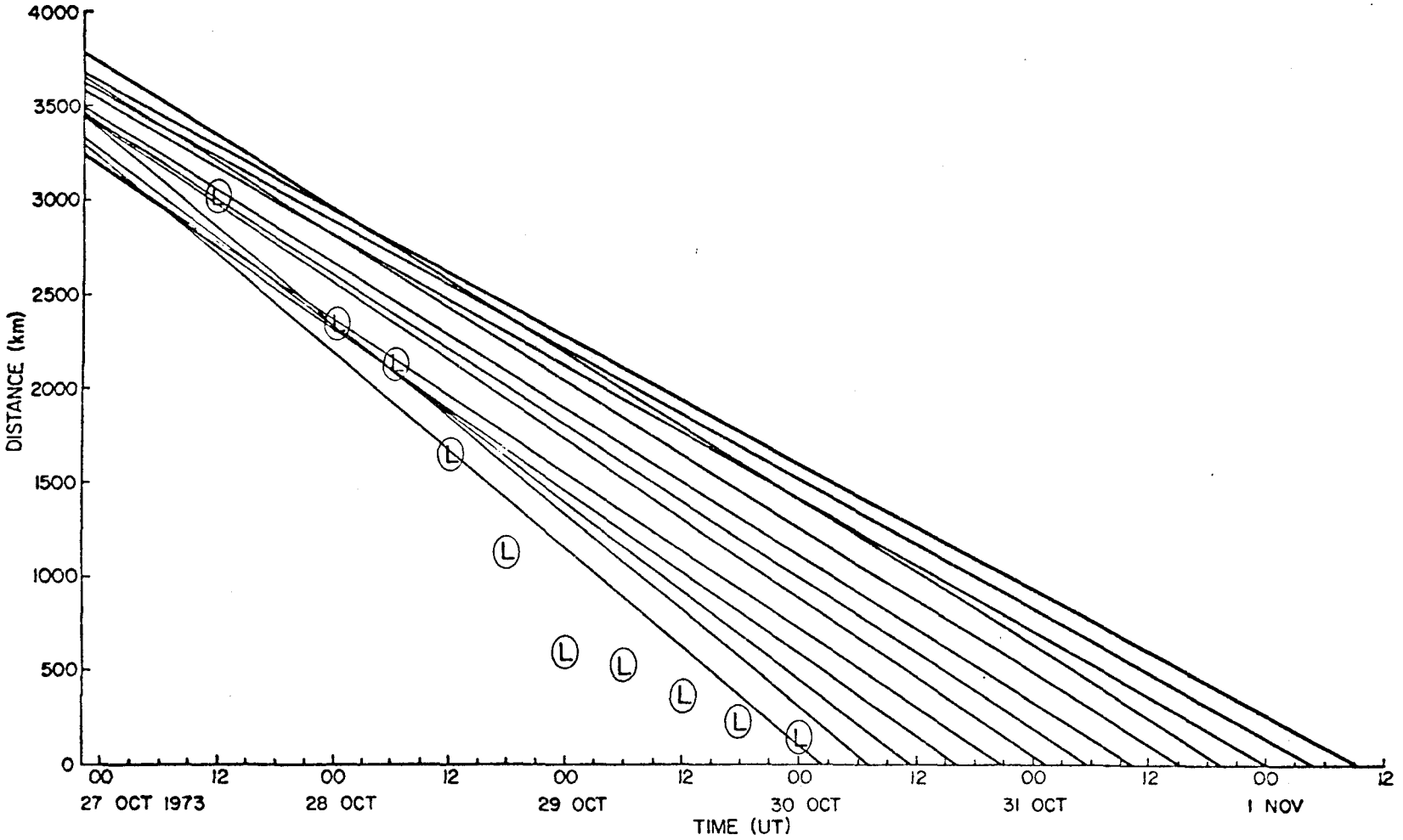

Figure 5-20. Circled L's show the distance from Middleton Island of the center of the storm shown in Figure 5-17. Lines show possible time and distance from Middleton Island for the source of waves associated with peaks in the spectra. Details of the construction of the lines are given in the text. Each line corresponds to the spectral peak whose frequencies are given in Figure 5-19.

In Figure 5-19 we see that the graph of frequency of the peak versus time may be broken into three main sections. In the first section, from the beginning of the record until 2053 UT 30 October, the frequency increases. In the middle section, 2053 UT 30 October to 1938 UT 31 October, the frequency of the peak remains nearly constant. After 1938 UT 31 October the frequency again increases. Specific correlations between each of these sections and features of the storm will now be made.

It is hypothesized that the peak at 0241 UT 30 October was caused by waves generated by the high winds (over 40 knots) which had a duration of at least 30 hours around 3500 km from Middleton Island. Figure 5-21 shows that such winds would be sufficient to generate waves with a frequency of 0.0653 Hz (T = 15.3 seconds). At around 0000 UT 28 October the storm paused around 2100 km from Middleton Island and grew in intensity. Around 0600 UT the same day it resumed its motion, moving faster than most of the waves it generated, thus effectively "turning off" the generating mechanism 2100 km away. Figure 5-22a shows a plot of frequency of a spectral peak versus time for a hypothetical, stationary storm which instantaneously generates waves with frequencies of 0.065, 0.07, 0.075, and 0.08 Hz, assuming the storm to be located 2100 km away from the site where the data are taken. The values for this plot are given in Appendix 3. Figure 5-22b shows a graph of the generation lines for the waves whose frequencies are shown in Figure 5-22a. Appendix 4 gives an analytic expression for finding the distance of the source from the wave gauge, given only the information in Figure 5-22a. Figure 5-22 agrees with those portions of Figures 5-19 and 5-20 between 0714 UT and

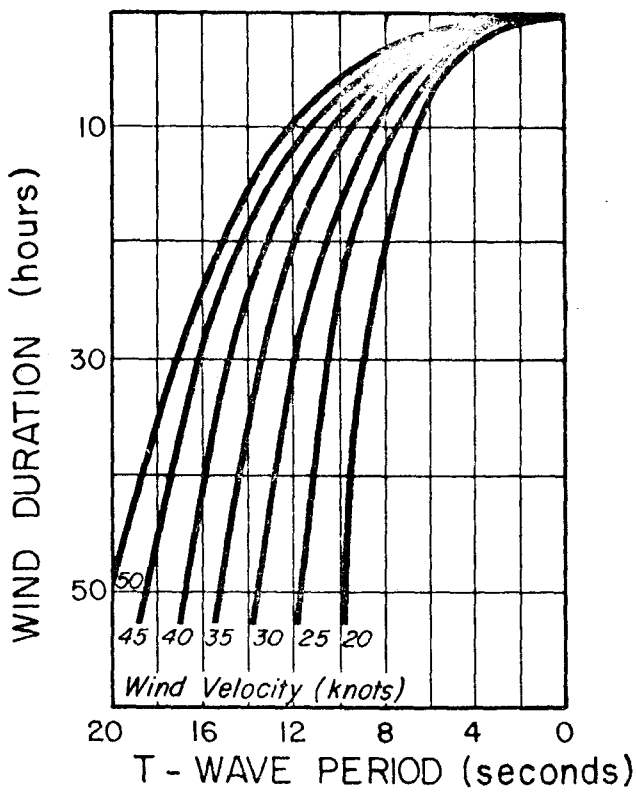

Figure 5-21. Empirical relationships between wind speed (1 knot = 0.5144 m/second), duration of the wind, and the periods of the waves. (After Reid, personal communication: 1967).

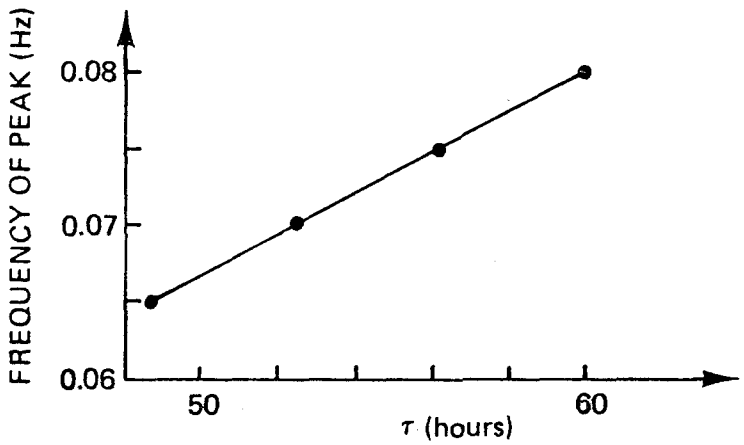

Figure 5-22a. Frequency of the peaks in spectra obtained by analyzing waves generated by a storm, 2100 km from the wave gauge, which instantaneously generated waves with frequencies of 0.065, 0.07, 0.075, and 0.08 Hz.

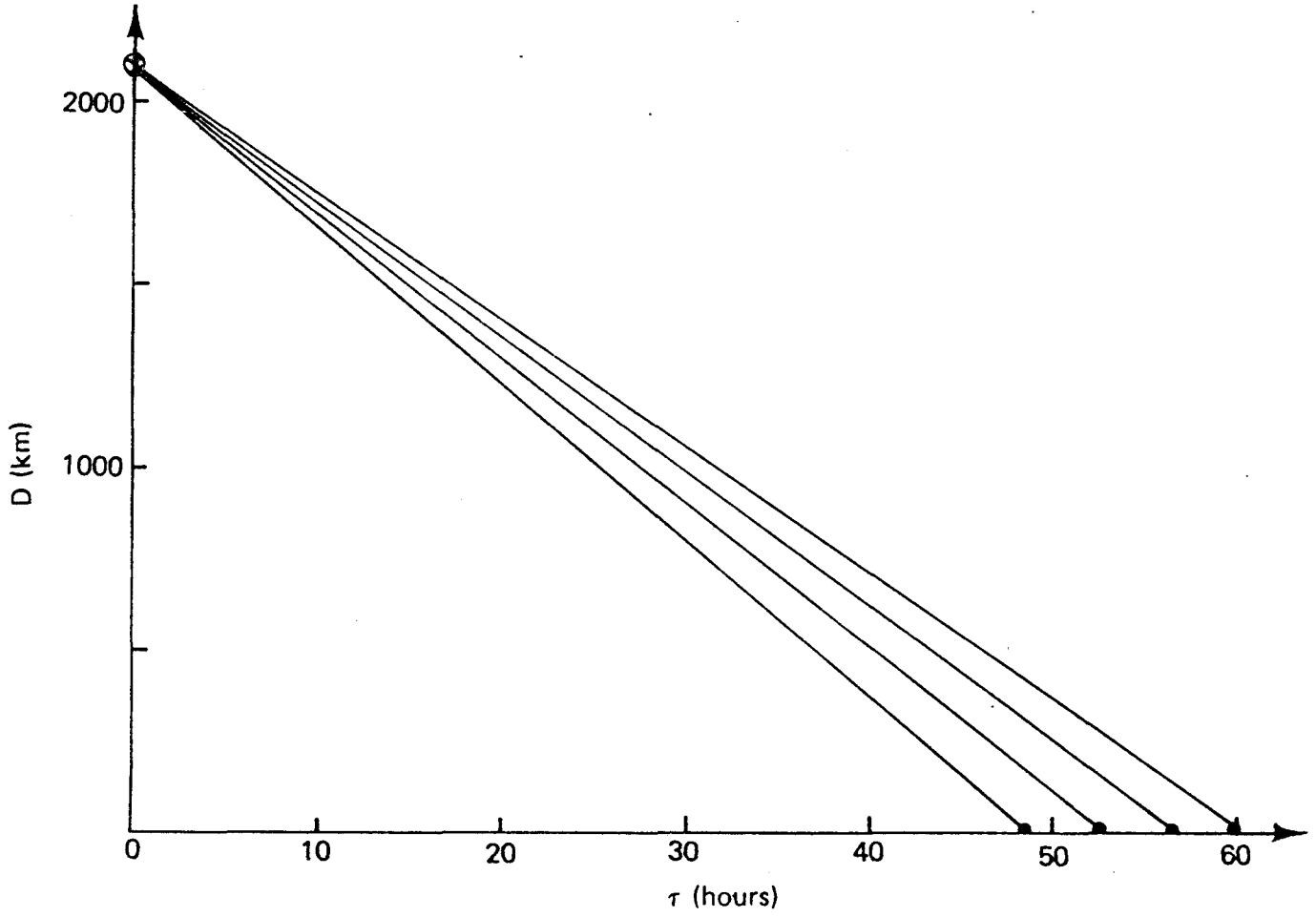

Figure 5-22b. Generation lines for the waves whose frequencies are shown in Figure 5-22a.

2053 UT 30 October.

From 0600 UT 28 October to 0000 UT 29 October the storm traveled about 23 m/second, faster than most of the waves it generated. This is evident in Figure 5-19, since the slope of the storm path is steeper than the slopes of the generation lines. The frequency of the peak from 2053 UT 30 October through 1938 UT 31 October remains nearly constant, consistent with a picture of higher frequency waves generated in an area around 2100 km from Middleton Island, after the departure of the main storm. According to Munk, Miller, Snodgrass, and Barber (1963), a moving storm will amplify waves whose group velocity equals the velocity of the storm. From equation (1), waves whose group velocity is 23 m/second will have a frequency of 0.039 Hz (T = 29.5 seconds). Thus, we would hope to see a spectral peak at 0.039 Hz from around 2053 UT 30 October to 2000 31 October. Consulting Figures 5-7 through 5-12, we see that there is indeed a peak, but it lies somewhat lower, around 0.03 Hz. This would put the speed of the storm at 26 m/second, not an unreasonable discrepancy for geophysical data.

The power of the spectral peak drops throughout this period, except around 0600 UT 31 October. This increase may be due to the high winds at 51°N, 142°W, 9900 km from Middleton Island, at 0000 UT 30 October which could have contributed additional power to waves of this frequency.

The increase in frequency from 1938 UT 31 October to 0011 UT 1 November occurred when the storm stopped moving, around 0000 UT 29 October, and the waves which it had been generating caught up with the storm. From 0011 UT to 0917 UT 1 November, the peak moved slowly toward higher frequencies as the stationary storm, now in the gulf, slowly decayed.

This is illustrated by an example. Suppose a storm, fixed 800 km away, instantaneously generates waves whose frequency is 0.095 Hz, 6 hours later generates waves with a frequency of 0.10 Hz, and 6 hours later generates 0.105 Hz waves. Figure 5-23a gives a plot of frequency of a spectral peak versus time for waves from such a storm (the values for this plot are given in Appendix 3), and Figure 5-23b shows the generation lines. Both are consistent with the last three points in Figures 5-19 and 5-20. Figure 5-23b shows that the generation lines for a stationary, decaying storm which is close to the wave gauge are the same as those for a stationary, instantaneous storm a great distance away.

The peak at 0.06 Hz which appears around 0126 UT 31 October (Figure 5-8) and continues into November is probably due to continuing storms and high winds in the northwest Pacific. For instance, at 0000 UT 27 October, 27.5 m/second (55 knot) winds were reported around 36°N, 161°E, 4550 km from Middleton Island. Travel time for 0.06 Hz waves from this location is

$$\tau = 4.55 \times 10^6 \text{m} \; / \; (13 \text{m/second})$$

$$= 97.22 \text{ hours}$$

giving an arrival time for these waves of around 0100 UT 31 October.

In order to see if the methods described above could be applied to other storms, we considered the work of Snider and Chakrabarti (1973). They used surface wave data obtained from the Ocean Weather Ship *Weather Advisor* which was in a storm in the North Atlantic from 15 to 19 March 1968. Records of from 17.4 to 33.7 minutes in duration were obtained every three hours, with $\Delta = 1.5$ seconds. Spectral analysis of

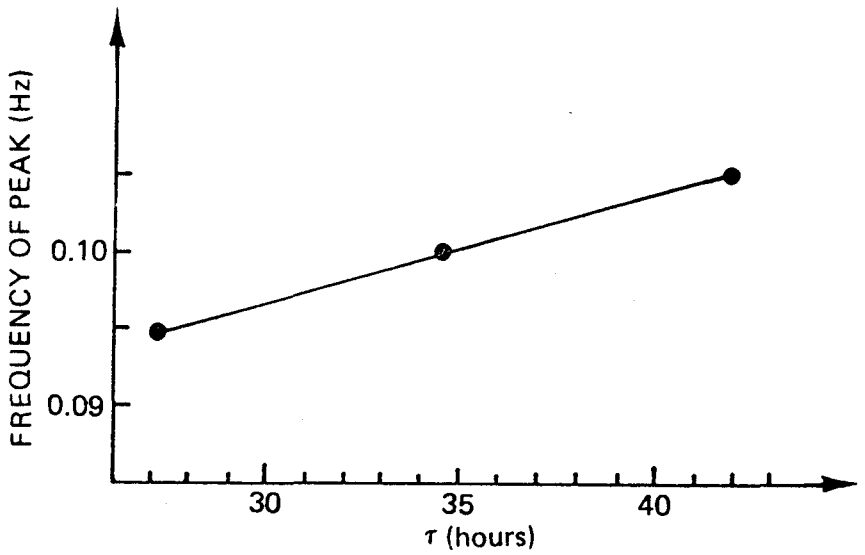

Figure 5-23a. Frequency of the peaks in spectra obtained by analyzing waves generated by a storm, 800 km from the wave gauge, which instantaneously generated waves with a frequency of 0.095 Hz, 6 hours later generated 0.10 Hz waves, and 6 hours later generated 0.105 Hz waves.

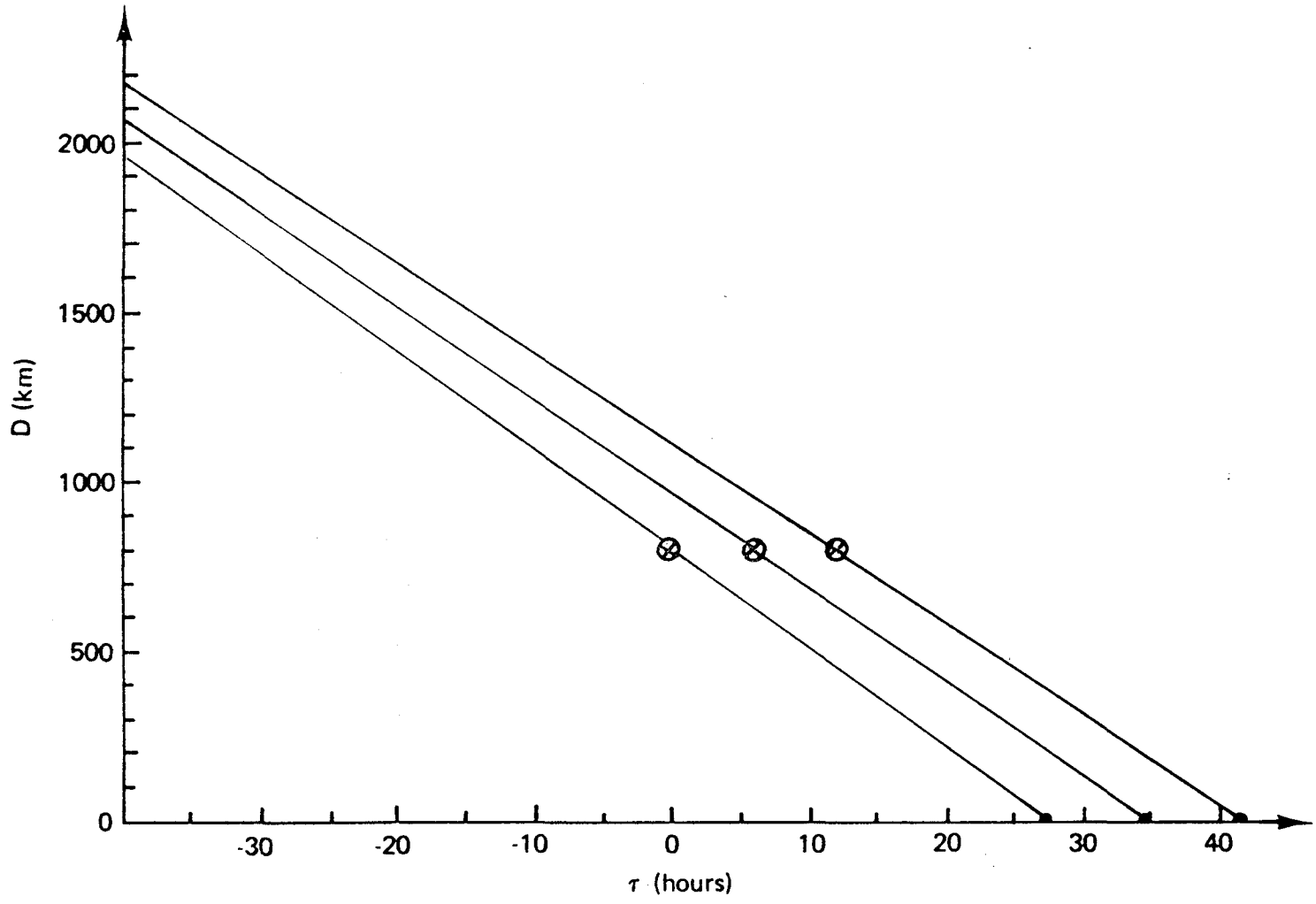

Figure 5-23b. Generation lines for the waves whose frequencies are shown in Figure 5-23a.

these records showed a well-defined peak, first small around 0.10 Hz before the storm, then quite large around 0.06 Hz at the height of the storm, then smaller and shifted to around 0.09 Hz as the storm subsided (Snider and Chakrabarti, 1973, Figure 3). Snider and Chakrabarti have tabulated the results of their spectral analysis for each record, so that it is a straighforward matter to plot frequency of the peak versus time. Such a plot exhibits the same slope during the time the storm was subsiding (from 0000 UT to 2100 UT 18 March 1968) as Figure 5-19 from 1400 UT 31 October to 0917 UT 1 November 1973 (Figure 5-24).

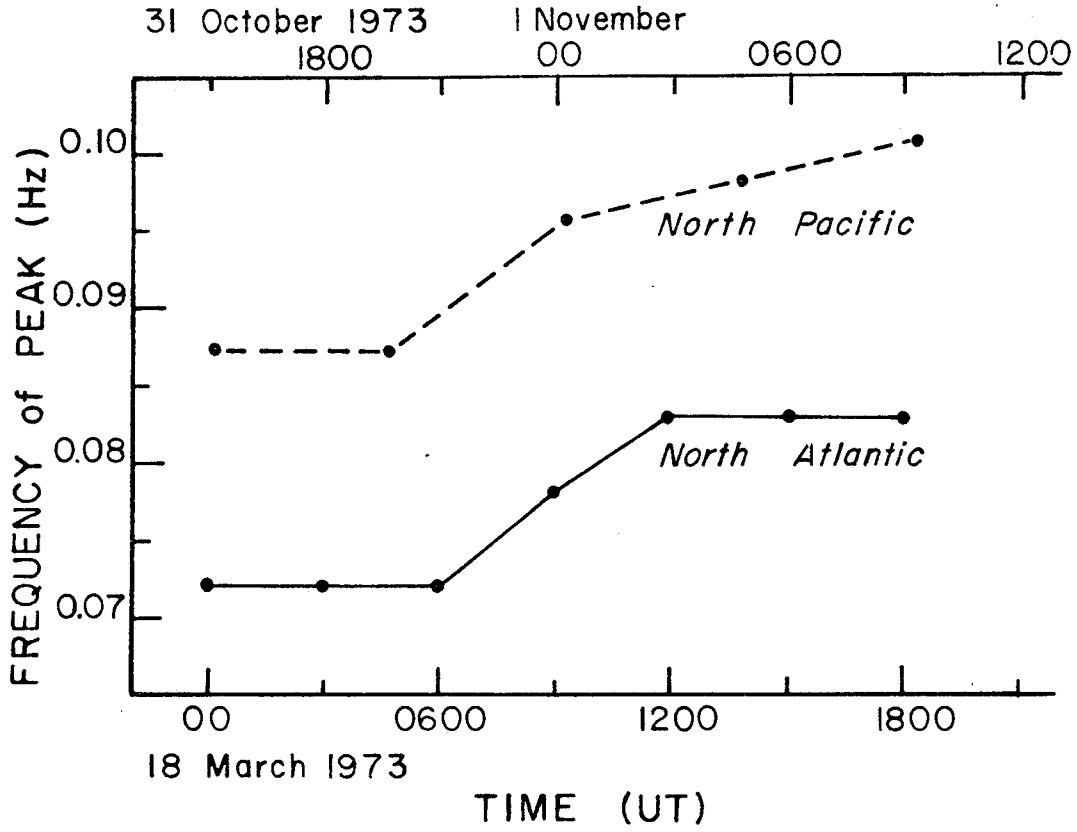

Figure 5-24. Comparison of frequency versus time of the spectral peak for the October 1973 storm in the North Pacific (dotted line) with a March 1968 storm in the North Atlantic (solid line).

CHAPTER 6

SUMMARY

Efficient and reliable methods based on the fast-Fourier transform have been developed to determine periodicities in time series. It has been shown that when the unfiltered record is sampled at large intervals, serious aliasing of the spectrum will occur, as indicated by Blackman and Tukey (1958). A second-order lowpass Butterworth filter with a cutoff frequency of 4.16×10^{-3} Hz (T = 4 minutes) effectively removes high-frequency components in the wave record, so that the record can be sampled at larger intervals without undue aliasing of the spectrum below 5.6×10^{-3} Hz (T = 3 minutes). Above this frequency, spectral aliasing has been shown still to occur.

Spectra for data taken after the occurrence of earthquakes of magnitude 5.9 in the Aleutians have shown that generation of ocean waves by these quakes is questionable, and that wave data following other similar quakes needs to be examined before any definite conclusions can be drawn.

When spectra from the first portion of the record were examined, it was found that a peak, which started out around 0.0625 Hz (T = 16 seconds), gradually shifted toward higher frequencies, simultaneously decreasing in amplitude. A plot of frequency of this peak versus time showed an increase for the first 18 hours of the record, then remained approximately constant for 24 hours, after which it again increased. These changes have been closely correlated with a large storm which remained stationary in the North Pacific, then moved rapidly into the Gulf of Alaska, after which it subsided. The correlation has

been clarified by showing, on the same graph, distance from Middleton Island of the center of the storm and of possible sources of waves whose frequency is the frequency of the peak.

A recent study by Snider and Chakrabarti (1973) of wave energy spectra obtained during a storm in the North Atlantic in 1968 also shows a shift and decay in the spectral peak. A comparison of plots of frequency of the peak versus time for the North Pacific and North Atlantic storms exhibit the same slope during the time the storms were subsiding.

APPENDIX 1

NOTATION

Numbers in parentheses after description refer to the section in which the symbol was first used.

A_m Discrete Fourier cosine transform of $\{x_k\}$; the Fourier coefficients for the cosine series (3.1)

a_i Filter coefficients (3.6); Fourier coefficients (3.1 only)

B_m Discrete Fourier sine transform of $\{x_k\}$; the Fourier coefficients for the sine series (3.1)

b Filter coefficient (3.7)

b_i Filter coefficients (3.6); Fourier coefficients (3.1 only)

C Arbitrary constant (Appendix 4)

c_g Wave group velocity (5.3)

c_p Wave phase velocity (4.2)

D Distance (5.3)

d Water depth (3.2)

f Frequency (5.3)

f_c Cutoff frequency (3.7)

$f(t)$ Arbitrary function of time (3.1)

g Gravitational constant (3.2)

$H(z)$ Z-transform of $\{h_k\}$; the transfer function of a filter (3.6)

h Tsunami height (4.1)

h_i Weighting sequence coefficients in convolution summation (3.6)

j $\sqrt{-1}$ (3.1)

K_p Pressure response factor (3.2)

K_{p_o} Approximated pressure response factor (3.2)

k Integer index (3.1)

L Wavelength (3.2); Integer index (3.3 only)

L_o Approximation to L (3.2)

log Logarithm to the base 10; also written $\log_{10}$ (3.1)

m Integer index (3.1)

N Total number of points in a time series, assumed to be even; $N = T_1/\Delta$ (3.1)

n N/2 (3.1)

$\mathcal{P}\{\cdot\}$ A number representing the probability of the quantity inside the curly braces (3.3)

p_1, p_2 Poles of a filter (3.7)

T Wave period (3.2)

T_1 Duration of a time series; $T_1 = N\Delta$ (3.1)

t Time (3.1)

X_m The m^{th} Fourier coefficient in the exponential series for $\{x_k\}$ (3.1)

$\mathcal{X}_m$ The m^{th} Fourier coefficient in the exponential series for the stochastic process $\{\mathcal{X}_k\}$ (3.3)

X(z) Z-transform of $\{x_k\}$, also written $Z\{x_k\}$ (3.6)

x_k The k^{th} measured value of a discrete-time series; k^{th} data point; also written $x(k\Delta)$ (3.1)

$\{x_k\}$ The measured discrete-time series; also written $\{x_{-n},\ldots,x_0,\ldots x_{n-1}\}$, or $\{x(k\Delta)\}$ (3.1)

$\tilde{x}_k$ Least-squares approximation to x_k in the interval $[-T_1/2, T_1/2]$; also written $\tilde{x}(k\Delta)$ (3.1)

$\mathcal{X}_k$ Stochastic process of which x_k is a member (3.3)

Y(z) Z-transform of $\{y_k\}$ (3.6)

$\{y_k\}$	Discrete-time series, the output of a filter whose input is $\{x_k\}$ (3.6)
$Z\{x_k\}$	Z-transform of $\{x_k\}$; also written X(z) (3.6)
z	At first an arbitrary finite complex number; later specified as exp(j2π/N) (3.6)
α	Parameter for a χ^2 statistic (3.3)
Δ	Time interval between data values (3.1)
ν	Degrees of freedom for a chi-squared variable (3.3)
π	Ratio of the circumference of a circle to its diameter (3.1)
τ	Elapsed time (5.3)
χ^2_ν	Denotes the chi-squared distribution with ν degrees of freedom (3.3)
ω	Radian frequency; $\omega = 2\pi/T$ (3.4)
*	Denotes complex conjugation (3.1)

APPENDIX 2

FOURIER TRANSFORM RELATIONSHIPS

From equation (3.1.2) we have

$$A_{-m} = \frac{1}{N} \sum_{k=-n}^{n-1} x_k \cos \frac{2\pi(-m)k}{N} = A_m$$

$$B_{-m} = \frac{1}{N} \sum_{k=-n}^{n-1} x_k \sin \frac{2\pi(-m)k}{N} = -B_m$$

$$B_{-n} = -\frac{1}{N} \sum_{k=-n}^{n-1} x_k \sin \frac{2\pi nk}{N}$$

$$= -\frac{1}{N} \sum_{k=-n}^{n-1} x_k \sin \frac{2\pi nk}{2n} = 0$$

$$B_o = 0 .$$

Also,

$$e^{j(2\pi nk/N)} = e^{j\pi k} = \cos \pi k = e^{-j\pi k} .$$

Thus, equation (3.1.1) becomes

$$\tilde{x}(k\Delta) = A_o + \sum_{m=1}^{n-1} \left\{ A_m [e^{j(2\pi mk/N)} + e^{-j(2\pi mk/N)} \right.$$

$$\left. - j B_m [e^{j(2\pi mk/N)} - e^{-j(2\pi mk/N)}] \right\} + A_n \cos \frac{2\pi nk}{N}$$

$$= (A_o - jB_o) + \sum_{m=1}^{n-1} (A_m - jB_m) e^{j(2\pi mk/N)}$$

$$+ \sum_{m=1}^{n-1} (A_m + jB_m) e^{-j(2\pi mk/N)} + A_n e^{j(2\pi nk/N)}$$

$$= (A_o - jB_o) + \sum_{m=1}^{n-1} (A_m - jB_m)e^{j(2\pi mk/N)}$$

$$+ \sum_{m=-1}^{-n+1} (A_m - jB_m)e^{j(2\pi mk/N)} + (A_{-n} - jB_{-n})e^{j(2\pi nk/N)}$$

$$= \sum_{m=-n}^{n-1} (A_m - jB_m)e^{j(2\pi mk/N)}$$

$$= \sum_{m=-n}^{n-1} X_m \, e^{j(2\pi mk/N)} \quad ,$$

which is equation (3.1.7).

We now prove equation (3.1.8). From equation (3.1.7) we have

$$\frac{1}{N} \sum_{k=-n}^{n-1} \tilde{x}_k \, e^{j(2\pi mk/N)} = \frac{1}{N} \sum_{k=-n}^{n-1} \left[\sum_{r=-n}^{n-1} X_r \, e^{j(2\pi rk/N)} \right] e^{-j(2\pi mk/N)} \tag{1}$$

$$= \frac{1}{N} \sum_{k=-n}^{n-1} \left[X_{-n} e^{-j(2\pi nk/N)} + \cdots + X_{n-1} e^{j[2\pi(n-1)k/N]} \right] e^{-j(2\pi mk/N)}$$

$$= \frac{1}{N} \sum_{r=-n}^{n-1} \left[X_r \sum_{k=-n}^{n-1} e^{j[2\pi(r-m)k/N]} \right]. \tag{2}$$

Consider the sum inside the brackets for the case $r \neq m$, say $r - m = \ell$. Since $N = 2n$, we have

$$e^{j[2\pi\ell(-n)/N]} = e^{-j\pi\ell} = e^{+j\pi\ell} = e^{j(2\pi\ell n/N)}$$

$$e^{j[2\pi\ell(-n+1)/N]} = e^{-j\pi\ell} e^{j(2\pi\ell/N)} = e^{j[2\pi\ell(n+1)/N]}$$

$$\vdots$$

$$e^{j(-2\pi\ell/N)} = e^{j2\pi\ell} e^{-j(2\pi\ell/N)} = e^{j[2\pi\ell(N-1)/N]} \, .$$

Thus,

$$\sum_{k=-n}^{n-1} e^{j(2\pi\ell k/N)} = \sum_{k=0}^{N-1} e^{j(2\pi\ell k/N)} \, .$$

But $e^{j(2\pi\ell/N)}$ is an N^{th} root of unity $[e^{j(2\pi\ell/N)N} = 1]$, and hence the sum inside the brackets of equation (2) is zero when $r \neq m$. When $r = m$, we have

$$\sum_{k=-n}^{n-1} e^{0} = N \ .$$

Therefore

$$\sum_{k=-n}^{n-1} e^{j[2\pi(r-m)k/N]} = \begin{cases} 0, & r \neq m \\ N, & r = m \end{cases}$$

and equation (1) becomes

$$\frac{1}{N} \sum_{k=-n}^{n-1} \tilde{x}_k \, e^{-j(2\pi mk/N)} = X_m \ ,$$

which is equation (3.1.8).

APPENDIX 3

VALUES USED IN CONSTRUCTING FIGURES 5-22a AND 5-23a

The formula for wave arrival time is from equations (5.3.1) and (5.3.2) and is given by

$$\tau = 4\pi Df / g \ .$$

Figure 5-22a, D = 2100 km

f	τ (seconds x 10^{-5})	τ (hours)
0.065	1.7503	48.62
0.070	1.8850	52.36
0.075	2.0196	56.10
0.080	2.1542	59.84

Figure 5-23a, D = 800 km

f	τ (seconds x 10^{-5})	τ (hours)	$\Delta\tau$ (hours)	Final τ (hours)
0.095	0.9745	27.07	0	27.07
0.100	1.0258	28.50	6	34.50
0.105	1.0771	29.92	12	41.92

APPENDIX 4

ANALYTIC EXPRESSION FOR WAVE SOURCE DISTANCE

Consider a plot of frequency of a spectral peak versus time of arrival of that peak, and suppose all the points lie on a straight line. For simplicity, consider only two points on the line, (τ_1, f_1) and (τ_2, f_2). Then the slope of the line is

$$\frac{f_2 - f_1}{\tau_2 - \tau_1} .$$

This slope will be non-negative, so long as the waves come from a single source, since waves with higher frequencies travel slower than those with lower frequencies.

Now consider a plot of the generation lines for waves of frequency f_1 and f_2. The equation for these lines is given by

$$D = -c_g \tau + C$$

$$= -(g/4\pi f)\tau + C ,$$

where C is the D-intersect, and the slope is negative because we are considering the prior positions of the waves. The line for f_1 is

$$D_1 = -(g/4\pi f_1)\tau + C_1 .$$

Since $D_1 = 0$ at $\tau = \tau_1$, we have

$$C_1 = (g/4\pi)(\tau_1/f_1) ,$$

so that

$$D_1 = \frac{g}{4\pi} \frac{\tau_1 - \tau}{f_1} . \qquad (1)$$

Similarly,

$$D_2 = \frac{g}{4\pi} \frac{\tau_2 - \tau}{f_2} \quad . \tag{2}$$

These lines intersect at the point $D_1 = D_2 = D_o$ when $\tau = \tau_o$, say. That is,

$$\frac{g}{4\pi} \frac{\tau_1 - \tau_o}{f_1} = \frac{g}{4\pi} \frac{\tau_2 - \tau_o}{f_2} \quad ,$$

or

$$\tau_o = \frac{f_1\tau_2 - f_2\tau_1}{f_1 - f_2}$$

and from equation (1),

$$D_o = \frac{g}{4\pi} \frac{\tau_1}{f_1} - \frac{f_1\tau_2 - f_2\tau_1}{f_1(f_1 - f_2)}$$

$$= \frac{g}{4\pi} \frac{\tau_1 - \tau_2}{f_1 - f_2} \quad \text{at} \quad \tau = \tau_o \quad . \tag{3}$$

Thus, the distance at which the generation lines cross (that is, the common source of the waves) is proportional to the inverse slope of the line of peak frequency versus arrival time.

For example, consider the frequency of a spectral peak versus wave arrival time shown in Figure 5-22a. Exact values for f and τ are given in Appendix 3. Let $f_1 = 0.065$ Hz, $\tau = 1.7503 \times 10^5$ seconds, $f_2 = 0.080$ Hz, $\tau_2 = 2.1542 \times 10^5$ seconds. Then the slope of the line f versus τ shown in Figure 5-22a is

$$\frac{f_2 - f_1}{\tau_2 - \tau_1} = \frac{0.015}{0.4039 \times 10^5} \text{ second}^{-2}$$

$$= 3.7138 \times 10^{-7} \text{ second}^{-2} \quad .$$

From equation (3),

$$D_o = \frac{g}{4\pi} \frac{10^7}{3.7138} \text{ second}^2$$

$$= 2.0999 \times 10^6 \text{ m}$$

$$\doteq 2100 \text{ km}$$

in agreement with the original assumption for D_o .

REFERENCES

Adams, W. M., and A. S. Furumoto (1970). Features of Tsunamigenic Earthquakes, pp. 57-68. In, *Tsunamis in the Pacific Ocean*, W. M. Adams (ed.), Honolulu: East-West Center Press.

Blackman, R. B., and J. W. Tukey (1958). *Measurement of Power Spectra.* New York: Dover Publ., 190 pp.

Braddock, R. D. (1970). Tsunami Propagation over Large Distances, pp. 285-303. In, *Tsunamis in the Pacific Ocean*, W. M. Adams (ed.), Honolulu: East-West Center Press.

Brenner, N. M. (1967). "Three FORTRAN Programs that Perform the Cooley-Tukey Fourier Transform." MIT Lincoln Lab., Lexington, Mass., Tech. Note 1967-2, 29 pp.

Cadzow, J. A. (1973). *Discrete-Time Systems.* Englewood Cliffs, N. J.: Prentice-Hall, 440 pp.

Chapman, S., and J. Bartels (1940). *Geomagnetism.* Oxford: Clarendon Press, 2 Vols., 1049 pp.

Danielsen, E. F., W. V. Burt, and M. Rattray, Jr. (1957). Intensity and Frequency of Severe Storms in the Gulf of Alaska. *Trans. Amer. Geophys. Un.* 38(1), 44-49.

Frankignoul, C. J. (1974). A Cautionary Note on the Spectral Analysis of Short Internal Wave Records. *J. Geophys. Res.* 79(24), 3459-3462.

Freeman, H. (1965). *Discrete-Time Systems, an Introduction to the Theory.* New York: Wiley, 241 pp.

Iida, K. (1963). Magnitude, Energy, and Generation Mechanisms of Tsunamis, and a Catalogue of Earthquakes Associated with Tsunamis, pp. 7-18. *In*, Proc. Tsunami Meetings Associated with the Tenth Pacific Science Congress, IUGG Monograph No. 24.

Iida, K. (1970). The Generation of Tsunamis and the Focal Mechanism of Earthquakes, pp. 3-18. In, *Tsunamis in the Pacific Ocean*, W. M. Adams (ed.), Honolulu: East-West Center Press.

Japan Meteorological Agency (1973). "Daily Weather Maps and Data, 16 October 1973-31 October 1973." Tokyo, Japan.

Jenkins, G. M., and D. G. Watts (1968). *Spectral Analysis and its Applications.* San Francisco: Holden-Day, 525 pp.

Kaiser, J. F. (1966). Digital Filters, pp. 218-285. In, *System Analysis by Digital Computer*, F. F. Kuo and J. F. Kaiser (eds.), New York: Wiley.

Kanasewich, E. R. (1973). *Time Sequence Analysis in Geophysics.* Edmonton: The University of Alberta Press, 352 pp.

Kinsman, B. (1965). *Wind Waves.* Englewood Cliffs, N. J.: Prentice-Hall, 676 pp.

Lahti, B. P. (1968). *An Introduction to Random Signals and Communication Theory.* Scranton, Pa.: International Textbook Co., 488 pp.

Laplace, P. S. (1779). *Oeuvres Complètes.* (Cited by B. Gold and C. M. Rader (1969). *Digital Processing of Signals.* New York: McGraw-Hill, on p. 2).

Miller, G. R., W. H. Munk, and F. E. Snodgrass (1962). Long-period Waves over California's Continental Borderland. Part II. Tsunamis. *J. Mar. Res.* 20(1), 31-41.

Munk, W. H., G. R. Miller, F. E. Snodgrass, and N. F. Barber (1963). Directional Recording of Swell from Distant Storms. *Phil. Trans. Roy. Soc., London* A255, 509-589.

Neumann, G., and W. J. Pierson, Jr. (1966). *Principles of Physical Oceanography.* Englewood Cliffs, N. J.: Prentice-Hall, 545 pp.

Otnes, R. K., and L. Enochson (1972). *Digital Time Series Analysis.* New York: Wiley, 467 pp.

Papoulis, A. (1965). *Probability, Random Variables, and Stochastic Processes.* New York: McGraw-Hill, 583 pp.

Podyapolsky, G. S. (1970). Generation of the Tsunami Wave by the Earthquake, pp. 19-32. In, *Tsunamis in the Pacific Ocean*, W. M. Adams (ed.), Honolulu: East-West Center Press.

Rosenberg, D. H. (1972). Coastal Weather, Tides and Wind Waves of the Northern Gulf of Alaska, pp. 131-141. In, "A Review of the Oceanography and Renewable Resources of the Northern Gulf of Alaska," Inst. Mar. Sci., Univ. Alaska, Rept. No. R72-23.

Royer, T. C. (1972). Physical Oceanography of the Northern Gulf of Alaska, pp. 5-22. In, "A Review of the Oceanography and Renewable Resources of the Northern Gulf of Alaska," Inst. Mar. Sci., Univ. Alaska, Rept. No. R72-23.

Royer, T. C., and R. O. Reid (1971). The Detection of Secondary Tsunamis. *Tellus* 23(2), 136-142.

Seitz, R. L. (1975). "A Tsunami and Long Wave Recording System." Inst. Mar. Sci., Univ. Alaska, Rept. (in preparation).

Snider, R. H., and S. K. Chakrabarti (1973). High Wave Conditions Observed over the North Atlantic in March 1968. *J. Geophys. Res.* 78(36), 8793-8807.

U.S. Department of Commerce (1973). "North American Surface Charts, October, 1973." National Weather Service, U.S.D.C., National Climatic Center, Asheville, N.C. 28801.

U.S. Department of the Interior (1973). "Preliminary Determination of Epicenters, Monthly Listings for October and November." National Earthquake Information Service, U.S.D.I., Geological Survey.